Advanced technologies for automated dynamic culture and electro-mechanical characterization of biological tissues for tissue engineering applications

Stefano Gabetti

* * * * * *

Supervisors
Prof. Alberto Audenino, Supervisor
Prof. Diana Massai, Co-Supervisor
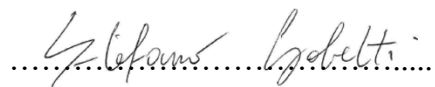
Doctoral Examination Committee
Prof. Sara Mantero, Referee, Politecnico di Milano
Prof. Toshiro Ohashi, Referee, Hokkaido University

Politecnico di Torino
2022

To mum, dad, Anna and Francesca

_____

I hereby declare that, the contents and organization of this dissertation constitute my own original work and does not compromise in any way the rights of third parties, including those relating to the security of personal data.

....

Stefano Gabetti

Turin, 19th July 2022

_____

Summary

Tissue engineering aims to develop functional substitutes of native biological tissues to be exploited as *in vitro* models for tissue development and disease research, with the ultimate but still challenging goal to be implanted for promoting *in vivo* regeneration. For the development of effective substitutes, alongside the cells and the architectural and biochemical support provided by three-dimensional (3D) scaffolds, a paramount role is played by the physical stimuli applied. Indeed, *in vivo* cells and tissues are continuously exposed to several physical stimuli arising from the extracellular matrix (ECM) and from the neighboring cells, which concur to tissue homeostasis and remodeling and that can be involved in disease pathogenesis. The ability of cells to sense and react to the physical cues of their microenvironment, dynamically adapting to its continuous modifications, is called mechanotransduction and it is based on cascades of interlaced molecular signaling pathways and complex cellular mechanisms.

Therefore, the characterization of the physical stimuli to which cells are exposed *in vivo* and the identification of the corresponding biological responses triggered at the cell and tissue scales are fundamental for translating the latest tissue engineering scientific knowledge into promising and efficient clinical strategies. To understand the interplay of phenomena implied in tissue regeneration and homeostasis, a considerable amount of research has been conducted exploiting approaches at the cell and tissue level. However, much uncertainty still exists about the mechanisms by which the cells perceive and transform physical stimuli into complex biological responses.

The objectives of this PhD thesis concerned the development and validation of advanced technologies for supporting the tissue engineering and mechanobiology research fields, in particular by: 1) providing cell/tissue dynamic culture environments replicating the native physical stimuli; 2) enabling characterization of physical properties of biological

_____

tissues and scaffolds; 3) *in vitro* investigating the native physical cues acting on cells and tissues. Applying advanced engineering methods, relying on state-of-the-art hardware and software platforms, and performing proof of concept biological tests, three technologies covering multiple aspects of tissue engineering and mechanobiology investigation were conceived, engineered, and validated.

As regards the development of technologies for dynamic cell/tissue culture, firstly a compact, easy-to-use, versatile electrical stimulator (ELETTRA) for cardiac tissue engineering applications, designed to provide tunable electrical stimuli to the cultured cells/constructs, was developed. Upon construction, the stimulator was coupled to customized culture chambers, designed for delivering uniform electrical stimulation to the samples, and was adopted for investigating the effect of different electrical stimulation waveforms on neonatal rat ventricular cells. Results demonstrated the reliability and versatility of ELETTRA, and confirmed the crucial role of electrical stimulation in promoting cardiac cell functionality and maturation, particularly when a biphasic waveform was imposed. Subsequently, an automated bioreactor for bone tissue engineering was designed, manufactured, and tested. Such bioreactor introduced the possibility to combine two different physical stimulations: flow-induced shear stress and pulsed electromagnetic field stimulation. Moreover, the automation strategy adopted for the perfusion control enabled delivering uni- or bi-directional direct perfusion within the same platform and without user intervention along the culture. Experimental tests were performed culturing 3D bone tissue models, based on a commercial scaffold seeded with human bone marrow stem cells, under both uni- and bi-directional perfusion. Perfusion culture promoted osteogenic differentiation and favored cells to deposit more ECM with respect to the static culture, and interestingly bi-directional perfusion better promoted ECM deposition across the constructs with respect to uni-directional perfusion, showing that the proposed bioreactor represents a powerful tool for in depth bone mechanobiology investigations.

Concerning the characterization of the physical properties of biological tissues and scaffolds, a novel test bench for permeability assessment was built. The test bench, developed on a pump-based hydraulic circuit, can house hard or soft samples within a customized permeability chamber and,

_____

upon imposing a defined flow rate (guaranteeing laminar flow), permeability is measured by using the Darcy flow transport model. Preliminary validation tests, performed testing commercial bone scaffolds within both the developed test bench and a reference one, confirmed the suitability of the proposed approach. The permeability test bench can be seen also as a complementary system to the perfusion bioreactor setup, allowing a complete quantitative characterization of scaffold performances.

All the proposed technologies were developed following an iterative design process based on the combination of advanced engineering tools and biological strategies for progressive refinement, testing, and on-site validation. This approach allowed optimizing the developed solutions through continuous refinements and taking into account the user feedbacks, with consequent reduced risk of failure at later stages of device development. The validation tests that were performed provided evidence that the proposed devices and test benches could overcome some of the current limitations affecting the tissue engineering research field (i.e., incomplete recapitulation of the physical cues, limited tunability and versatility of the equipment, uncertainty in characterizing material properties and stimuli), strongly contributing to the advancement of different research fields. This fulfils the main purpose of this PhD thesis, which was providing advanced engineering tools for increasing the robustness and repeatability of research experiments in tissue engineering, paving the way for the investigation of specific open questions related to mechanotransduction.

In the near future, the proposed technologies will be used as powerful investigation tools for unravelling cell-scale mechanotransduction signaling pathways, providing meaningful insights to increase the tissue regeneration knowledge base, finally contributing to boost the translation of promising tissue engineering strategies to clinical use.

_____

Acknowledgements

First and foremost, I wish to thank Prof. Diana Massai, for seeing potential in me and giving me the opportunity to do this work. Every day (and every night) she has been the example of what a researcher should be: upright, accurate, determined, and open-minded. I am deeply grateful for the countless hour she spent in following my activities, providing meaningful suggestions and intriguing perspectives. But most of all, for encouraging me when I could only see the downside and for dealing with my stubbornness and melancholy.

I would like to thank Prof. Alberto Audenino for advising me during my research activities and helping me in appreciating the hidden beauty of technology. Furthermore, I wish to thank Prof. Umberto Morbiducci for showing me the intertwining of science and art and for his critical suggestions, inspirational comments, and music recommendations.

I thank Dr. Anna Marsano for welcoming me in her group at Universitätsspital Basel and giving me the opportunity to work on the applications of our project. Many thanks to Antonio Sileo, with whom I collaborated during the seven months I spent in Basel and to Deborah, Gregory and Laia for making time fly.

I wish to thank all my colleagues, with a special mention for Beatrice and Giovanni, for the constructive discussions and for making our offices and labs places where to share the ups and downs of our work, usually with heaps of food from all over the World.

Thanks also to all the colleagues from the external institutions with whom I collaborated over the course of my PhD.

A special thank goes to all the people who decided to undertake the mission to make knowledge and technology open and free, especially those on which this work relies: Arduino founders and community, KiCAD developers, Zotero developers and Alexandra Elbakyan.

_____

I am thankful to my friends, for keeping alive the special relationships we have built even during the last troubling periods, and for the patience to listen to me explaining what I actually do.

I would like to thank my parents, which always trusted and supported me, assisting me in important decisions, without imposing their view. With them I thank my sister Anna, for giving me another perspective on all the things in life and for showing me the huge amount of evidence proving that physicists are better than engineers.

Last but not least, heartfelt thanks to my fiancée, Francesca, who relieves my worries, shares insights, enlightens every day and, more importantly, stands me for most of the time.

My warmest thanks to all of you, without your support I could not say now that, you know, I am something of a scientist myself.

_____

Contents

_____

List of Tables

List of Figures

Chapter 1

Introduction

1.1 Mechanotransduction and physical stimuli in *vivo*

The cell is the basic structural and functional unit of life and constitutes the building block of organisms. Individual cells themselves are highly complex living entities, performing a variety of functions: the synthesis, sorting, storage and transport of molecules; the expression of genetic information; the recognition, transmission and transduction of signals; and the powering of molecular motors and machines[1]. A cell is covered by a phospholipid bilayer membrane reinforced with protein molecules, and the interior comprises a liquid phase (cytosol) and subcellular components: a nucleus, the cytoskeleton, organelles of different sizes and shapes, and other proteins (Figure 1.1).
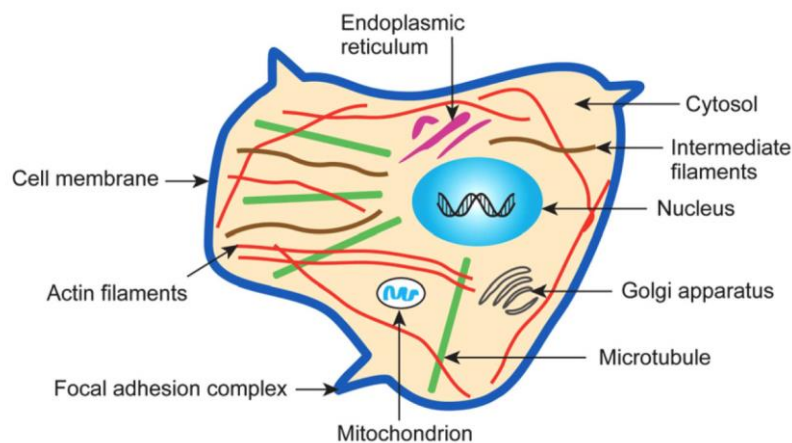
Figure 1.1: Schematic illustration of the subcellular structure of a typical eukaryotic cell (from Suresh (2007), Acta Biomaterialia[2]).

_____

Cells live in a constantly changing biomechanical environment, which constantly exposes them to mechanical stimuli arising from the surrounding extracellular matrix (ECM) and from neighboring cells. Depending on their location within the body, cells are selectively exposed to a set of different stimuli such as pressure, fluid shear stress, stretch, and compression[3]. Externally applied mechanical loads play a significant role in tissue homeostasis and remodeling and cells in tissues are responsible for this remodeling in response to mechanical forces[4].

The intracellular molecular processes through which physical stimuli are translated to a biological response are termed mechanotransduction and are of fundamental importance to help the cell adapt to the continuous dynamic modifications of the microenvironment[5].

Although the concept that cells can interpret and respond to mechanical cues was established at the beginning of the 20th century, only in the recent years intense investigation has been devoted to elucidating the molecular mechanisms by which the cell perceives and transforms mechanical stimuli. In fact, the origins of mechanobiology can be traced back to 1917, when it was first suggested by Thompson that the shape of living organisms can reflect mechanical forces[6]. However, the research technologies to better understand the cellular and molecular mechanisms for how forces are crucial in biological processes were introduced in the 1990s, with the development of instruments capable of mechanically probing and manipulating single cells and biomolecules at forces and displacements smaller than 1 pN and 1 nm respectively[7,8].

The identification of mechanotransduction mechanisms is further complicated by the fact that cells are highly dynamic and their complex structure changes in response to mechanical forces. When cells sense a change in their net external loading, they actively alter their internal forces to counteract external forces and the balance between intracellular tension and externally applied loads is a key determinant of cell fate[9,10]. Even small changes in the magnitudes or distribution of these forces may lead to compensatory remodeling of cell-matrix and cell-cell contacts and may initiate a variety of cell behaviors[11]. Cellular behaviors that are modulated by cell-generated forces or associated changes in cell shape include growth, differentiation, apoptosis, motility, signal transduction, gene expression, chromosome movement and extracellular matrix (ECM) remodeling. Furthermore, when these same forces are transmitted across the cell surface they can influence tissue development[9].

Knowledge of these mechanotransduction mechanisms will aid in a better understanding of the physiological responses of various tissues and will also help elucidate the pathogenesis of many diseases caused by mechanical loads[4]. Ultimately, the quantification of the physical stimuli to which cells are exposed, and the identification of the triggered molecular mechanisms will be fundamental for the development of new medical therapies.

1.1.1 Mechanosensing

The human body has more than 200 different types of cells that vary in size, shape, and function. Despite the considerable differences, the ability to sense external forces is shared by most, if not all, cell types[1].

From a general perspective, the cellular response to a mechanical stimulus is based on the cascade of three main phenomena:

- Mechanoreception: first, a cell must detect the stimulus and relay the message from outside the cell (where the stimulus acts) to inside the cell (where a response will ultimately be generated).
- Signal transmission: the mechanical signal needs to be relayed within the cell to various targets throughout the cell.
- Target activation: when the signal reaches its target (usually a protein), the target is activated, causing alterations in cell behavior through a variety of molecular mechanisms[3].

On a cellular level, a mechanical stimulus generates a biochemical signal, which in turn brings about several intracellular processes (e.g.: activation of complex signaling pathways, upregulation or downregulation of gene expression, and alteration of protein synthesis), resulting in adjustment of the intracellular and extracellular environment[12]. Although intracellular signaling events triggered by external forces have been elucidated in many cell types, the primary mechanosensory for transducing mechanical input into biochemical signals remains elusive.

It is hypothesized that forces may physically alter the molecular structure or displace the position of a sensor, thereby altering/triggering chemical signal transduction events. In conjunction, mechanosensors should be located at a site where the force acts directly or can be transmitted to efficiently. As most forces act directly on the plasma membrane, the majority of the mechanosensors that have been proposed are structures on

the plasma membrane. Membrane structures that have been implicated in the role of mechanosensors in several cell types include stretch-activated ion channels, G protein-linked receptors, tyrosine kinase receptors, and integrins (Figure 1.2).
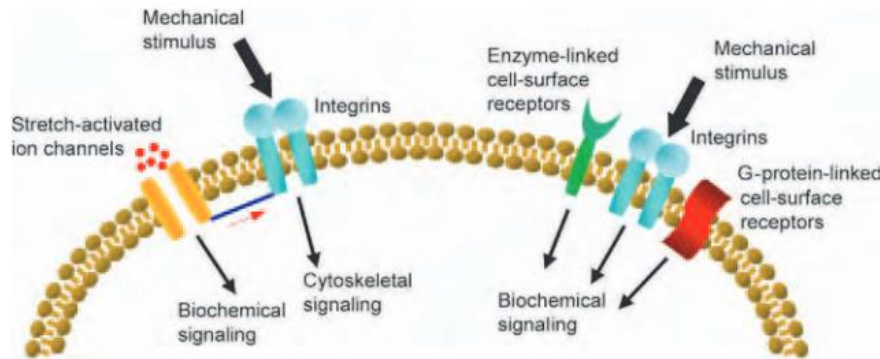
Figure 1.2: Candidate mechanoreceptors for relaying extracellular mechanical signals to the cell's interior to activate intracellular signaling pathways (from Ethier and Simmons (2007) Introductory biomechanics from cells to organisms[3]).

Of the proposed mechanosensors, integrins have been the most extensively studied, as they are transmembrane proteins that link the ECM to the cytoskeleton via focal adhesion proteins in the cytoplasm. Through the focal adhesion complex, forces applied to the plasma membrane are transferred to the cytoskeleton[13], which is then connected to the nucleus, where the mechanosensitive genes are eventually activated, leading to the ECM-integrin-cytoskeleton-nucleus axis (Figure 1.3).

In response to externally applied forces, cells actively rearrange the adhesion sites and the organization and contractile activity of the cytoskeleton and redistribute their intracellular forces to equalize the external force. The resulting change in cytoskeletal tension may convey a regulatory signal to the cell and subsequently alter its functional state. Dynamic changes in cytoskeleton organization, integrin-ECM binding, and traction forces may thus play a critical role in regulating mechanotransduction.

Alternatively, because forces applied to the plasma membrane are transferred to the cytoskeleton, it too could act as a mechanosensor[5,14]. Cytoskeleton filaments are anchored in the plasma membrane at several sites, in association with: focal adhesions, intercellular adhesion proteins, integral membrane proteins, and the nuclear membrane[15]. Through the cytoskeleton, the cell generates an internal tension on the extracellular matrix[16]. This internal tension produces forces on the adhesion sites of the

cell, which balance external forces, leading to a mechanical equilibrium resembling architectural tensegrity[17,18].

Furthermore, the cytoskeleton also binds to stretch-activated ion channels and cell-surface receptor proteins, whose conformation may be altered by physical deformation of the membrane, leading to their activation or inactivation[19].
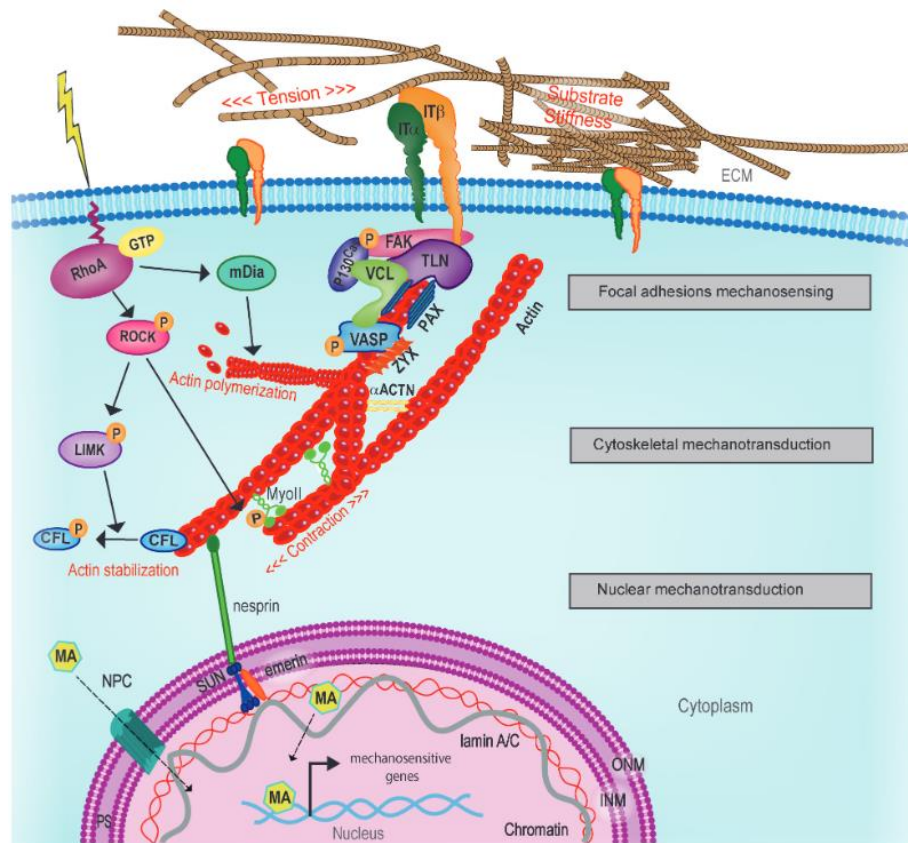
Figure 1.3: Schematic representation of cellular mechanotransduction layers (from Martino et al. (2018), Cellular Mechanotransduction[5]).

Although the stress transmission pathway is shared, different responses may be determined by the nature of the association between cytoskeleton and mechanotransducers at the different locations in the cell and possibly also by transducers that are independent of the cytoskeleton[15]. Interestingly, evidence suggests that integrins also regulate mechanotransduction via biochemical signaling[20].

Finally, it should be noted that all the candidate mechanosensors mentioned have a high degree of association with one another. Forces acting on one region of the cell surface are also transmitted by the cytoskeleton to other locations where signaling can occur, such as focal adhesions at the cell-ECM interface, cell-cell junctions, the nuclear membrane (Figure 1.4). It is therefore likely that forces may be transduced

to biological signals through interactions of several activated mechanoreceptors.

Such "decentralized model" was first proposed by Davies to describe endothelial cell responses to mechanical stresses and is applicable to mechanically induced responses in other cell types[15,21].

Since this thesis mainly deals with techniques and tools for investigating mechanotransduction phenomena occurring cardiac tissue and bone tissue, the following sections will briefly introduce the properties and stimuli of these two types of biological tissues.
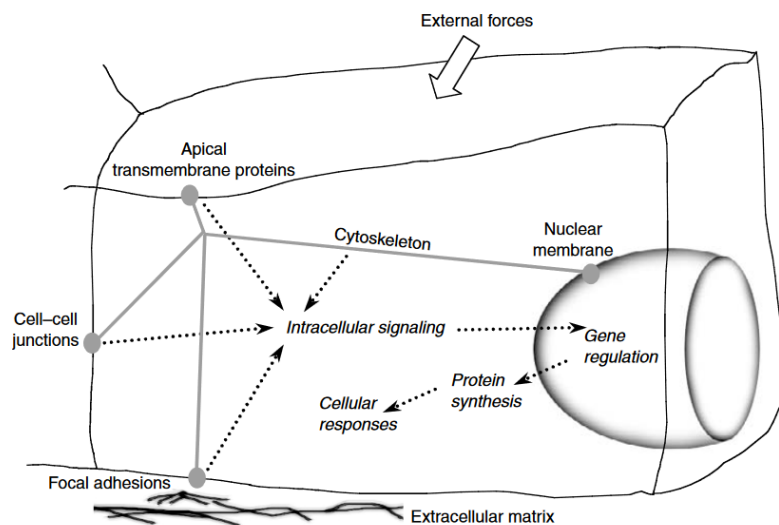
Figure 1.4: Model of initiation of signal transduction in cells in response to external forces (from Bronzino and Peterson (2006) Tissue Engineering and Artificial Organs[10]).

1.1.2 Electromechanical properties and physical stimuli of cardiac tissue

The heart is a dynamic electromechanical system, where the myocardial tissue is subjected to cyclic stresses from very early development, without pause, for a person's entire life. The bulk of the heart tissue is the contractile myocardium, a structure with asymmetrical and helical architecture, composed of tightly packed rod-shaped myocytes forming fibers and fibroblasts, with dense supporting vasculature and collagen-based ECM[22]. Myocardial structure experiences both active stretching during filling and self-generated mechanical force during ejection. In addition, consistent portions are subjected to fluid shear stress either pulsatile, oscillatory, or even turbulent. In details, in a healthy human heart, pressure during one cardiac cycle ranges between 10 and 120 mmHg for the left ventricle and between 5 and 30 mmHg for the right ventricle[23]. Local mechanical loads

can reach 50 kPa, with 22.9% longitudinal and 59.2% radial mean strain[24]. Active contraction loads measured on isolated human cardiac strips were evaluated between 14 and 23 kPa[25,26].

As cardiomyocytes (CMs), the contractile cells comprising heart muscle, contract rhythmically, the stresses and strains that these cells experience are very sensitive both to the mechanical properties of the surrounding tissue and to the rheological properties of the blood being pumped[27]. Healthy myocardium has a Young's modulus E evaluated in the range 10–15 kPa by atomic force microscopy measurements whereas fibrotic tissue is notably stiffer ($E \sim 20$–100 kPa)[28].

The mechanical properties of myocardium are determined by both the properties of the cells and of the ECM. Inside the CMs, the active contractile force is generated in the sarcomeres, the basic contractile units of cardiac muscle, by the interaction of the actin and myosin filaments (Figure 1.5). The passive mechanical properties are primarily determined by the intracellular protein titin, a large elastic protein that constitute the interconnections between the sarcomeres[29]. The ECM, whose synthesis and degradation is regulated by fibroblasts, is composed of structural proteins such as collagen and elastin as well as non-structural proteins such as proteoglycans, proteases, and growth factors[30].
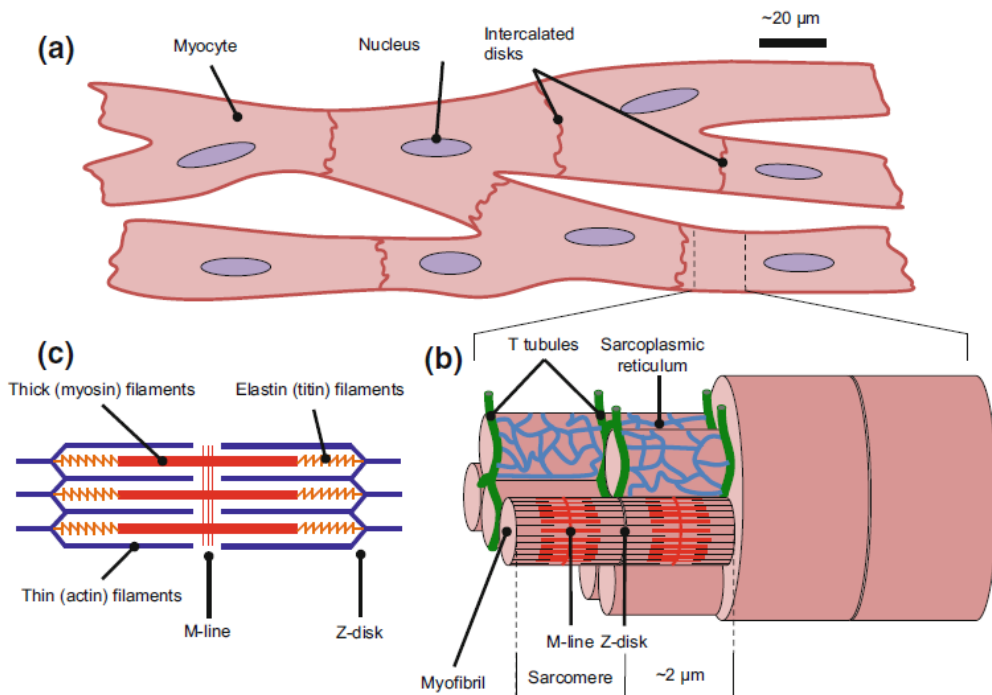
Figure 1.5: Structure of cardiac tissue and myocytes. a. Arrangement of cardiac myocytes and connections between them. b. Internal structure of a cardiomyocyte. c Diagram showing the contractile apparatus within a myofibril (from Hoskins et al. (2017) Cardiovascular Biomechanics[31]).

7

CMs are electrically excitable cells, *in vivo* the mechanical contraction of myocardium is initiated and synchronized by electrical excitation that originates in the sinus node. About 1% of CMs in the heart constitute the pacemaker cells, which are responsible for generating electrical impulses or action potentials that maintain the electrical connectivity across the tissue.

Endogenously produced pulsatile electrical field has amplitude of 0.1-10 V/cm and pulse duration of 1-2 ms[32]. Typically, the resting rate in adults is 60-100 beats per minute (bpm), corresponding to 1-1.7 Hz.

Cardiac tissue is surrounded by highly conductive extracellular fluid (3-12 mS/cm)[33]. Coordinated contraction and rhythm maintenance are controlled by the network of interconnected CMs, which communicate via gap junctions between neighboring cells and though voltage gated ion channels that control internal and external ion levels. Electrical impulse propagation is regulated primarily through gap junctions (in particular the family named connexins), which synchronize action potentials between cells and play an important role in the development of regular synchronous contractions[34]. Voltage gated ion channels are important regulators of the pacemaker mechanisms and also contribute to atrio-ventricular impulse conduction[35]. Electrical excitation of CMs is converted into movement through excitation-contraction coupling, a series of intracellular processes involving regulation of cytosolic calcium and cycling of actomyosin cross-bridges[36,37].

The development and maturation of CMs is driven by the balance between extrinsic and intrinsic mechanical loads that regulate protein synthesis, sarcomere assembly, cell size, contractile activity, and interactions with other cells and the ECM[36,38]. Changes in flow, shear stress, and cell shape, as well as ECM remodeling, all greatly influence the cardiac developmental process. As a response of continual exercise, myocardium remodels undergoing hypertrophy. However, improper mechanical signaling from surrounding tissue can lead to the development of defects, as in the case of pathological hypertrophy, which is characterized by an increase in fibronectin and collagen deposition, ultimately leading to fibrosis and myocardial stiffening[26,39].

Several proteins have been proposed as key mechanosensors and mechanotransducers, able to directly sense and respond to mechanical loads, triggering various cellular processes such as regulation of electrophysiology via stretch-sensitive channels, contractile function, calcium regulation, myocardial fibrosis, and the downstream effect of

cardiac muscle growth via hypertrophy and atrophy. As they constitute the primary site for force generation, proteins composing the sarcomere and its connections to the cytoskeleton have been identified as main mechanotransducers, since the generated forces are transmitted both longitudinally and laterally to the cell sarcolemma. Also the intercalated discs, which maintain mechanical and electric coupling between CMs are possible key sites for mechanotransduction, as well as transmembrane proteins coupling the cytoskeleton to the ECM (e.g.: integrins)[40].

1.1.3 Mechanical properties and physical stimuli of bone tissue

Mechanotransduction is a critical determinant of new bone formation, repair and regeneration, and adaptation of the skeleton to its external environment. Wolff first postulated that bone is a dynamic entity and that its internal structure can be influenced by and adapt to its surrounding environment in order to meet varying physical demands[41]. Bones *in vivo* are stressed by direct physical loading during normal activities which derives from external forces and from the pull of contracting muscles. These generate a complex distribution of stresses, as bone is subjected to tension, compression, torsion, shear and bending[42]. Under unloading conditions, bone mass is rapidly lost, as observed in consequence of bed rest or in astronauts after long duration space flights.

Strains resulting from habitual activity, which are sufficient to maintain bone structure, hardly exceed 400 $\mu\varepsilon$ (0.04%) and vigorous exercise can induce bone strains up to 1000-2000 $\mu\varepsilon$ (0.1-0.2 %)[43]. The elastic moduli of human bone tissue normally range between 1 and 20 GPa, with significant difference between trabecular ($E \sim 2$ GPa) and cortical bone ($E \sim 14$-18 GPa), which also exhibit different tensile strength (10-100 MPa for trabecular bone, 50-150 MPa for cortical bone)[44].

Despite its apparent rigidity, bone can withstand physical loading as it is a flexible material characterized by viscoelastic behavior[45]. In fact, bone is a porous and hydrated tissue, in which cells are distributed throughout its volume and connected to each other through porosities of the ECM.

Osteoblasts, which produce bone matrix, are found on bone surfaces along with bone-lining cells. Osteocytes lie in lacunae in the mineralized bone ECM, their dendrites pass through small channels called canaliculi and connect to each other and to bone surface cells via gap junctions[46]. This intricated system is collectively called the lacuno-canalicular network. In the lacuno-canalicular network, osteocytes are surrounded by the

interstitial fluid. Loading and unloading of the bone originates mechanical strains to the ECM and pressure gradients that cause oscillating fluid flow in the lacuno-canalicular system[12] (Figure 1.6).
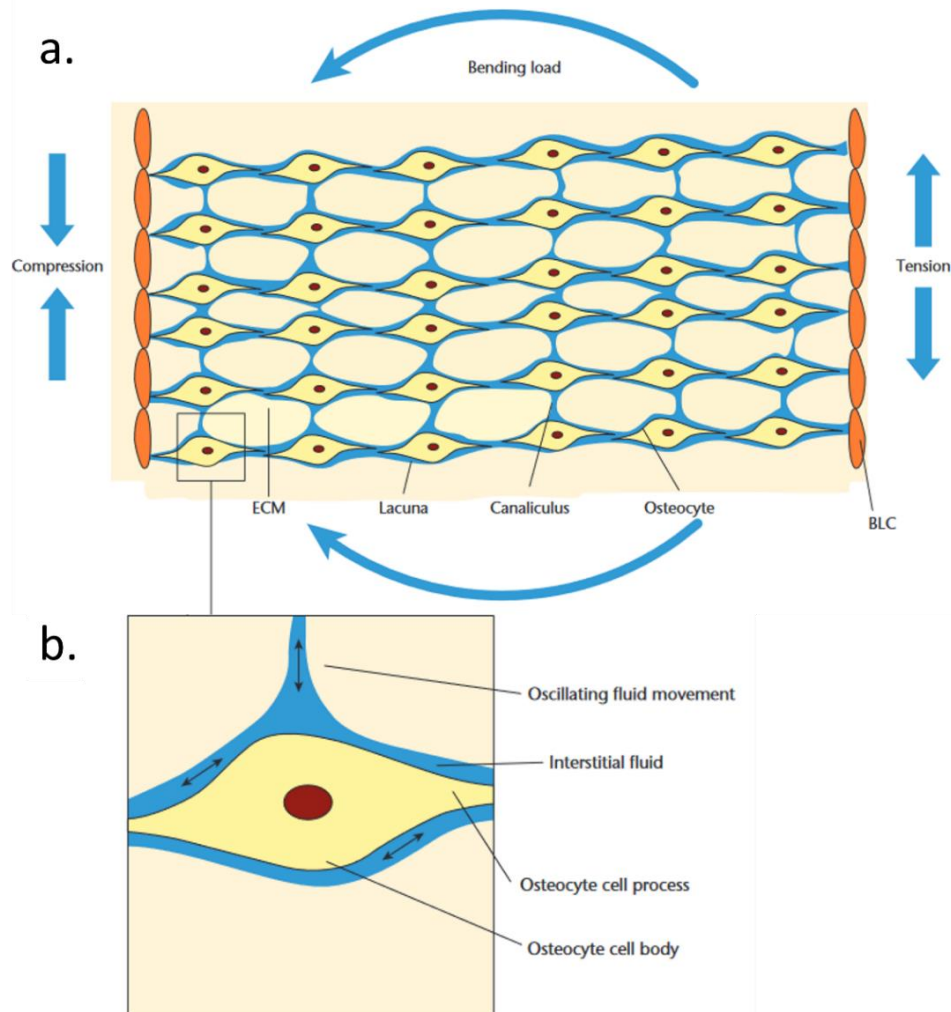
Figure 1.6: Bone cellular architecture. a. Mechanical loading of bone is transmitted to the lacuno-canalicular network. b. induced interstitial fluid flow within the lacuna-canalicular network. BLC, bone lining cell; (adapted from Stewart et al. (2020) Bone & Joint Research[12]).

The interstitial fluid acts as the medium through which stresses act on the osteocytes, as its oscillating flow exerts shear stress on the cell membranes, which is estimated between 0.8 and 3 Pa[47]. Through this mechanocoupling mechanisms, mechanical loading is transmitted to the cell in form of fluid shear stresses, which are detected by the cell mechanosensors.

However, despite the development of several fluid transport models in bone[46,48], the overall mechanism is not fully elicited. Paradoxical results are obtained when comparing tissue-level strains *in vivo*, which rarely exceed 0.2%, to the strains necessary to elicit biochemical responses *in vitro* (>0.5%). Moreover, *in vitro* experiments reported the positive effects of fluid shear

stress at much lower values (1-100 mPa) with respect to the ones estimated *in vivo*[49]. One possible explanation is that most *in vitro* systems (e.g.: flow chambers) do not replicate the *in vivo* stimulation: a uniform fluid shear stress in a flow chamber is more likely to deform the soft cell body, while *in vivo* is much more likely to stimulate the osteocyte processes in the canaliculi[46].

Furthermore, interstitial fluid flow is not the only medium for mechanocoupling in bone. Although mechanocoupling physiology has been researched most extensively in osteocytes, other cells also play a pivotal role. In detail, whereas osteocytes are mostly responsive to fluid flow, deformation of osteoblasts leading to mechanotransduction has been shown to occur in the presence of stretch[12].

In vivo, bone cells are also exposed to another type of physical stimulation: in fact, bone is piezoelectric material[50]. Application of a mechanical load results in the generation of electrical potentials, with amplitude dependent upon the magnitude and rate of deformation and polarity determined by the direction of bending[51]. This behavior is due both to the properties of the ECM and to the streaming potentials generated inside the cells in response to mechanical loading[52]. Bone resorption and bone formation are activated by electrical potential via pathways related to the activation of voltage gated calcium channel or release of intracellular calcium[53]. The discovery of the electrical nature of bone osteogenesis has led to the development and investigation of techniques for applying electrical fields to fracture sites to promote healing[54]. Among these, pulsed electromagnetic field (PEMF), has been successfully applied in the clinic for the treatment of non-union fractures, also thanks to its non-invasiveness. However, despite its clinical use and the demonstrated positive effects in terms of bone cell proliferation, differentiation, and ECM protein expression, a complete understanding of the biological mechanisms induced by PEMF is yet missing[55].

1.2 Bioreactors as advanced *in vitro* models

The ability of cells to sense and react to physical stimuli determines tissue development *in vivo*. Most tissues function under specific biomechanical environments and deranged tissue response to mechanical stimuli is implicated in a wide range of diseases and disorders. The study of mechanotransduction is therefore vital for translating the latest basic

scientific understanding into clinically useful therapies. Up to now, cell-level approaches have provide a consistent knowledge base about the main mechanisms, but to understand the complex mechanisms of mechanotransduction there is the need to overcome this approach and build research platforms enabling the analysis at the tissue level[56].

In this view, tissue engineering is an interdisciplinary field of research which aims to bridge this gap by developing and maintaining live tissues *in vitro*. Engineered tissues could serve as model systems, offering the opportunity to isolate controllable factors, ultimately facilitating the analysis of structure-function relationships in normal and pathological conditions and enabling basic understanding of tissue remodeling mechanisms[56–58].

Although these three-dimensional (3D) *in vitro* tissue models are necessarily a simplification of the more complex native tissue, they can recapitulate a subset of relevant physiological functions for the tissue of interest and be used to investigate specific tissue response to external or internal stimuli[59]. In this perspective, they could constitute a viable alternative to *in vivo* experiments and to traditional two-dimensional (2D) cell culture assays in early-stage research aimed at investigating the efficacy, safety, and mode of action of therapeutic agents[60]. In fact, the reliability of animal models is limited because different species often respond differently to treatments or compounds, while 2D in vitro models often give false predictions due to the oversimplified cell environment[61].

To develop biomimetic and functional substitutes, tissue engineering needs to replicate the complex interplay of three fundamental elements of the native tissue: cells, ECM and physical stimuli. In a typical approach, 3D tissue structures are generated by seeding cells inside porous biomimetic scaffolds, which provide the template for tissue development and degrade or are resorbed at defined rates. The enabling technology which contributes to complete the triad is the bioreactor.

Bioreactors are devices in which biological processes develop under closely monitored and accurately controlled environmental and operating conditions[62]. When properly designed, bioreactors can provide a 3D culture environment with suitable mass transport and chemical and physical stimuli, mimicking the physiological native conditions[63,64]. In general, the functions that need to be performed by a bioreactor for tissue engineering can be summarized as follows:

- providing uniform cell distribution;
- maintaining the desired concentration of gases and nutrients in the medium;
- providing mass transport to the cultured cells/tissues;
- exposing the cells/tissues to physical stimuli;
- providing information about the cell development or about 3D tissue formation.

The design and manufacturing of a tissue-specific bioreactor is therefore a demanding task requiring multidisciplinary team effort. In fact, it presupposes thorough knowledge of anatomical and functional characteristics of the target tissue, together with deep technical background related to the numerous engineering parameters involved, which include material design, mass transfer, mechanical stimulation, and electrical stimulation[65] (Figure 1.7).
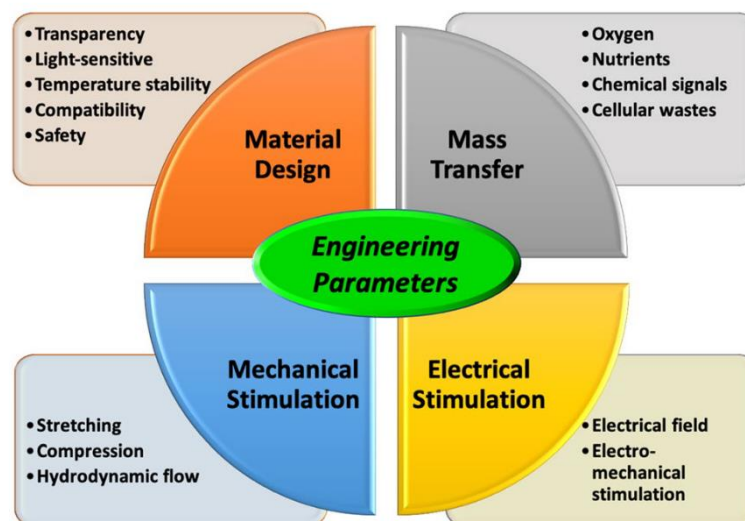
Figure 1.7: Engineering parameters for bioreactor design (from Lim et al. (2022) Bio-Design and Manufacturing[65]).

Firstly, an important aspect to consider when designing a bioreactor is the appropriate material for constructing the device. This must be biocompatible, non-leachable, non-degradable, non-porous, and easily sterilized. As the most used way of sterilization in cell culture labs is the steam autoclave, sterilizability of the material usually brings in the requirement of stability at appropriate temperatures. To allow rapid and cost-effective prototyping, the material also need to be compatible with standard manufacturing techniques. Moreover, since the bioreactor should enable to deliver physical stimulation to the cultured tissue and to analyze

the outcome of the experiment, it has to be considered whether the material needs to be transparent or light sensitive.

In a bioreactor system, mass transfer is of paramount importance. Tissue engineering constructs often lack a vascular network, and this is a considerable limiting factor in maintaining cell survival. In static culture, the construct is commonly submerged in the culture medium and nutrient and oxygen delivery to the construct occur by diffusion, as well as the removal of metabolic waste. This limits the thickness of cultured tissue to about 100-200 μm[66]. Cells in the center of a construct with clinically relevant thickness (~ 0.1 - 1 cm) die because of oxygen diffusional limitations and buildup of metabolic waste[67]. Therefore, bioreactors should incorporate elements and components that facilitate efficient mass transfer. Widely established solutions are based on convection of the culture media, either induced by stirring elements located inside the culture chamber, or using pumps and tubing to build a hydraulic circuit for medium recirculation[68].

As previously stated, the key function of a bioreactor is to replicate the physical cues to which the tissue is subjected in its native environment. These include a variety of mechanical forces such as stretching, compression and fluid shear stresses and electrical stimuli in form of time-varying electrical fields and currents. For the development of clinically relevant and translational *in vitro* models, tissue-specific physical cues must be provided by the bioreactor system. In this regard, bioreactors need to be able to provide different regimes of mechanical and electrical conditioning, to enable the possibility of running series of hypothesis-driven experiments aimed at elucidating the mechanisms of downstream processes of cellular responses. As it happens for the *in vivo* environment, inside the bioreactor it is the interplay of forces and signals inside a bioreactor that drives tissue maturation, therefore the design of its components has always to be conceived by looking at the whole picture. As an example, the removal of waste by convection of the culture media also stimulates the cells by means of hydrodynamic shear stresses. This complexity brings about the need to use computer-aided design (CAD) tools and modelling tools such as computational fluid dynamics (CFD) or Multiphysics modelling when designing a bioreactor.

To carry on these functions in an automated and replicable way, bioreactors need to accurately control the biophysical cues delivered and comprehensively monitor the environmental factors *in vitro* by using biosensors.

Given all the requirements described, and considering the tissue-specificity, bioreactors are conceived as systems and notably different architecture have been built for the various applications of tissue engineering. Anyway, modern advanced bioreactors share a common architectural setting, which is based on the following subsystems (Figure 1.8):

- the culture chamber, where cell/tissue constructs are housed in a sterile and closed vessel;
- the recirculation/perfusion system, assuring medium replacement and/or optimized cell and/or nutrient distribution within the 3D environment;
- the physical stimulation system, delivering physical stimuli mimicking the native physiological/pathological conditions;
- monitoring system, enabling real time, automatic monitoring of culture and construct parameters (i.e., temperature, pH, biochemical gradients, gas concentrations, pressure, physical stresses, waste removal, etc.) within the culture chamber;
- control system, providing real time, automatic control of culture parameters (i.e., temperature, pH, biochemical gradients, gas concentrations, pressure, physical stresses, waste removal, etc.) within the culture chamber.
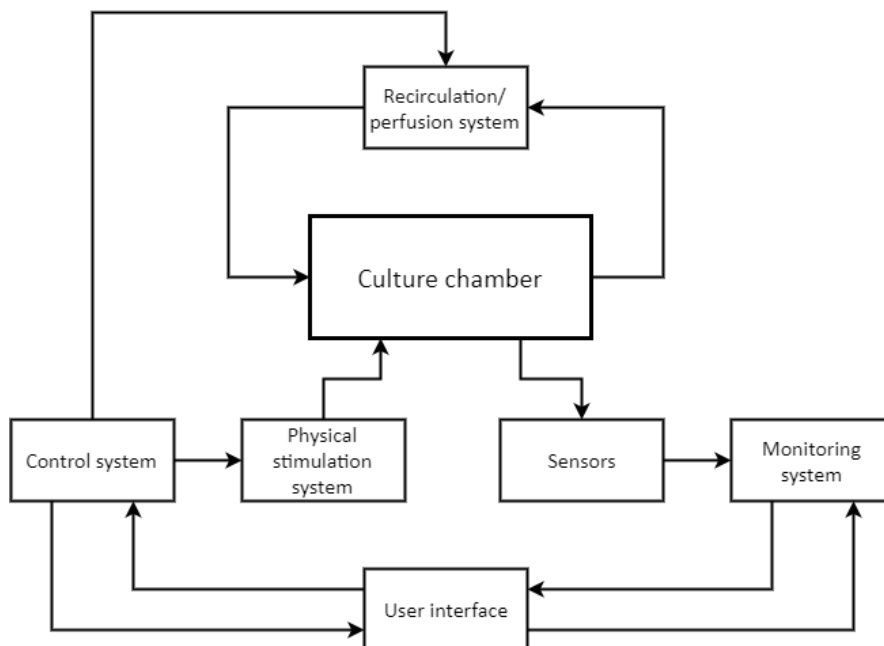
Figure 1.8: block diagram of bioreactor subsystems and their relations.

Well-designed bioreactors can provide the technological means to perform controlled studies aimed at understanding which specific biological, chemical, or physical parameter plays which function in engineering a defined tissue.

As the scope of this thesis mainly concerns *in vitro* models of cardiac and bone tissue, the following sections will briefly detail the most common solution for the 3D cell culture of these tissues.

1.2.1 Bioreactors for cardiac tissue engineering

Functional substitutes of myocardium should propagate electrical impulses and respond to these impulses by synchronized contractions. This inner complexity of cardiac tissue makes the fulfillment of a reliable *in vitro* model highly challenging, as the cultured cardiomyocytes should mature into an interconnected syncytium. Moreover, adult CMs are highly sensitive cells that quickly dedifferentiate in the absence of physical cues and the maintenance of their differentiation *in vitro* is still an open issue[26].

Physiologic-like bioreactors for cardiac tissue engineering (CTE) rely on the use of components to deliver electrical and mechanical stimuli to the culture construct, either in combination or individually.

As specifically concerns mechanical cues, dynamic stretch mimics the cyclic filling of the ventricles with blood during diastole and has been identified as the most relevant type of mechanical stimulation. This has led to the development of bioreactors, providing mechanical stretch to tissue patches or stretchable scaffolds, including some devices resulting from research conducted in this group[34,69–71]. Several solutions are commercially available, such as those developed by Flexcell, Bose, CellScale or Ion Optix. Moreover, the emergence of open-source and low-cost electronics and of 3D printing technologies has considerably boosted the development of custom-made bioreactors providing *in vitro* mechanical stretch for CTE[69,72–74]. Even before the introduction of these prototyping techniques, a variety of bioreactors had been developed to cyclically stretch 3D cardiac tissues[75,76]. One of the first bioreactors to achieve functional improvement of cardiac tissues with stretch was developed by the Eschenhagen group[77]. Their pioneering approach consisted in the casting of ring-shaped rat cardiac engineered tissues, which were submitted to unidirectional cyclic stretch (10% strain, 2 Hz), resulting in the development of a construct characterized by longitudinally oriented cell bundles, with morphological features of adult tissue[78]. Although the contractile force was still much lower than that

of the native tissue, the subsequent refining of the model brought to some impressive results, such as the successful implantation of the constructs in infarcted rat hearts[79]. The approach developed by Eschenhagen and colleagues has shown that immature cardiac cell populations can assemble into cardiac constructs, if subjected to appropriate mechanical cue during culture.

In parallel, also electrical stimulation of 3D CTE constructs has been investigated, leading to the development of systems for electrical pacing of constructs. Commonly, electrical stimulation is delivered as field stimulation, by applying a voltage between two parallel electrodes immersed in the culture medium. Commercial systems are available for electrical stimulation, and they usually consist of voltage-controlled stimulators, such as those by Grass or Ion Optix. Also in this case, conceptual lab prototypes have been developed based on open-source technologies[80,81]. In this regard, considerable insights have been provided by the Vunjak-Novakovic group. The first setup consisted of a modified cell culture dish in which the constructs were placed between two cylindrical carbon electrodes. These were contacted by platinum wires and connected to a stimulator providing rectangular voltage pulses at a physiological amplitude and frequency[82]. Electrical stimulation induced cell alignment and coupling, and promoted the establishment of gap junctions, propagation of signals and generation of action potentials that induced synchronous macroscopic contractions. Subsequent research built upon these preliminary results lead to the definition of important parameters such as electrode material, amplitude, duration, and frequency of stimulation[83]. Subsequently, electrical pacing has been coupled to passive mechanical stimuli from support structures, leading to the development of CTE constructs based on the maturation of pluripotent stem cells[84] and to the development of a translational research platform, the BioWire[85].

Aside from stretching, other methods for inducing mechanical stimulation via physical strain of the biomaterial construct have been tested. Strain can be applied as dynamic compression, which stimulates the cells in the opposite way native muscle stretches. Secondly, fluid shear stress can be applied to a construct via perfusion, which also improves mass transport. From a technical point of view, perfusion is also simpler to integrate with electrical stimulation. Different bioreactor platform combining the two stimulations have been proposed and tested, obtaining structural and functional enhancement of constructs[86,87].

Regarding combined electromechanical stimulation, a significant contribution was provided by Morgan and Black, which built a bioreactor platform mimicking isovolumic contractions and used it to study the influence of different timing between electrical and mechanical signals on the development of CTE constructs[88]. The bioreactor is based on an innovative architecture in which flexible tubing expands stretching the constructs circumferentially and provided remarkable insights on electromechanical stimulation regimes. Notably mechanical and electrical stimulation alone affected the construct similarly in the system, while combined electromechanical stimulation improved the expressions of proteins responsible for calcium handling and contractility when the two stimulations were delayed as it happens *in vivo*, while it did not when they had a synchronous start.

1.2.2 Bioreactors for bone tissue engineering

Forces applied to bone *in vivo* result in changes of hydrostatic pressure, direct cell strain, fluid shear stress, and electric fields. The accurate recapitulation of these mechanisms is fundamental for the formation of mature bone tissue substitutes *in vitro*[89].

Historically, the first challenge faced by bioreactors developed for bone tissue engineering (BTE) has been to ensure adequate mass transport to maintain 3D constructs of relevant size. At first, viability of constructs was ensured with the help of systems based on agitation of the culture medium in which the culture constructs are immersed. A basic bioreactor used for this function is the spinner flask bioreactor, which provides mixing of the medium using a stir bar or an impeller[57]. Another notable example is the rotating wall vessel, originally developed by the NASA to simulate microgravity[90], which reduces diffusional limitations of nutrients and waste products and ensures low levels of shear stress generated by the laminar flow[91]. However, for both these systems the presence of a free volume around the constructs limited the efficiency of fluid transport towards the inside of the constructs.

The incomplete overcoming of the diffusional limitations by these systems brought about the introduction of perfusion bioreactors, systems based on a hydraulic circuit made of a pump and tubing, which recirculates the medium and enables its passage through the culture chamber where the construct is placed[47,57,91]. These systems are classified as indirect or direct perfusion bioreactors, depending on whether the culture medium is

perfused around or throughout the cell/scaffold constructs. Understandably, direct perfusion bioreactors have been consistently adopted as systems for BTE, since they improve mass transfer both at the construct periphery and within its internal pores and subject the constructs to flow-induced shear stress that can mimic the *in vivo* stimulation caused by interstitial fluid flow on osteocytes. Moreover, oscillating perfusion can be used as an effective method to improve cell seeding efficiency and uniformity in 3D scaffolds[92]. This idea was at the base of the design of bioreactors systems that subsequently became commercially available solutions such as the U-Cup by Cellec and the P3D by Ebers. The possibility to use direct perfusion to deliver flow-induced shear stress via perfusion bioreactors has been exploited thanks to the development of different system architectures that allow to deliver unidirectional, pulsatile or bidirectional flow[93]. Considerable differences have been reported in the results obtained with different systems and perfusion strategies. Anyway, direct perfusion bioreactors in general have been shown to enhance cell density in the scaffold center, cell proliferation and differentiation of osteoprogenitor cells, as well as the deposition of mineralized ECM[91].

The design of BTE bioreactors has also considered the possibility to condition the construct by the application of mechanical strain. In principle, perfusion bioreactors can also achieve this goal by applying dynamic hydraulic pressure on the constructs. Besides this approach, other architectures have been considered. The first bioreactor of this kind actually evolved machines originally fabricated for material testing, which were subsequently optimized for BTE[91]. One example is constituted by compression bioreactors, which consist of a motor, a system providing linear motion and one or more pistons applying static or dynamic compressive loads directly to the constructs[47]. Mechanical compression systems have also been combined with perfusion circuit to develop bioreactors system with combined stimulation[94]. Other strategies adopted for applying mechanical load to BTE constructs include the uniaxial cyclic stretch of deformable supports or bending of flexible scaffolds[91].

The electrical stimuli characterizing the *in vivo* environment have also been replicated *in vitro* as strategies to optimize the outcomes in BTE systems or to study the effects of such stimuli on cell behavior[95]. Similarly to what has been done in CTE, electrical stimulation has been applied in BTE by using electrodes in direct contact with the culture medium. In most of the studies constructs were stimulated with direct current, which for

electric field amplitudes of 100-200 mV/mm resulted in improved mineralization and osteogenic differentiation of stem cells[54]. However, the application of this stimulation has the significant drawback of the generation of high quantities of cytotoxic byproducts, which limit the duration of experiments and require the need of a perfusion system. Another way of inducing electrical fields in the constructs is through the use of PEMF stimulation which, as previously mentioned, is used in clinic for the treatment of non-union fractures. PEMF-based bioreactors consisting of multi-well plates positioned between two Helmholtz coil have been used for the investigation of stimulation of parameters on BTE constructs, with reported results of increased osteogenic differentiation and proliferation of osteoprogenitor cells[96–98].

1.3 Characterization of substrates

In functional living tissues, physical signals acting on the cells are mediated by the surrounding ECM, to which cells bind by establishing focal adhesions. *In vitro*, cells adhere to the substrate where they are seeded (either a porous scaffold or a planar patch) through the same kind of interactions. To develop reliable *in vitro* models, scaffolds should not only provide support and physiological chemical stimuli to the cells, but also exhibit a similar physical behavior with respect to the native tissue. In particular, the structure and composition of the substrate play a major role in the application and transmission of mechanical loads and impact significantly on mass transport phenomena. Characterizing the properties of the target biological tissue and of the scaffold used to mimic it is crucial for the development of reliable *in vitro* models in tissue engineering.

Concerning structural mechanical properties, cells not only react to externally applied loads via mechanotransduction pathways, but also actively exert forces on the ECM. Through focal adhesions, cells anchor and pull on the surrounding environment, probing its stiffness[99]. This mechanism is fundamental for anchorage-dependent cells, for which the ability to sense the substrate is essential for cell survival and proliferation. Several studies have demonstrated the effects of substrate stiffness on cell growth, differentiation, migration and alteration of functional properties[28,99,100]. This aspect must therefore be considered when developing a new scaffold for tissue engineering. Several techniques are available for characterizing biological tissues and scaffolds mechanical properties, such

as uni- or bi-axial tensile testing, compressive testing or nanoindentation. Although biological soft tissues are often not suitable for testing with conventional machinery, research in tissue biomechanics is an active field which in the recent years is bringing about a consistent optimization of testing techniques to allow the characterization of these tissues[101–104].

In parallel, tissue microstructure has a considerable impact on transport phenomena, which drive the delivery of oxygen and nutrients to the cells and the removal of waste substances. A must-have requirement for a biomimetic scaffold is therefore to have an interconnected porous structure ensuring adequate transport of nutrients to its core, thus guaranteeing cell survival inside its whole volume. Pore size, geometry, and 3D distribution shape the flow inside the scaffold, with significant effects on cell attachment, proliferation and differentiation[105]. The characterization of transport phenomena inside tissues and scaffold is fundamental for achieving accurate recapitulation of the *in vivo* stimuli in *in vitro* models. Despite some geometrical parameters such as porosity or mean pore size can be measured quite easily, the use of these quantities to characterize transport phenomena is questionable, as they are not directly related to transport phenomena in a unique way[106]. Not necessarily a more porous scaffold performs better than one with lower porosity, while scaffolds with the same porosity might yield different results when used in cell culture. Recent advancements in additive manufacturing technologies offer the possibility to design scaffolds characterized by a fine, detailed and repeatable microarchitecture[107]. However, this does not represent a solution to the problem, but rather justifies the need for the evaluation of transport phenomena in view of a proper optimization of scaffold design.

In this term, permeability has been identified as a macroscale property that can allow a detailed and comprehensive evaluation of transport phenomena occurring inside the tissue or scaffold considered. Permeability affects the magnitude of pressure and shear stresses inside scaffolds, the principal triggers of cell mechanotransduction. Due to these aspects, significant effort has been put towards the development of technologies and protocols to determine biological tissues and scaffolds permeability[106]. However, most of the technologies so far are tissue specific and at basic research level. Differently from mechanical characterization with testing machines, the measure of permeability in biological tissues is not standardized. Widely accepted protocols are still missing and the proposed methods lack metrological rigorousness[106,108].

The development of a versatile test bench for permeability measurements on biological soft and hard tissues is still an open issue and constitutes one of the objectives of this thesis. Details on the development of such a system are detailed in Chapter 4, where an overview of significant setups developed for measuring permeability in biological tissues will be detailed.

1.4 Research outline

There is a consistent body of literature recognizing the pivotal role played by mechanotransduction in the development and maintenance of functional living tissues *in vivo* and the need for the precise recapitulation of physical cues in view of developing reliable and robust *in vitro* models. However, much uncertainty still exists about the exact mechanisms driving cellular response to external stimuli.

The generalizability of much published research on this issue is problematic, due to the substantial differences in the developed approaches and the unsolved limitations. Commonly, *in vitro* models recapitulate a small subset of physical cues with limited accuracy, falling short of faithfully replicating *in vivo*-like conditions. In parallel, testing tools and machinery were developed for materials and substrates used in the industrial sector and are not easily adaptable for testing biological tissues and substrates.

These shortcomings bring about the need for the development of different technological platforms:

- devices enabling *in vitro* dynamic culture of engineered tissues under the application of tunable physical stimuli;
- test benches providing the means for characterizing physical properties of biological tissues and scaffolds.

The development of such technologies constitutes the research topic of this thesis. This dissertation will introduce new technologies developed to advance the ongoing research in mechanobiology, discuss their advantages and limitations, and suggest future perspectives for the use and further development of such technologies.

1.4.1 Thesis objectives

The objectives of this thesis project can be summarized as follows:

1. to design, develop and test a versatile and compact system for studying the effect of different protocols of electrical stimulation on cardiomyocytes *in vitro*.

2. to design, develop and validate a novel automated perfusion bioreactor that allows culturing 3D constructs under tunable perfusion and that can be combined with PEMF stimulators.

3. to design, develop and validate a versatile test bench for the measurement of biological tissues and scaffolds permeability.

To comprehensively address all the objectives, the overall structure of the dissertation is subdivided in chapters, which will cover the manifold aspect of the conducted research as follows:

Chapter 2 – Versatile Electrical Stimulator for Cardiac Tissue Engineering Investigations

Among the native-like stimuli applied in vitro for generating functional *in vitro* cardiac tissue models, pulsatile electrical stimulation plays a crucial role in promoting and supporting cardiac maturation and functionality. In this view, this chapter describes the design, development, and validation of a versatile electrical stimulator for cardiac tissue engineering, named ELETTRA. The most significant advantage and novelty of ELETTRA is the possibility to program up to 3 independent channels to provide electrical stimuli to several sets of culture chambers in parallel and to provide this at a competitive cost with respect to currently available technologies. The stimulator was developed interfacing an open-source electronics board with custom-designed printed circuit boards. Culture chambers to use the stimulator in biological tests were designed using CAD software and optimized based on the results of computational simulations of electric field and currents. The stimulator was validated in biological experiments aimed at investigating the effects of 3 different electrical stimulation patterns on neonatal rat cardiomyocytes functionality.

Chapter 3 – An Automated 3D-Printed Perfusion Bioreactor Combinable with Pulsed Electromagnetic Field Stimulators for Bone Tissue Investigations

In this chapter, a novel automated bioreactor providing tunable perfusion and combinable with pulsed electromagnetic field (PEMF) stimulators for bone tissue investigations is described. The most significant

advantage and novelty of the proposed bioreactor is the automated perfusion control, which allows selecting uni- or bi-directional perfusion mode within the same platform and without user intervention along the culture. The chapter details the procedure of design, optimization, and validation of the bioreactor platform. Open-source hardware and 3D printing technologies were used to design and manufacture bioreactor components. Computational fluid dynamics simulations supported the culture chamber design and allowed the estimation of the shear stress values within the construct. Electromagnetic field simulations were run to evaluate the magnetic field distribution in case of combination of the bioreactor with a PEMF stimulator. The bioreactor was validated by preliminary biological tests aimed at investigating the effects of uni- and bi-directional perfusion conditions on osteogenic differentiation of the cultured 3D bone tissue models.

Chapter 4 – Permeability Test Bench for Characterizing Hard and Soft Samples for Tissue Engineering Applications

Scaffold effectiveness is strongly influenced by its microstructure and ability to be permeated by fluids and species. Several methods were proposed to characterize the permeability of hard and soft scaffolds, however defined protocols are still missing. Inspired by this context, this chapter deals with the development and preliminary validation of a test bench for determining the permeability of hard and soft biological scaffolds. Considerations of the fluid dynamics of porous media and of soft tissues mechanics guided the development of the test bench. A pump-based method for recirculating water was selected. Additive manufacturing techniques were used to build the components permeability chamber, where the sample is positioned. Pressure sensors were selected, and data acquisition and processing algorithms were developed. For validation, commercial cylindrical hard scaffolds were tested, and results were compared with those obtained with a reference test bench for hard samples.

Chapter 5 – Conclusions and Future Work

In this last chapter, concluding remarks of each section are summarized, limitations of the proposed approaches are analyzed, and suggestions for future research are given.

Chapter 2

Versatile Electrical Stimulator for Cardiac Tissue Engineering Investigations

The work described in this chapter was performed in collaboration with Antonio Sileo and Anna Marsano from Universitätsspital Basel, Basel, Switzerland.

A paper on the work presented in this chapter is under preparation for submission to:

Biotechnology & Bioengineering,

Gabetti, S., Sileo, A., Montrone, F., Putame, G., Audenino, A., Marsano, A., Massai, D., Versatile and tunable Monophasic/Biphasic Electrical Stimulator for Cardiac Tissue Engineering Investigations

Abstract

The application of physical stimuli recreating the *in vivo* environment is crucial for the *in vitro* development of functional cardiac tissues. In detail, electrical stimulation (ES) has been shown to significantly affect the functional properties of *in vitro* cultured cardiomyocytes. Currently, the available stimulators are expensive and allow limited modulation of stimulation parameters, constraining the possible analysis of the effects of different ES parameters. In this study, a tunable electrical stimulator (ELETTRA) designed for delivering ES in a stable, accurate and controlled way at a highly competitive cost is presented. Adopting a customizable electronic platform combined with free and open-source software allowed developing a versatile device combinable with different cell/tissue culture set-ups, which allows testing different stimulation patterns simultaneously while stimulating multiple samples in parallel. Customized culture chambers were designed and manufactured in view of demonstrating the performances of ELETTRA, and the electrical field developing inside was characterized with the support of computational modelling. In-house validation tests confirmed the accuracy and compliance of the ES parameters delivered by ELETTRA and its reliability during cell culture. Finally, biological experiments performed to evaluate the influence of different ES modes (monophasic or biphasic) on the *in vitro* maturation neonatal rat cardiac cells, demonstrated that monophasic ES at 5 V/cm and particularly biphasic ES at ±5 V/cm were effective in enhancing cardiac electrical functionality.

2.1 Introduction

The *in vitro* development of functional and reliable substitutes of myocardium is the main goal of cardiac tissue engineering (CTE) and can play a fundamental role for basic and pre-clinical research. Engineered *in vitro* models of heart tissue can serve as platforms to study cardiac tissue development and function in healthy and pathological conditions or to test new drugs[60,109–112]. In detail, by recapitulating a subset of relevant physiological functions, *in vitro* heart models can be used to investigate specific response to external or internal stimuli, offering the opportunity to isolate controllable factors, ultimately facilitating the analysis of structure-function relationships and enabling basic understanding of tissue remodeling mechanisms[59,113,114].

To perform this function, *in vitro* substitutes of myocardium should mature into an interconnected syncytium which manifests the functional properties of the native heart: propagate electrical impulses and respond to these impulses by synchronized contractions[115,116]. In order to achieve this result, cardiac cells in vitro need to be seeded on appropriate scaffolds which provide architectural and biochemical support[38,100,112,117] and cultured in a controlled environment which subjects them to *in vivo*-like physical stimulation[26,34,118].

Focusing on the stimuli, several bioreactors imposing dynamic mechanical stretch to tissue patches or stretchable scaffolds were developed to mimic the cyclic filling of the ventricles[69,71,77,78,119–121] and several solutions are commercially available nowadays, such as those developed by Flexcell, Bose or CellScale. Besides this approach, several studies demonstrated that in vitro electrical stimulation (ES) affects the rate, duration, and number of action potentials of CMs, increasing the percentage of spontaneously beating cells and promoting cell–cell coupling and calcium handling[82,122–124]. ES is commonly delivered to the cultured tissue as field stimulation, i.e. by the application of an electric field issued from the voltage between two parallel electrodes immersed in the culture medium[32,80,87,125]. In literature, two main ES modes have been experimented: monophasic and biphasic. Pioneering studies used monophasic ES, which is simple to generate, and demonstrated that this stimulation mode improves electrical coupling of cardiac cells, increases the production of functional Connexin 43 (Cx-43), and enhances inter-connectivity between cells[82,83]. Biphasic ES was firstly considered as a way to reduce the accumulation of by-products in the

27

culture medium resulting by faradaic reactions at the electrode-medium interfaces[32]. Preliminary comparative studies demonstrated that biphasic ES induced higher levels of maturation in neonatal rat CMs[126] and in human cardiac progenitor cells[127] with respect to monophasic ES[125,128–132]. However, apart from the two mentioned studies, a clear advantage of biphasic ES was not reported in literature and monophasic ES has been widely adopted in CTE to promote cell maturation[84,133].

To deliver monophasic or biphasic ES modes in CTE applications, different setups have been developed, mostly connecting the electrodes to commercial electrical stimulators, such as those developed by Grass (USA)[81,83,85,87,133,134] or Ion Optix (USA)[135–138] or with pacemakers[139]. However, commercial electrical stimulators are highly expensive and allow limited modulation of stimulation parameters, constraining the possible analysis of the effects of different ES parameters and ultimately hindering the adoption of ES protocols in CTE[81]. In this perspective, there is a growing need for cost-effective and versatile solutions to implement electrical stimulation for CTE applications. In the recent years, the availability of affordable open-source and low-cost electronic solutions for control purposes enabled the development of lab-made stimulators[73,80,81]. These setups however are affected by several limitations such as small ES tunability, little adaptability to different cell culture setups, and often limited versatility in terms of ES mode.

Inspired by this scenario, we developed a novel electrical stimulator (ELETTRA) designed for delivering ES in CTE applications in a stable, accurate and controlled way at a highly competitive cost. Open-source and low-cost technologies were adopted for the stimulator implementation. To demonstrate the performance of ELETTRA, customized culture chambers were designed and manufactured. Computational modelling supported the optimization of the culture chamber design, allowing the characterization of the electric field across it. Accuracy and compliance tests were performed to characterize the ES parameters delivered by ELETTRA and its reliability during cell culture. Finally, to investigate the influence of different ES modes on the *in vitro* maturation of cardiac cells, preliminary biological tests were performed on neonatal rat cardiac cells, exposed to monophasic or biphasic ES. The biological effects of the different applied ES modes were evaluated in terms of electrical functionality, expression of Cx-43 and sarcomeric α-actinin, and sarcomeric organization.

2.2 Materials and Methods

2.2.1 ELETTRA electrical stimulator

The following design requirements guided the development of the ELETTRA electrical stimulator. Firstly, it was designed for providing *in vitro* electrical stimuli in the range of the physiological pulsatile electric field experienced by human cardiac cells *in vivo* (electric field = 0.1-10.0 V/cm, resting rate = 1.0-1.7 Hz, pulse duration = 1-2 ms[32,140,141]). Moreover, inspired by several studies[83,84,87,126,127,131], ELETTRA was developed to deliver a voltage-controlled stimulation either as monophasic or as biphasic square wave pulses. With a view to reduce the number of sequential experiments and to increase the number of possible conditions to be tested simultaneously, parallelization, modularity and versatility guided the stimulator development. Lastly, ELETTRA was devised to be compact and easy to use in a cell culture laboratory following conventional Good Laboratory Practices (GLP). During the development process, an iterative optimization approach, together with low-cost manufacturing and assembly procedures, allowed progressively refining the ELETTRA features.

In detail, ELETTRA is embedded in a compact case (21 cm x 18 cm x 7 cm) and it is composed of five subsystems: 1) the control unit; 2) the waveform generation unit; 3) the dual power supply unit; 4) the monitoring unit; and 5) the user interface (Figure 2.1a). The control unit consists of an Arduino Due micro-controller board (Arduino, Italy) running a purpose–built software. The code, loaded on the microcontroller, communicates with the user interface and allows controlling multiple outputs with accurate timing. A USB port allows direct connection to the micro-controller board for possible software update, without disassembling the device. The waveform generation unit allows generating square-wave stimuli with monophasic or biphasic waveform, controllable in pulse duration (1-10 ms), voltage (0.25-12 V), and frequency (0.5-10 Hz), with maximum output current of 700 mA, for 3 independent outputs in view of stimulating multiple constructs in parallel (Table 2.1). For each output, the stimulation is obtained by sending controlled digital signals from two Arduino Due digital pins as input of a voltage divider circuit made up of a 10 kΩ digital potentiometer (MCP41010, Microchip Technologies, USA) and an operational amplifier (LM358, STMicroelectronics, Italy) configured in unity gain, and subsequently relaying the two modulated signals as input of a differential amplifier circuit with a gain of 4.7 on both channels built

with an operational amplifier (L272M, On Semiconductor, USA). The dual power supply unit is based on two DC/DC converters (TSR-3 24150, TracoPower, Switzerland) interfaced to custom-designed passive filters for converting the 18 V single supply from a standard AC/DC adapter to a balanced ±12 V dual supply, enabling the delivery of biphasic stimulations. A fan guarantees the system cooling. The electric circuits were assembled on RoHS-compliant printed circuit boards (PCBs), designed by using the open-source free software KiCAD 5.1.6 and manufactured externally (JLCPCB, China). The monitoring unit is based, for each output, on a sensing resistor (10 Ω) placed downstream of the reference electrode port and two standard connectors mounted on the stimulator frame. During stimulation, by connecting an oscilloscope to the connectors and measuring the voltage drop on the sensing resistor for each output, the user can indirectly measure the current flowing between the electrodes. The user interface is composed of a LCD display, two push buttons, and a rotary encoder that allow setting the stimulation parameters for each independent output and switching on/off the ES. During the stimulation, the elapsed time and the stimulation parameters are showed. ELETTRA can be connected to different experimental set-ups by Bayonet Neill–Concelman (BNC) sockets (Figure 2.1b). For the here adopted set-up, an output cable equipped with a splicing connector (Wago, Germany) makes possible connecting up to 6 culture chambers in parallel.

_____
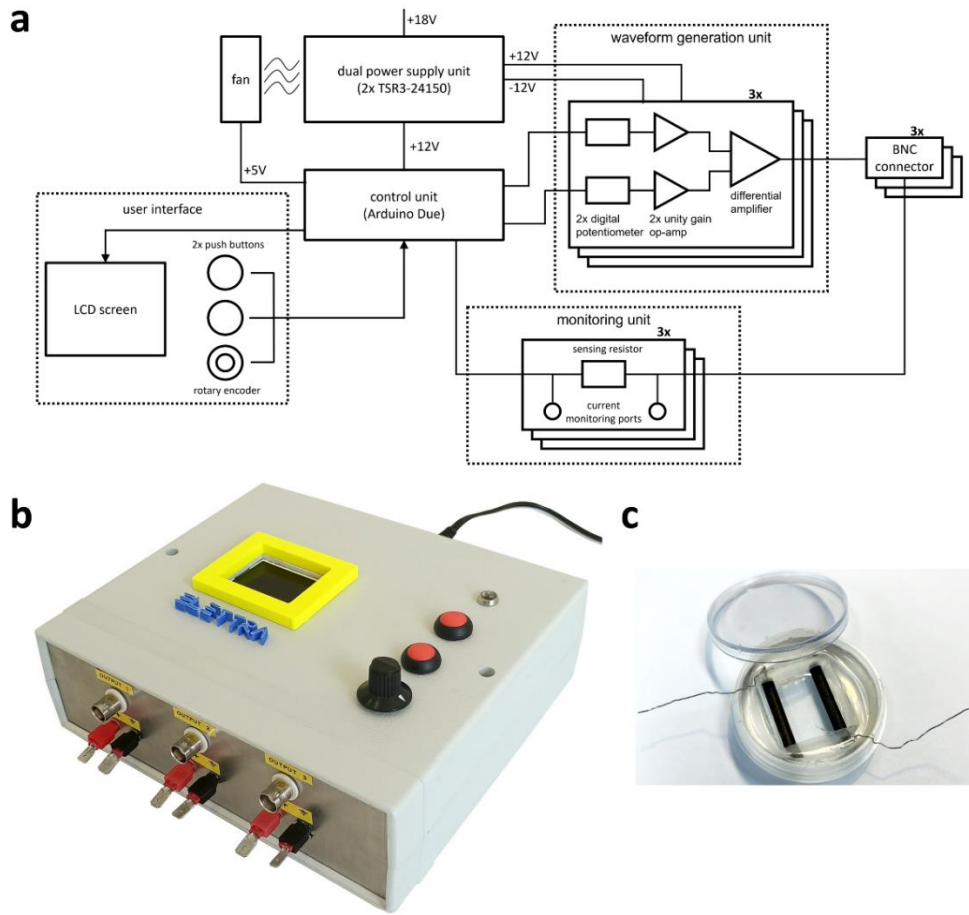
Figure 2.1. ELETTRA and culture chamber. a) schematic drawing of ELETTRA showing the relations between its subsystems and components; b) picture of the ELETTRA electrical stimulator; c) picture of the assembled culture chamber.

Table 2.1. ELETTRA stimulation parameters

Parameter	Range
Waveform type	Monophasic/Biphasic
Amplitude (V)	0.25 – 12.0
Frequency (Hz)	0.5 – 10.0
Pulse duration (ms)	1 – 10

2.2.2 Culture chambers

In view of investigating the influence of biomimetic ES on the *in vitro* maturation of cardiac cells, a set of culture chambers to be connected to ELETTRA was designed and manufactured (see Supplementary Material). Each culture chamber is based on a μ-Dish chamber (ibidi GmbH,

Germany), with diameter of 35 mm, in which a polydimethylsiloxane (PDMS, Sylgard 184, Dow Corning, USA) cylindrical structure with a central rectangular hole is press-fit inserted. Two carbon rod electrodes (length =26 mm, diameter = 3 mm; Sigma-Aldrich, Germany), linked to platinum wires (Sigma-Aldrich, Germany) to be connected to ELETTRA, are embedded in parallel within the PDMS structure at a fixed distance of 1 cm, with their facing sides exposed to air/culture medium for a length of 20 mm (Figure 2.1c). Carbon rods were selected among different electrode materials due to their properties of biocompatibility, charge transfer and resistance to corrosion[142]. The PDMS structure is autoclavable and, once sterilized, it can be press-fitted in a sterile μ-Dish chamber. Each culture chamber can house up to 4 mL of culture medium.

2.2.3 ELETTRA characterization

Lumped-parameter model

For characterizing the voltage and the current waveforms provided by ELETTRA, an equivalent lumped-parameter model of the culture chamber and of the ELETTRA waveform generation unit was developed and simulations were run (Simulink, MathWorks, USA). The culture chamber was modelled as a Simplified Randles Cell circuit[143], which is composed of three key elements: 1) the resistor R_e (resistance of the solution); 2) the resistor R_p (electrodes' resistance to corrosion); and 3) the capacitor C_p (non-ideal double layer at the electrode/electrolyte interface), with R_p and C_p put in parallel. Considering the materials and the geometry of the manufactured culture chambers, the following values were adopted: 1) R_e = 53 Ω; 2) R_p = 5.13 x 10^8 MΩ; 3) C_p = 240 μF (for details on adopted assumptions see Supplementary Material).

The ELETTRA waveform unit was modelled by its ideal equivalent circuit. The simulations were run varying the number of chambers (from 1 to 6) connected in parallel to ELETTRA and applying a monophasic waveform (voltage = 5 V, frequency = 1 Hz, pulse duration = 2 ms).

Electric field modelling

For characterizing the spatial distribution of the electric field and of the current density within the culture chamber, a finite element method (FEM) analysis was performed (Comsol Multiphysics 5.3, Comsol Inc., USA). The geometry of the culture chamber, composed of 5 sub-domains (PDMS structure; carbon rod electrodes; culture medium; polyethylene derivate

coverslip and chamber; air above the culture medium), was meshed with 1.7×10^6 tetrahedral elements and 1.7×10^5 triangular elements. Each sub-domain was assumed as a homogenous isotropic medium with respective electrical properties (Supplementary Table 2.S1). For the culture medium, 2.5 mL were modelled, and the cell monolayer was assumed as part of the culture medium volume due to its high-water content[80]. Using the Electric Currents interface in the AC/DC module, a stationary simulation was performed, solving the continuity equation in absence of distributed current sources:

$$\nabla \cdot J = \nabla \cdot (\sigma E + J_e) = 0$$

where J is the current density (A/m²), σ is the electrical conductivity (S/m), E is the electric field distribution (V/m), and J_e is the externally generated current density (A/m²), which was set to 0 in the simulation. The electric field distribution was then derived by computing the gradient of the electric potential V:

$$E = -\nabla V$$

As boundary conditions, uniform electric potentials at the external sides of the electrodes (5 V at the positive electrode, 0 V at the ground electrode) and electric insulation at the external faces of the model were imposed.

Experimental in-house tests

The ELETTRA performances in terms of compliance of delivered stimulation parameters and reliability during cell culture application were preliminary tested in-house. A culture chamber was filled with 2.5 mL of culture medium (Dulbecco's Modified Eagle Medium (DMEM), Sigma-Aldrich, USA) and was connected to ELETTRA. Each of the 3 outputs was set to deliver monophasic ES or biphasic ES (frequency = 1 Hz, pulse duration = 2 ms) varying the voltage from 1 to 12 V with steps of 1 V (from ±1 V to ±12 V for the biphasic ES). By using a digital oscilloscope (PicoScope 2204A, Pico Technologies, UK) and connecting the probe to the positive output and to the ground port of the monitoring unit on ELETTRA's chassis, the delivered voltage was measured. A second oscilloscope probe was connected to the monitoring ports of ELETTRA to measure the voltage drop across the sensing resistor. For both measurements, 10 consecutive pulses were recorded. Recorded values were compared with the nominal voltage value set on ELETTRA. The percentage errors of measured values

with respect to nominal values were calculated as the mean of the differences between the imposed voltage and the measured voltage, and were expressed as mean ± standard deviation (SD). The current waveforms were extracted by dividing the voltage drop on the sensing resistor by its resistance value. For each test, the current peak was extracted and its mean and SD were calculated. Subsequently, the reliability of ELETTRA in stimulating multiple culture chambers in parallel was tested. From 1 and up to 6 culture chambers were filled with 2.5 mL of DMEM and were connected in parallel to ELETTRA. Monophasic and biphasic stimulations (voltage = 5 V for monophasic mode, ± 5 V for biphasic mode; frequency = 1 Hz; pulse duration = 2 ms) were delivered. Tests were repeated for each output, the current was monitored connecting the oscilloscope probe to the ELETTRA monitoring ports, 10 consecutive pulses were recorded and the mean and SD of the current peak were calculated. For each characterization test, voltage waveforms were recorded at a sample rate of 780 kS/s. Acquired signals were post-processed using MATLAB R2020b (MathWorks, USA). Experimental results for monophasic stimulation were then compared with the lumped parameter model outcomes. Moreover, data from the current measurements were used for setting the voltage for biological tests, in order to deliver the desired electric field to the cell culture for each tested condition.

2.2.4 Cell culture experiments

Cell isolation

Neonatal rat cardiomyocytes (CMs) were isolated from 2-3-days old Sprague Dawley rats as previously described[144]. Briefly, rat ventricles were cut into small pieces and digested overnight in 0.06% w/v trypsin solution (trypsin from bovine pancreas, Sigma-Aldrich, USA) at 4°C with continuous shaking at 50-60 oscillations per minute. Five continuous 4-min cycles of 0.1% w/v collagenase solution (collagenase type 2, Worthington-Biochem, USA) treatment were used to continue digestion of the minced tissues. To allow fibroblast (FB) attachment and enrich the cell population for CMs, isolated cardiac cells were pre-plated in culture flasks for 45 min at 37°C and 5% CO_2. The enriched cardiac population was seeded at a density of 6 x 10^4 cells/cm^2 and cultured for 48 h, before starting the experiments, in a seeding medium composed of high glucose DMEM (Sigma-Aldrich, USA), supplemented with 1% Hepes buffer (Sigma-Aldrich, USA), 1% Penicillin/Streptomycin (Sigma-Aldrich, USA), 1% L-

glutamine (Sigma-Aldrich, USA) and 10% Fetal Bovine Serum (FBS, Sigma-Aldrich, USA).

Cell characterization

After isolation, cardiac cells were harvested, washed with phosphate buffered saline (PBS, Sigma-Aldrich, USA), fixed for 20 min at 4°C (4% PFA (Sigma-Aldrich, USA)), permeabilized for 15 min at room temperature (0.5% Triton 100X (Sigma-Aldrich, USA) in PBS) and stained for 30 min at 4°C with the following antibodies: anti-alpha-actinin (sarcomeric) antibody (conjugated with phycoerythrin (PE), Miltenyi Biotec, Germany) and anti-cardiac Troponin T antibody (conjugated with allophycocyanin (APC), Miltenyi Biotec, Germany). All the antibodies were used at 1:200 dilution in FACS buffer (PBS w/o Ca^{2+} and Mg^{2+} (Sigma-Aldrich, USA), 0.5% v/v FBS (Sigma-Aldrich, USA) and 2mM EDTA (Sigma-Aldrich, USA)). Life and dead staining was performed using violet fluorescent reactive dye (read at BV421 (Invitrogen by Thermo Scientific, USA) diluted 1 µl in 1 ml PBS (Sigma-Aldrich, USA)). Cells were then suspended in FACS buffer and at least 50.000 events per sample were collected with a flow cytometer (LSRfortessa, BD, USA).

2D cell culture under ES

Before starting the experiments, the autoclaved PDMS structures were press-fit inserted in the µ-Dish 35 mm chambers (Ibidi, Germany). Cells were then seeded at a density of 6×10^4 cells/cm^2 corresponding to 2.5×10^5 cells per chamber using 2.5 mL of seeding medium. From the following day, the seeding medium was changed with 2.5 mL of low glucose DMEM (Sigma-Aldrich, USA), supplemented with 1% Hepes buffer (Sigma-Aldrich, USA), 1% Penicillin/Streptomycin (Sigma-Aldrich, USA), 1% L-glutamine (Sigma-Aldrich, USA), and 1% FBS (Sigma-Aldrich, USA) to limit FB proliferation (culture medium). Samples were statically pre-cultured for 3 days, to allow the cell recovery from the isolation process[82], then followed by additional 4 days without (control) or with ES, according to previous publications[80,126,127,145]. Culture medium was changed every two days to provide fresh nutrients to the cells and to remove toxic by-products that may be produced during the ES. Three different ES modes were tested simultaneously (frequency = 1 Hz, pulse duration = 2 ms): 1) monophasic ES at 5 V/cm; 2) biphasic ES at ± 2.5 V/cm; 3) biphasic ES at ± 5 V/cm (Figure 2a). The biphasic ES at ± 2.5 V/cm mode was chosen to deliver the same absolute value of the electric field variation of the monophasic ES at 5 V/cm mode, while the biphasic ES at ± 5 V/cm mode was chosen to deliver the same amount of charge released by the monophasic ES at 5 V/cm mode

(Supplementary Figure 2.S1). ES modes were applied to up to 4 culture chambers in parallel (Figure 2.2b), and all samples were cultured in total for 7 days in a standard incubator (37°C, 95% humidity, 5% CO_2) (Figure 2.2c).
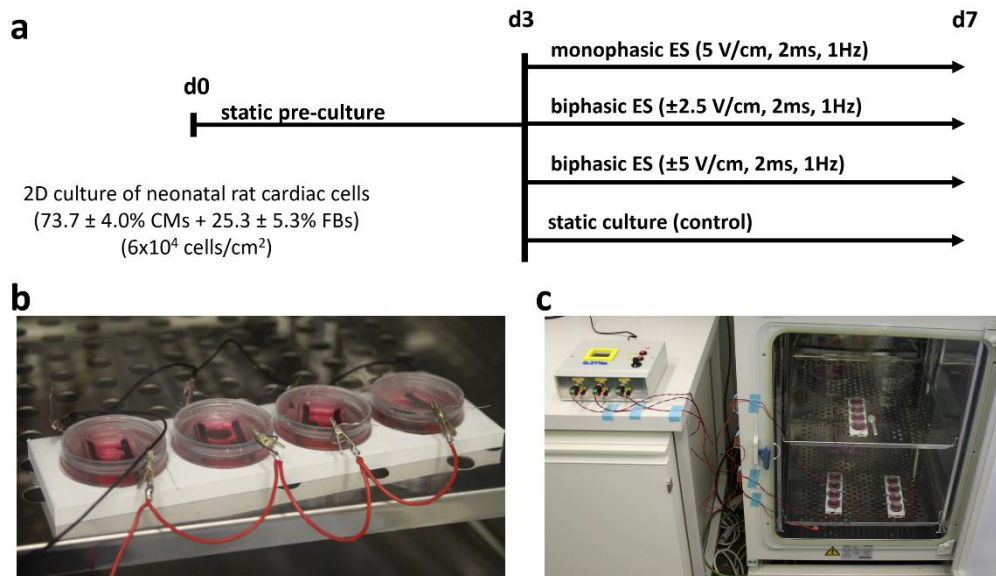
Figure 2.2. Biological experiments. A) timeline of the performed culture protocols; b) 4 culture chambers connected in parallel during the experiments; c) picture of the whole setup during the biological experiments: each output of ELETTRA is connected to a set of 4 culture chambers placed inside the incubator.

Electrical functionality assessment

After 7 days of culture, cell contractile activity in response to external electrical pacing was assessed by measuring two electrical maturation parameters, the Excitation Threshold (ET) and the Maximum Capture Rate (MCR)[146]. The pacing tests were performed inside a live-imaging microscope incubator (ZEISS X91, Olympus, Japan), with controlled temperature (37°C) and CO_2 (5%). Electrical pulses (1 Hz, 2 ms) were imposed using ELETTRA and, starting from 1 V/cm, a progressively increasing voltage amplitude was applied to determine the minimum electric field needed for generating a synchronous cell contraction (ET). Once ET was established, the electric field was imposed equal to 150% ET and, increasing the frequency, the maximum frequency that the cells can follow (MCR) was assessed. Movies of the electrically paced cells were acquired using 10X objective lens at 30 frames per second with the live-imaging microscope incubator. Data from functionality assessment were analysed by GraphPad Prism 8 (GraphPad Software, USA) adopting Kruskal-Wallis test with post-hoc Dunn's multiple comparison test. Data were averaged and expressed as the mean ± SD. The statistical significance

was denoted as ∗ for p-value ≤ 0.05, ∗∗ for p-value ≤0.01, and ∗∗∗ for p-value ≤0.001.

Immunofluorescence analysis

To investigate the CMs/FBs ratio and the cardiac maturation at the end of the culture, immunofluorescence analysis was performed. Cells were washed with PBS (Sigma-Aldrich, USA) and fixed using 4% PFA (Sigma-Aldrich, USA) for 15 min. Afterwards, the immunostaining was carried out. In detail, cells were washed 2 times with PBS (Sigma-Aldrich, USA), then they were incubated for 1 h at room temperature in 5% normal goat serum (Sigma-Aldrich, USA) with 0.25% Triton 100X (Sigma-Aldrich, USA) in PBS (Sigma-Aldrich, USA). After washing 2 times with PBS, cells were incubated for 1 h in the dark with the following primary antibodies: mouse monoclonal anti-sarcomeric α-actinin (ABCAM9465, Abcam, UK) and rabbit polyclonal IgG anti-connexin-43 (C6219, Sigma-Aldrich, USA). Cells were again washed twice with PBS and then incubated in the dark for 30 min with fluorescently labelled Alexa546 anti-mouse and Alexa647 anti-rabbit secondary antibodies (Life Technologies, Thermo Fisher Scientific, USA). Nuclei were stained using 4′,6-diamidino-2-phenylindole (DAPI, Invitrogen, Thermo-Fisher Scientific, USA) at 1:40 for 15 min. Incubations were performed at room temperature and antibodies were diluted in PBS 1X with 0.1% bovine serum albumin (BSA, Sigma-Aldrich, USA). Primary and secondary antibody dilution was 1:200. Images were acquired using 40X objective lens on a Nikon-CSU1 spinning-disk confocal microscope (Nikon, Japan) and analyzed by using ImageJ software (NIH, USA).

The number of cells was assessed counting the DAPI positive nuclei, while the numbers of CMs and FBs were defined counting the number of cells positive and negative for the sarcomeric α-actinin, respectively.

2.3 Results

2.3.1 ELETTRA characterization

Experimental in-house tests and lumped parameter model

ELETTRA performances were first characterized experimentally. The measurements of the pulse train, the voltage waveform, and the resulting current waveform on a single culture chamber filled with culture medium are shown in Figure 2.3 for a monophasic (5 V, 1 Hz, 2 ms, Figures 2.3a-c) and for a biphasic (±5 V, 1 Hz, 2 ms, Figure 2.3d-f) stimulation, respectively. The pulse train graphs demonstrate that, with respect to the imposed frequency, ELETTRA delivered the stimulations accurately (Figures 2.3a and 2.3d). The voltage waveform graphs show square waves with low noise (noise root mean square voltage = 0.022 V for both ES modes, Figures 2,3b and 2.3e). The percentage errors of the measured voltage with respect to the imposed one were lower than 5% for imposed voltages between 2 and 11 V, with a maximum error of 8.1% at 1 V for monophasic ES (Supplementary Figure 2.S2). As regards the current flowing between the electrodes (Figures 2.3c and 2.3f), for both stimulations the current increased instantly in magnitude when ELETTRA was switched on, while during the active phases the current magnitude decreased due to the induced polarization of the culture medium and the consequent shielding effect of charges accumulated at the electrode-solution interfaces. During the passive phases, the current reversed its direction as the accumulated charges were released in the solution. Moreover, for the biphasic ES, the greater negative peak in current amplitude was due to the combination of the release of charges accumulated during the positive half-wave with the current directly induced by the applied negative voltage (Figure 2.3f). For both waveform modes, different voltages (1 - 12 V with 1 V step) were imposed and the peak current values measured on each output showed negligible differences among the three outputs (see Supplementary Table 2.S2). The highest peak current value was equal to 170.79 ± 0.56 mA for monophasic ES and equal to 205.80 ± 1.38 mA for biphasic ES, when imposing a 12 V stimulation voltage. Such values are considerably lower than the maximum current output of the stimulator (700 mA), confirming the suitability of ELETTRA to stimulate multiple chambers in parallel.
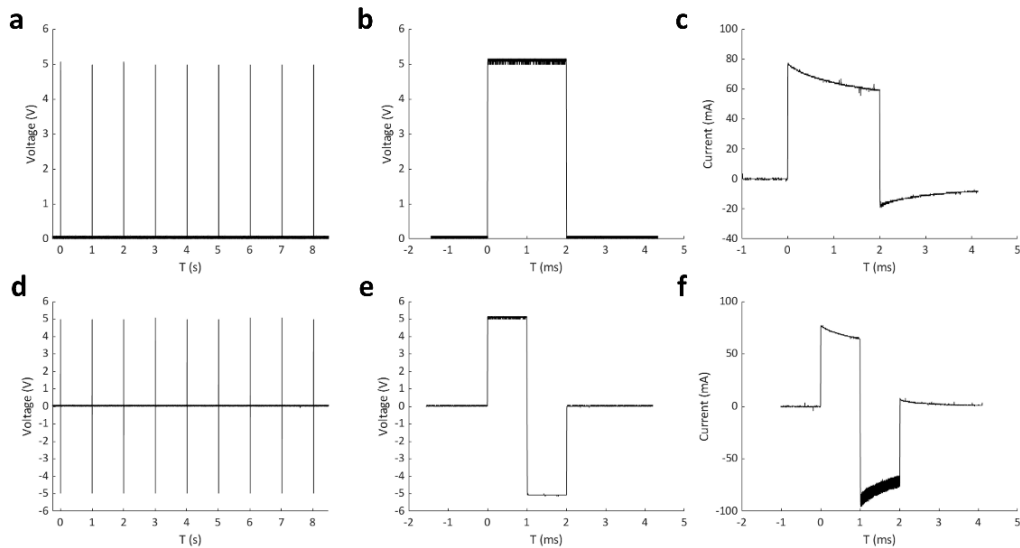
Figure 2.3. Measurements of pulse train, voltage waveform and resulting current waveform on a single culture chamber for monophasic ES (a, b, c) and biphasic ES (d, e, f).

Up to 6 culture chambers were then connected in parallel and stimulated with monophasic waveform (5V), and the measured current waveforms and peak currents were compared with the corresponding lumped parameter model results. For each condition, the simulated current was slightly higher than the measured one (Figure 2.4a), with a maximum discrepancy of the current peak equal to 13 mA (5%) when 6 chambers were connected in parallel (Figure 2.4b), because of the lump parameter model neglects the non-ideal behavior of the components and the additional sources of voltage drop (e.g., the connectors). Moreover, a nonlinear increase of the peak current occurred for both measured and simulated tests when multiple chambers were connected (Figure 2.4b), with a consequent decrease of the delivered electric field. This is related to the voltage drop on the ELETTRA sensing resistor, which increases with the number of chambers connected. Such effect was taken into account during the biological tests, and the voltage was appositely adjusted to deliver the desired electric field to the cell culture for each tested condition.

39
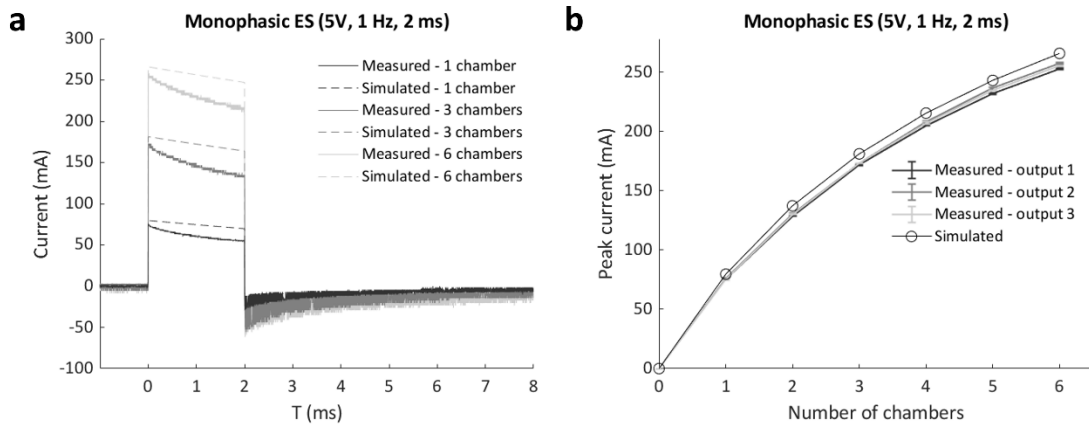
Figure 2.4. Comparison of measured currents and lumped parameter model results for multiple chambers connected in parallel to ELETTRA. a) current waveforms for 1, 3 and 6 chambers connected; b) peak currents for 1 to 6 chambers connected.

Electric field modelling

The distributions of the electric field and of the current density within the culture chamber were characterized performing the FEM analysis. Figure 2.5a shows representative results of the electric field distribution within the culture chamber at three planes perpendicular to the electrodes, when a 5 V voltage and 2.5 mL of culture medium were simulated. The electric field magnitude was about 7.5 V/cm around the electrodes with an almost uniform value (4.5-5 V/cm) between the electrodes (Figure 2.5a). On the central plane, the electric field magnitude was also calculated along two lines located, respectively, at the height of the electrode centers (gray line, Figure 2.5a) and at the bottom of the culture chamber, where the cells are seeded (magenta line, Figure 2.5a). At the height of the electrode centers, the electric field magnitude ranged from 4.5 to 7.5 V/cm (Figure 2.5b), while at the culture chamber bottom it was characterized by an average value of 4.5 V/cm over a wide central region (6 mm) (Figure 2.5c).

The vector diagram of the current density over the central cross section of the culture chamber highlights that the direction of the current was well aligned along the electrode-electrode direction, where the cells are cultured (Figure 2.5d). Due to the uniformity of the electric field, the current density was uniform with an absolute value of 660 A/m^2 in the central region. The total current flowing between the electrodes, calculated as the surface integration of the current density on one electrode, was 112.5 mA, in agreement with the peak current (114.5 mA) measured when a monophasic electrical stimulation (5 V/cm, 2 ms, 1 Hz) was applied to a culture chamber filled with 2.5 mL of culture medium.

40
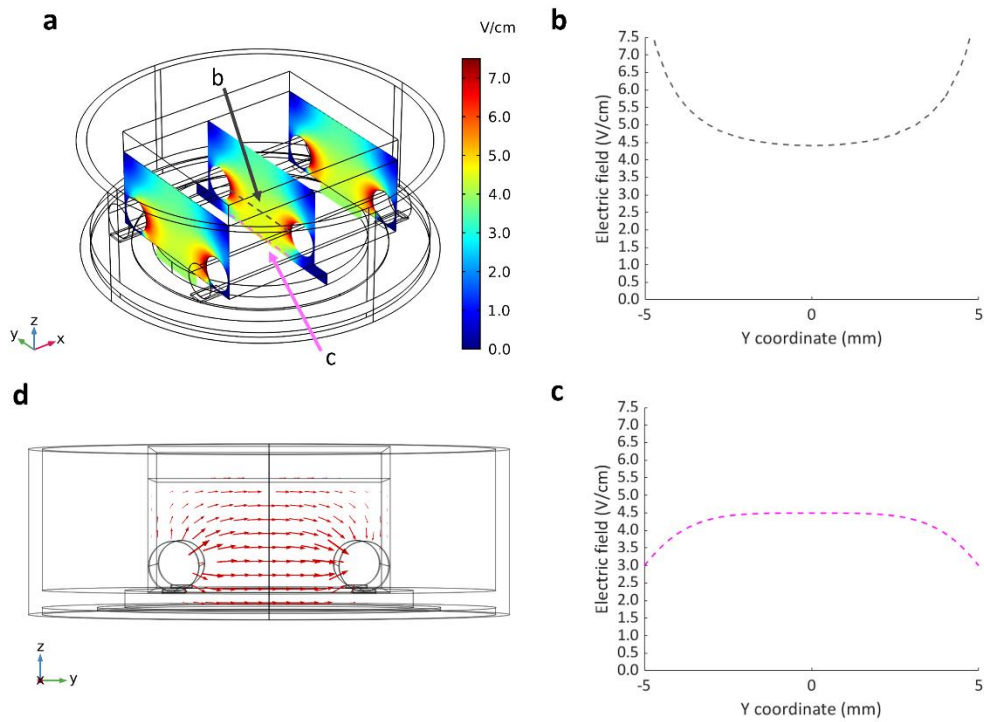
Figure 2.5. Distributions of electric field and current density within the culture chamber. a) contour plot of electric field magnitude at three planes perpendicular to the electrodes' main axes, located at x=-10 mm, x=0 mm, x= 10 mm; b, c) electric field magnitude on the central plane of the chamber along a line at the height of the electrodes centers and at the bottom of the chamber, respectively; d) vector diagram of the current density over the central cross section of the culture chamber.

2.3.2 Cell culture experiments

Electrical functionality assessment

Following 7 days of culture in either static (control) or ES conditions, the electrical functionality of neonatal rat CMs was assessed evaluating their response to an external electrical pacing. Figure 2.6a shows that, when exposed to external pacing, CMs cultured under monophasic ES at 5 V/cm or under biphasic ES at ±5 V/cm started to synchronously contract at a significantly lower ET (3.50 ± 0.41 V/cm and 3.58 ± 0.41 V/cm, respectively) compared to the control (4.93 ± 0.46 V/cm), but no statistically significant differences were observed among the ES groups. As regards the maximum electrical pacing frequency that the cells can follow, all the ES groups showed an overall increasing trend of MCR compared to the control (2.57 ± 0.53 Hz), however only the CMs cultured under biphasic ES at ±5 V/cm showed a significantly higher MCR (3.71 ± 0.49 Hz). Interestingly, all the ES group reached the normal rat heart frequency (around 3 Hz) (Figure 2.6b).
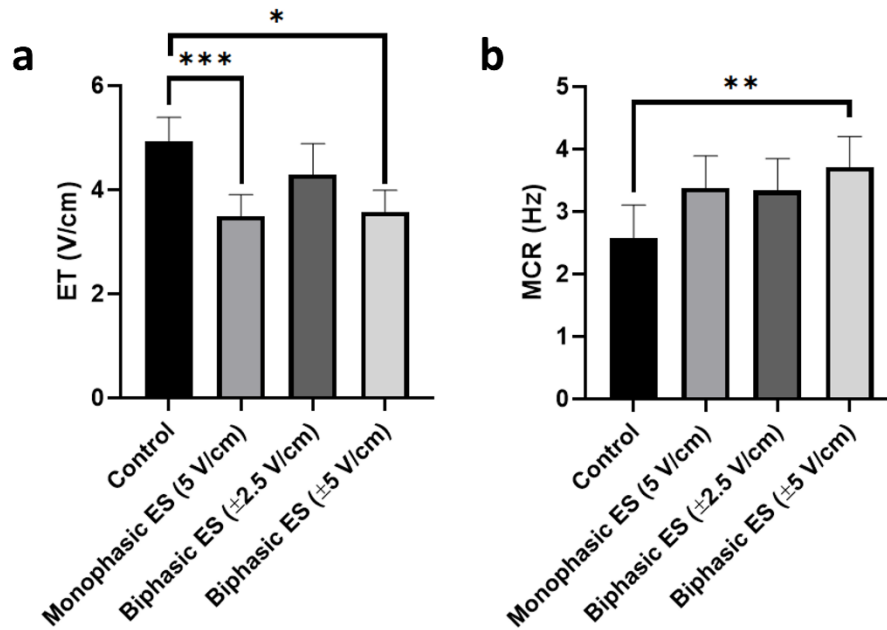
Figure 2.6. Functional properties after different stimulation modes: (1) no stimulation, (2) monophasic ES (5V/cm, 1 Hz, 2 ms), (3) Biphasic ES (±2.5V/cm, 1 Hz, 2 ms) and (4) Biphasic ES (±5V/cm, 1 Hz, 2 ms). a) Excitation threshold (ET), b) Maximum capture rate (MCR). Asterisks (*) denote statistically significant difference (*$p < 0.05$, **$p < 0.01$, ***$p < 0.001$).

Cardiac cell characterization and immunofluorescence analysis

The percentages of CMs and FBs were evaluated both immediately after isolation and at the end of the ES culture. Following the isolation process, cardiac cells were analyzed by flow cytometry and, among the living cells, the CMs resulted to be 73.7 ± 4.0% (double positive for anti-cardiac Troponin T and anti-alpha-actinin (sarcomeric)), while FBs were estimated to be 25.3 ± 5.3% (double negative for the same antibodies). At the end of the culture and after the electrical functionality analysis, the different cultured groups were fixed and stained, and the immunofluorescence image analysis showed almost 55% CMs and 45% FBs for all groups (Supplementary Figure 2.S3).

To assess the level of cardiac maturation, the presence of specific cardiac proteins, namely the gap-junction protein Connexin-43 (Cx-43) and the sarcomeric α-actinin for the contractile structure, was investigated. Unlike the control group, most of the cells cultured under ES were positive for Cx-43 (Figure 2.7). In particular, cells cultured under monophasic ES at 5 V/cm or under biphasic ES at ±5 V/cm were characterized by the Cx-43 mainly localized at the cell membrane in proximity of neighboring CMs, suggesting

its functional role as gap junction. For cells cultured under biphasic ES at ±2.5 V/cm, the Cx-43 was present both in the cytoplasm and at the cell membrane. For the control condition, Cx-43 was less present and mainly localized within the cytoplasm (Figure 2.7). Moreover, electrically stimulated CMs appeared to be characterized by a better organization of sarcomeres compared to control CMs. Moreover, the number of elongated, rod-shape CMs was higher in the ES groups then in the control group (Figure 2.7).
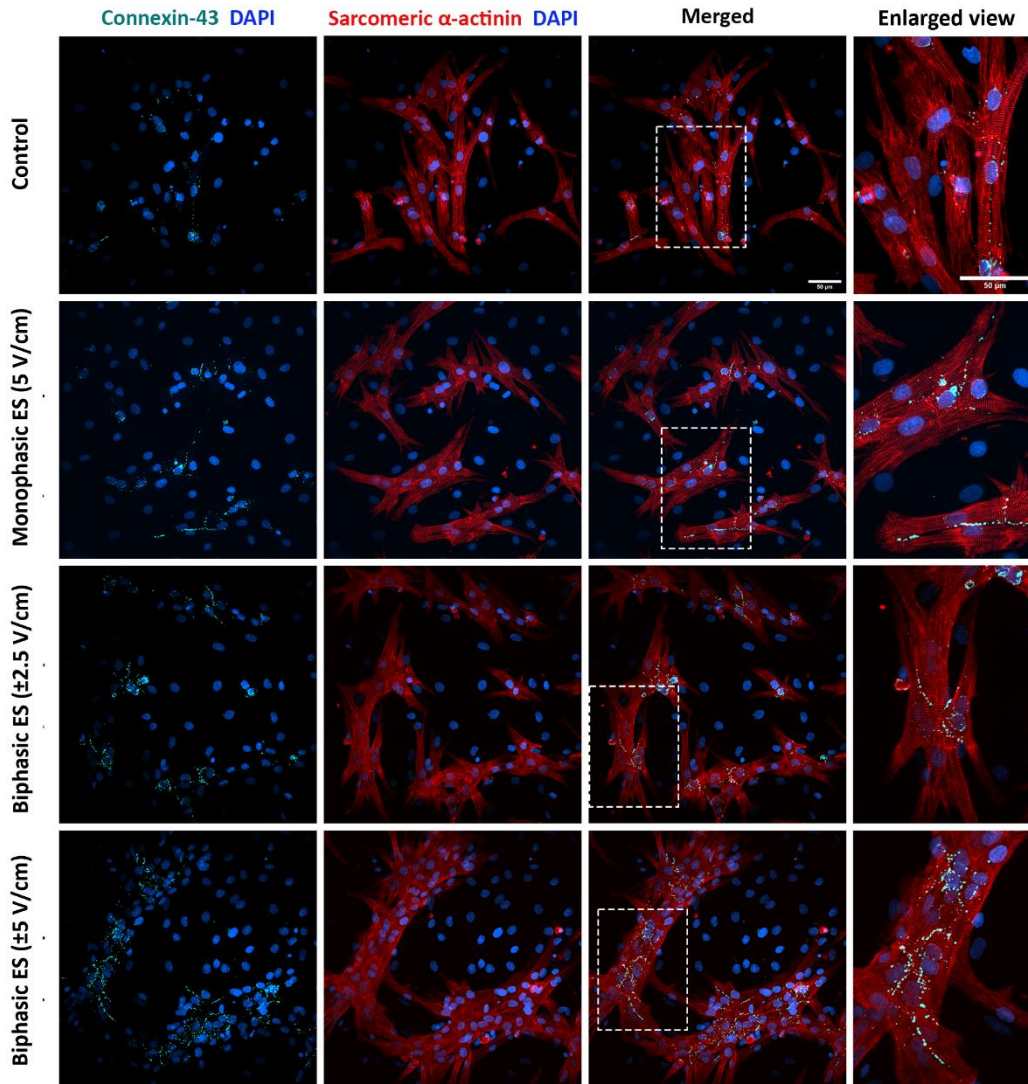
Figure 2.7. Immunofluorescence images of neonatal rat CMs for the four conditions. The images show the Cx-43 (cyan) with the nuclei in blue (DAPI), Sarcomeric α-actinin (red) with the nuclei in blue (DAPI) in separated images and the merged signals for each experimental group.

2.4 Discussion

In CTE research, it has been demonstrated that for the *in vitro* development of functional cardiac substitutes a controlled culture environment and native-like mechanical and/or electrical stimuli are fundamental[34,147]. As concerns the ES, several studies investigated the effects of electrical stimuli on cardiac cells and constructs under controlled conditions and their potential in promoting cardiac maturation. In particular, it was shown that *in vitro* ES affects the rate, duration, and number of action potentials of CMs, improves the organization of sarcomeres and the establishment of gap junctions promoting cell–cell coupling and calcium handling, thereby, increasing the electrical and contractile functionality of stimulated cells[82,124,125]. In most of the studies, ES was delivered as electric field stimulation by applying a voltage between two parallel electrodes immersed in the culture medium[32,87], and the electrical stimulus was generated by using commercial electrical stimulators[81,83,85,87,125,133–138]. Although commercial stimulators are versatile and allow testing different ES patterns simultaneously, they are characterized by limited waveform modulation, high cost, and bulkiness, which limit the adoption of ES protocols in CTE. Alternatively, cost-effective and portable prototypes have been purposely developed[73,80,81], however such devices are limited to a single output with limited ES tunability and/or can be used only with a specific setup.

Taking into account the limitations of commercial and custom-made electrical stimulators, we developed the electrical stimulator ELETTRA, appositely designed for CTE applications. Particular attention was paid to guarantee versatility, indeed, ELETTRA can deliver a wide range of cardiac-like electrical stimuli (voltage $= 0.25 - 12.0$ V, frequency $= 0.5 - 10.0$ Hz, pulse duration $= 1$- 10 ms, tunable monophasic or biphasic waveforms) and, being equipped with three standard outputs, it can be coupled to multiple custom-made culture chambers or to already existing dynamic culture devices. Moreover, during the development phase, the choice of the open-source Arduino platform guaranteed high customizability and cost-effectiveness compared to commercial computer-based systems, and the use of custom-designed PCBs avoided cumbersome and heavy parts, leading to a compact and portable device (Figure 2.1b). Lastly, the integrated user-friendly interface allows quick setting and easy tuning of the stimulation parameters and provides real-time feedbacks to the operators, facilitating laboratory operations. In order to test the ELETTRA

44

performances in a representative CTE application, we then developed customized culture chambers to be connected to ELETTRA for investigating the influence of different ES waveforms on the *in vitro* maturation of cardiac cells. Autoclavable PDMS structures, each one including two electrodes and combinable with standard cell culture dishes, were manufactured to be connected in parallel to ELETTRA, allowing ease of use and rapid assembling/disassembling procedures.

Firstly, characterization tests were performed on ELETTRA, without and with culture chambers connected, for assessing reliability and accuracy of the device. As regards the voltage tests (1-12 V), the mean percentage errors between the measured and the nominal voltage values were almost negligible (< 5%) for imposed voltages ranging from 2 to 11 V, and did not overcome 9% when 1 V or 12 V were set (Supplementary Figure 2.S2). The higher inaccuracy at 1 V has to be ascribed to the limited resolution of the waveform generation unit, while at 12 V it is related to the output voltage saturating the differential amplifier. However, it should be noted that electric field amplitudes commonly applied in CTE range between 2 and 5 V/cm[34,83], values that can be accurately delivered by ELETTRA. As concerns the characterization of the current flowing between the electrodes, the tests confirmed the suitability of ELETTRA to stimulate multiple culture chambers in parallel for each output (up to 6 for an imposed voltage of 5V). Indeed, the lumped parameter model outcomes (for which the culture chambers were modeled as Randles cells) were in good agreement with the experimental results, although they slightly overestimated (~ +5%) the current flowing within the culture chambers (Figure 2.4). This is related to the fact that the simulation did not account for the non-ideal behavior of the adopted components and neglected possible voltage drops (e.g., at the connectors). Moreover, observing the differences between simulated and experimental data, they were lower at the peak current than during the subsequent active phase (Figure 2.4a), suggesting that the model was accurate in determining the resistive effects of the solution, while it slightly overestimated the capacitive ones. Thus, as the critical parameter is the peak current, the lumped parameter model can be considered a suitable tool for defining the number of culture chambers that can be connected in parallel to each ELETTRA output and, in case different culture chambers would be used, it can be adapted by appropriately tuning the Randles cell parameters. In addition, the characterization of the current allowed assessing the effect of the sensing resistor and thereby adjusting the imposed voltage during the biological tests for ensuring the desired electric field. Lastly, the FEM analysis confirmed that the cells seeded at the bottom of the culture

chamber, between the electrodes, are exposed to almost uniform electric field and current density, with some perturbations around the electrodes (Figure 2.5). Experimental measurements validated the computational results, with a difference in the total current between the simulation and the experimental measurements lower than 2%. For the computational analysis, a stationary condition was adopted thus the transient behavior of the delivered pulses was neglected, however, in accordance with previous studies, such assumption was considered acceptable as the modelled system was much smaller than the wavelengths of interest[87,148]. Thus, the characterization tests confirmed that ELETTRA is a reliable device in providing accurate and repeatable ES within a range of interest for CTE applications.

ELETTRA was then adopted for investigating the effect of different ES waveforms on cardiac cells cultured *in vitro.* In detail, cardiac cells isolated from neonatal rats were seeded in the manufactured culture chambers, statically pre-cultured for 3 days and then exposed for 4 days to different ES modes (monophasic ES at 5 V/cm; biphasic ES at ±2.5 V/cm; biphasic ES at ±5 V/cm) provided by ELETTRA. Before starting the experiments, the percentages of CMs and FBs were assessed to be $73.7 \pm 4.0\%$ and $25.3 \pm 5.3\%$, respectively. Since after 7 days of culture in either control or ES conditions the percentage of CMs (around 55%) and FBs (around 45%) was similar for all experimental groups, we can conclude that CM survival was not affected by the ES conditions (Supplementary Figure 2.S3), and the increase of the FB percentage was most likely due to FB proliferation. As regards the imposed ES waveforms, to our knowledge this is the first time that the effects of different biphasic waveforms, equivalent to the monophasic waveform (5V/cm) either in the absolute value of the electric field variation (biphasic ES at ±2.5 V/cm) or in charge (biphasic ES at ±5 V/cm), were compared. Indeed, most of the CTE studies applying ES compared monophasic waveforms with biphasic waveforms balancing the absolute value of the electric field variation, avoiding to investigate the charge balance[80,126,127]. In our study, the electrical functionality tests revealed that CMs cultured under monophasic ES at 5 V/cm or under biphasic ES at ±5 V/cm showed a significantly lower ET compared to the control, and moreover the CMs cultured under biphasic ES at ±5 V/cm presented a significantly higher MCR. Differently, among the ES groups, the CMs exposed to biphasic ES at ±2.5 V/cm were characterized by low functional properties in terms of both ET and MCR (Figure 2.6). The charge delivered by the biphasic ES at ±2.5 V/cm was half of the charge delivered by the other applied ES conditions, thus the cells were overall less stimulated with

respect to the other ES groups and presented limited electrical functionality. Our results differ from a previous work[126], where a significant reduction of ET for cells cultured under biphasic ES at ± 2.5 V/cm compared to the control was shown, without significant differences compared to monophasic ES at 5 V/cm. However, in the work of Chiu and colleagues, organoids resembling cardiac myofibers cultivated in matrigel-coated microchannels were used, thus the differences in construct and culture conditions could explain the different outcomes of the two works. In terms of maintenance of cell survival and Cx-43 localization, our findings are in agreement with previous studies[80,126,127]. Indeed, unstimulated cells showed less Cx-43, mainly localized at the cytoplasm level, while in ES groups Cx-43 was detected particularly at the cell membrane, in proximity of neighboring cells (Figure 2.7).

2.5 Conclusions

In this study, we developed, characterized, and tested a compact, easy-to-use, tunable electrical stimulator, ELETTRA, appositely developed for CTE applications. The adoption of a customizable electronic platform combined with free and open-source software allowed developing a device offering control accuracy, indirect monitoring, versatility, and portability at a competitive cost. ELETTRA is combinable with different cell/tissue culture set-ups and allows both testing different stimulation patterns simultaneously and stimulating multiple samples in parallel, representing a powerful tool for CTE investigations. The biological experiments, showing for the first time a comparison between biphasic ES conditions, demonstrated that monophasic ES at 5 V/cm and particularly biphasic ES at ±5 V/cm were effective in enhancing cardiac electrical functionality.

These findings constitute the basis for the future use of ELETTRA in advanced investigations aimed to identify the effects of different stimulation protocols and to define the combinations of parameters inducing specific biological effects. Moreover, coupled with existing bioreactors, ELETTRA could be used to provide combined physical stimuli in a physiologically relevant way, for future production of functional CTE constructs.

Supplementary Material

Culture chamber manufacturing

For manufacturing the PDMS structure, at first a mold was designed (SolidWorks, Dassault Systemes, France) and then manufactured with the Replicator+ 3D printer (MakerBot, USA) using a polylactide acid (PLA) filament. The PDMS solution (Sylgard 184, Dow Corning, USA) was prepared in standard 10:1 proportion of pre-polymer and curing agent. The mold was then placed in the center of a μ-Dish chamber (ibidi GmbH, Germany), where the PDMS was poured, and degassing was performed in a vacuum jar at room temperature for 4 h. In parallel, the carbon rods (Sigma-Aldrich, Germany) were cut at a length of 26 mm. Once the PDMS structure was polymerized, the carbon rods were inserted to serve as electrodes. For electrically connecting the carbon rods to ELETTRA, a hole was drilled through each carbon rod and through the PDMS structure and, with the help of a cannula, a platinum wire (Sigma Aldrich, Germany) was passed through. Platinum wires, which are thin enough to pass through the space between the μ-Dish chamber and the lid, were cut long enough to access the external environment guaranteeing sterility to the cultured cells.

Lumped-parameter model assumptions

The three parameters of the Randles Cell (R_e, R_p, C_p) were evaluated considering the materials and geometry of the chamber described in the Materials and Methods section.

To determine R_e it must be taken into account the conductivity of the solution σ and the geometry of the electrolyte where the current flows in. For an electrode area A exposed to the electrolyte carrying a uniform current, being d the spacing between the electrodes, the solution resistance is calculated as follows [145]:

$$R_e = \frac{d}{\sigma A}$$

where σ is the conductivity of the solution and A is the area of the electrode exposed to the solution.

The value of A was calculated assuming that the cylindrical carbon rod electrodes in the chamber expose 2/3 of their lateral surface to the electrolyte:

$$A = 2\pi \cdot r \cdot l \cdot \frac{2}{3}$$

_____

Considering the length of the portion exposed by the electrode to the electrolyte l = 20 mm, the electrode radius r = 1.5 mm a the interelectrodic distance d = 1 cm, the area resulted A = 1.26 cm².

Considering the value for the conductivity of the culture media reported in literature (1.5 S/m [83]), R_e was estimated at 53 Ω.

The polarization resistance R_p and the double layer capacitance C_p were evaluated starting from literature data relative to electrochemical impedance spectroscopy (EIS) studies which gave the normalized values over a unit area (R_p/A = 4.06*10¹³ Ω/cm²; C_p/A = 190 µF/cm² [142]) and resulted R_p = 5.13 x 10⁸ MΩ and C_p = 240 µF.

Supplementary Table 2.S1. Electrical conductivity and relative permittivity values of the modelled sub-domains.

	PDMS	Carbon Rods	Medium	PE derivate	Air
Electrical conductivity (S/m)	0.83*10⁻¹² [80]	1,28*10⁶	1.5 [83]	1*10⁻¹⁵	0
Relative permittivity	2.69 [149]	12	80 [150]	2.3	1

Supplementary Table 2.S2. Peak current flowing inside the culture chamber for all the tested stimulation conditions. To compare monophasic and biphasic stimulations, current values were expressed as absolute values.

Stimulation voltage (V)	Peak current (mA)					
	Monophasic			Biphasic (symmetric)		
	Output 1	Output 2	Output 3	Output 1	Output 2	Output 3
1	16.78 ± 0.19	16.70 ± 0.82	17.09 ± 0.78	21.01 ± 0.77	21.15 ± 0.87	20.75 ± 0.58
2	33.05 ± 0.19	32.65 ± 0.72	32.91 ± 0.67	39.65 ± 0.28	40.18 ± 0.31	40.22 ± 0.43
3	47.63 ± 0.23	47.24 ± 0.31	47.37 ± 0.68	57.24 ± 0.28	59.09 ± 0.37	58.56 ± 0.45
4	63.33 ± 0.41	62.72 ± 0.43	62.98 ± 1.11	76.15 ± 0.46	78.43 ± 0.37	77.73 ± 0.45
5	77.84 ± 0.46	77.40 ± 0.03	77.05 ± 0.45	94.00 ± 0.50	95.93 ± 0.28	95.50 ± 0.45
6	93.94 ± 0.37	93.50 ± 0.83	92.44 ± 0.28	112.72 ± 0.56	114.30 ± 0.83	112.89 ± 0.74
7	109.05 ± 0.02	108.70 ± 0.74	107.65 ± 0.74	130.12 ± 0.03	130.48 ± 0.74	129.60 ± 0.85
8	124.71 ± 0.56	123.83 ± 0.91	123.12 ± 0.03	147.71 ± 0.03	147.71 ± 0.05	145.60 ± 0.74
9	137.37 ± 0.56	138.95 ± 0.03	137.37 ± 0.56	162.31 ± 1.45	163.89 ± 0.74	161.43 ± 1.11
10	154.78 ± 0.04	153.91 ± 0.93	153.03 ± 0.03	179.72 ± 1.11	179.19 ± 0.99	175.68 ± 0.56
11	169.20 ± 0.74	167.27 ± 0.56	167.27 ± 0.56	195.20 ± 0.03	193.61 ± 0.56	191.15 ± 0.85
12	170.79 ± 0.56	167.27 ± 0.56	169.03 ± 0.56	205.80 ± 1.38	205.36 ± 0.03	205.36 ± 0.04
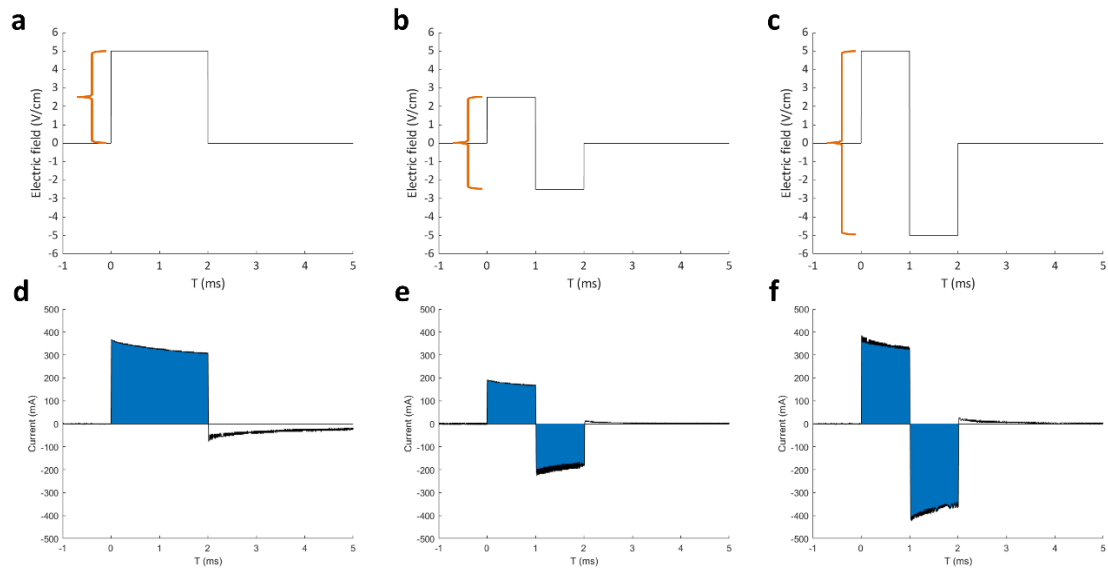
Supplementary Figure 2.S1. Comparison of the ES modes used in biological experiments. The absolute value of the electric field variation of the monophasic ES at 5 V/cm (a) and of biphasic ES at ± 2.5 V/cm (b) are equal, while that of biphasic ES at ± 5 V/cm is twice as much. The total charge delivered by monophasic ES at 5 V/cm (blue area, d) is twice the charge delivered by biphasic ES at ± 2.5 V/cm (e) and equal to that of biphasic ES at ± 5 V/cm (f).
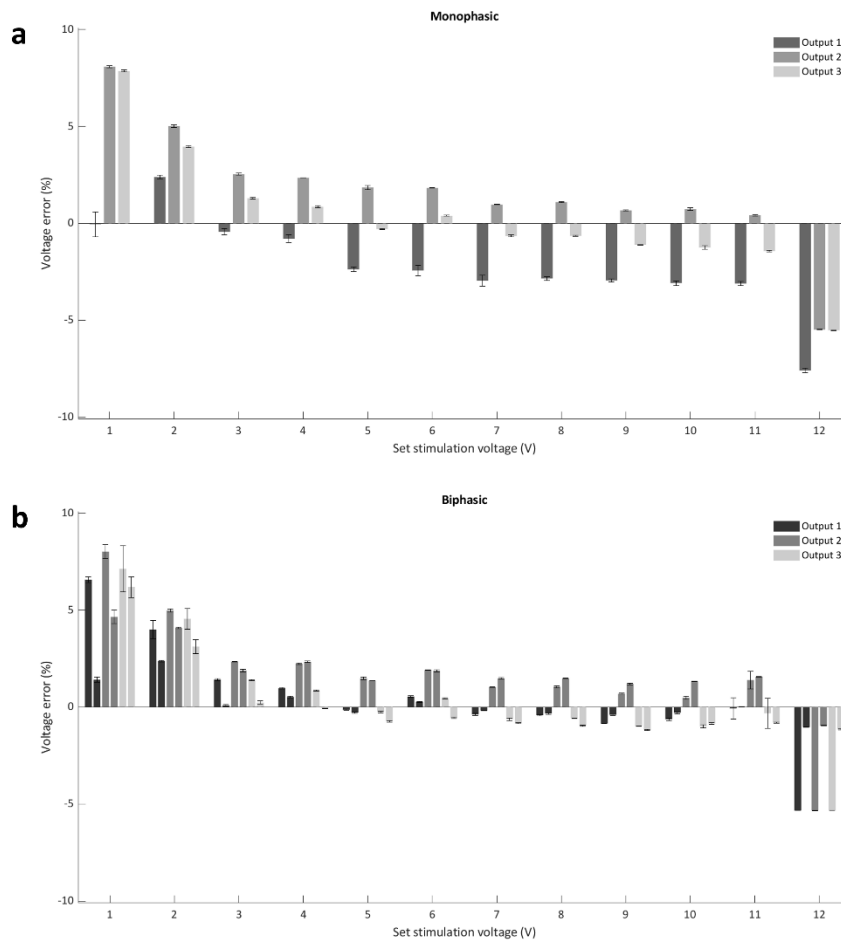
Supplementary Figure 2.S2. Percentage errors of the measured voltage with respect to the imposed voltage for monophasic ES (a) and biphasic ES (b)
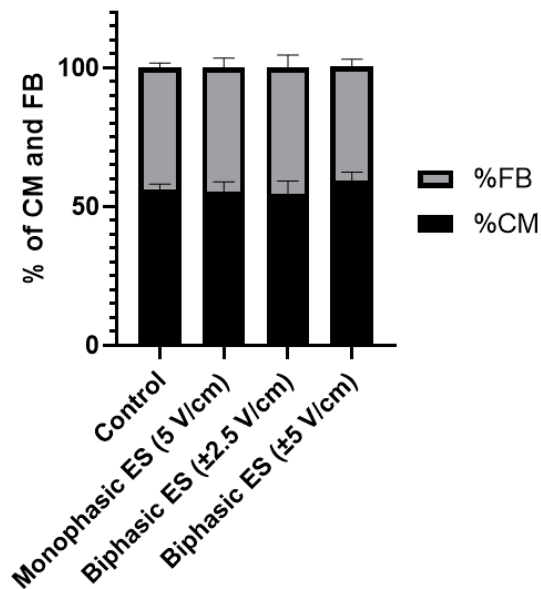
Supplementary Figure 2.S3. Percentage of CMs and FBs after 7 days of culture for each experimental group.

Chapter 3

An Automated 3D-Printed Perfusion Bioreactor Combinable with Pulsed Electromagnetic Field Stimulators for Bone Tissue Investigations

Abstract

In bone tissue engineering research, bioreactors designed for replicating the main features of the complex native environment represent powerful investigation tools. Moreover, when equipped with automation, their use allows reducing user intervention and dependence, increasing reproducibility and the overall quality of the culture process. In this study, an automated uni-/bi-directional perfusion bioreactor combinable with pulsed electromagnetic field (PEMF) stimulation for culturing 3D bone tissue models is proposed. A user-friendly control unit automates the perfusion, minimizing the user dependency. Computational fluid dynamics simulations supported the culture chamber design and allowed the estimation of the shear stress values within the construct. Electromagnetic field simulations demonstrated that, in case of combination with a PEMF stimulator, the construct can be exposed to uniform magnetic fields. Preliminary biological tests on 3D bone tissue models showed that perfusion promotes the release of the early differentiation marker alkaline phosphatase. The histological analysis confirmed that perfusion favors cells to deposit more extracellular matrix (ECM) with respect to the static culture and revealed that bi-directional perfusion better promotes ECM deposition across the construct with respect to uni-directional perfusion. Lastly, the real-time PCR results of 3D bone tissue models cultured under bi-directional perfusion without and with PEMF stimulation revealed that the only perfusion induced a ~40-fold up-regulation of the expression of the osteogenic gene collagen type I with respect to the static control, while a ~80-fold up-regulation was measured when perfusion was combined with PEMF stimulation, indicating a positive synergic pro-osteogenic effect of combined physical stimulations.

3.1 Introduction

Nowadays, due to the population ageing coupled with rising of obesity and decreased physical activities, bone fractures and their clinical management represent a heavy socio-economic burden[151,152] complemented by a dramatically growing need for bone replacement worldwide[153,154].

In fact, although bone can usually regain functionality by self-healing, there are pathological conditions such as nonunion or large bone defects due to trauma, infections, tumors or osteoporosis in which self-healing fails, causing severe pain and immobility to patients[155,156]. Besides the conventional surgical procedures adopted for managing critical-sized bone defects, bone tissue engineering (BTE) is emerging as a promising strategy for generating *in vitro* functional bone tissue substitutes to be implanted for promoting *in vivo* bone regeneration[44]. BTE approaches are based on the effective interplay among osteogenic cells, three-dimensional (3D) porous scaffolds, and physiological chemical and physical stimuli[157,158]. Currently, a direct translation of BTE strategies to clinical use still remains challenging due to scientific, technical, and regulatory limitations[159–161], and BTE substitutes are mostly adopted as 3D bone tissue models for in vitro bone research and pre-clinical studies[60,162]. For example, it has been demonstrated that mechanical forces, such as compression and fluid flow-induced shear stress, influence or even drive stem cells differentiation into mature bone lineages[163–165]. Therefore, for a clear understanding of the mechanotransduction mechanisms driving bone tissue development, homeostasis, and regeneration, the in vitro modelling and analysis of 3D bone tissue models exposed to controlled native-like physical stimuli would be essential[166].

In this context, several bioreactors have been developed and adopted as powerful investigation tools for providing in vitro defined native-like physical stimuli[49,57,65,71,167–171]. Technically, bioreactors imposing hydrostatic pressure were developed to mimic the native-like compression[172–175]. Along with this approach, a variety of studies showed that direct perfusion, by guaranteeing continuous medium flow through the 3D cultured constructs, ensures efficient mass transport during both cell seeding and tissue culture[176,177] and exposes the constructs to fluid flow-induced shear stress profiles that can promote proliferation and differentiation of osteoblasts and foster bone mineralization[175,178–180]. For example, Bancroft and colleagues developed a direct uni-directional perfusion bioreactor (total

medium volume = 200 mL) based on a peristaltic pump and observed increased deposition of mineral extracellular matrix (ECM) produced by marrow stromal osteoblasts seeded on titanium fiber mesh scaffolds, when cultured under perfusion for 16 days[178,181]. Moreover, adopting the same setup and constructs, the combination of uni-directional perfusion and osteogenic medium resulted in enhanced proliferation and differentiation of mesenchymal stem cells[182]. Subsequently, the bi-directional/oscillating perfusion mode, which was at first introduced to improve cell seeding efficiency[92,183–185], has emerged as an effective strategy to stimulate the constructs more uniformly by better recapitulating the multi-directional movement of the interstitial fluid within the native bone[46,48], promoting osteogenic differentiation as well[186–188]. In 2018, Beşkardeş et al. developed a bi-directional perfusion bioreactor based on a syringe pump and found that bi-directional perfusion, combined with osteogenic culture medium, enhanced osteogenic differentiation of pre-osteoblasts seeded on chitosan-hydroxyapatite scaffolds after 21 days of culture[188]. However, only one study compared the effects of uni- and bi-directional perfusion on 3D bone constructs, demonstrating that after 6 days bi-directional flow promoted more uniform cell proliferation and increased early osteogenic effects with respect to uni-directional flow[189]. This result was obtained by using two different non-automated perfusion systems: a uni-directional perfusion bioreactor (total culture medium volume = 250 mL) based on a pump for chromatography, and a bi-directional perfusion device based on a syringe pump acting on a flexible membrane (total culture medium volume = 1.5 mL). Moreover, due to their peculiar architectures and to the lack of automated control, the two perfusion devices needed different manual operating procedures. For overcoming the intrinsic limitations of manual procedures, a further crucial feature in advanced bioreactors is automation, which allows enhancing environmental control and reducing user intervention, thus increasing process reproducibility and standardization. In 2018, Schmid and co-workers developed a perfusion bioreactor with automated cell seeding and active control of oxygen concentration during the culture, facilitating the investigation of BTE constructs with high homogeneity and viability[177].

Besides the well-known mechanical stimuli characterizing the bone tissue environment in vivo, in the last decades further physical stimuli, clinically applied for boosting bone tissue regeneration, have been investigated. In particular, the non-invasive pulsed electromagnetic field

(PEMF) stimulation was demonstrated to foster bone cell proliferation, differentiation, and ECM protein expression, with evident beneficial effects in promoting endogenous bone healing[55,190–192]. PEMF stimulation induces a secondary electric field in the exposed tissue, like the one generated in native bone during the transduction of mechanical energy into electrical energy (bone piezoelectric behavior)[193], which can trigger the cell membrane depolarization and consequently stimulate ion currents[194]. However, due to the variety of PEMF stimulators and setups adopted, a complete understanding of the biological mechanisms induced by PEMF is yet missing and PEMF stimulation is empirically applied in the orthopedic clinical practice[98,193,195]. Thus, new investigation tools and approaches are required for performing in-depth studies that could lead to define optimal standardized PEMF protocols for treating the different pathological conditions.

Inspired by this scenario, we developed a novel automated perfusion bioreactor that allows culturing 3D constructs under tunable, automated uni- or bi-directional perfusion and that can be combined with PEMF stimulators. Computational modelling supported the design optimization of the bioreactor culture chamber, allowing characterizing the fluid dynamics and the magnetic field across it. Rapid, flexible and cost-effective 3D-printing techniques were adopted for the manufacturing phase. A user-friendly control unit was appositely developed for enabling setting and automated control of the perfusion unit, with the final aim of reducing the user dependency and increasing process reproducibility. For assessing the bioreactor performances in terms of perfusion, preliminary biological tests were performed on 3D bone tissue models, obtained by seeding human mesenchymal stem cells (hMSCs) on commercial bone substitutes, cultured under uni- or bi-directional perfusion. The biological effects of the different imposed culture conditions were evaluated in terms of cell viability, release of the early osteogenic differentiation marker alkaline phosphatase (ALP), and ECM deposition. Lastly, to verify the performances of the combined platform and to investigate the biological effect of combining bi-directional perfusion and PEMF stimulation, a real-time PCR-based test was performed culturing 3D bone tissue models for 14 days under three defined conditions: static condition, bi-directional perfusion, and bi-directional perfusion combined with PEMF stimulation. The expression of the osteogenic genes ALP and collagen type I were evaluated at the end of the culture.

3.2 Materials and Methods

3.2.1 Bioreactor design, components and working principle

The proposed bioreactor was designed for providing, in a controlled manner, tunable direct perfusion and to be combinable with a PEMF stimulator. In detail, the bioreactor is composed of: 1) a culture chamber, for housing the cultured 3D construct; 2) a perfusion unit, for providing uni- or bi-directional perfusion; 3) a control unit, for setting and automatically controlling the perfusion unit from outside the incubator. The bioreactor is combinable with a PEMF stimulation device (Figure 3.1a) to deliver individual or combined physical stimulations (uni- or bi-directional perfusion and/or PEMF stimulation) to the cultured constructs.

As regards the bioreactor development, supported by computational fluid dynamics (CFD) simulations, two versions of the culture chamber (identified as "CC1" and "CC2") were designed (SolidWorks, Dassault Systèmes, France). Both chamber layouts consist of two cylindrical screwable parts, equipped with inlet and outlet channels and luer threads (Figures 3.1b and 3.1c). Tailored flexible cylindrical holders, to be press-fit inserted within the culture chamber, allow to house 3D cylindrical constructs of different size (diameter (d) = 7-10 mm; height (h) = 1-15 mm). CC1 is characterized by an external (d = 48 mm, h = 61 mm) and internal (d = 20 mm, h = 42 mm) cylindrical geometry (culture chamber working volume = 10 mL), the inlet and outlet channels connect laterally to the internal volume, and watertightness is achieved by combining an interlocking mechanism and an O-ring inserted in the bottom part of the chamber for axial sealing (Figure 3.1b). CC2 layout was designed to improve the flow field distribution within the chamber and to reduce the working volume. In detail, CC2 has an external cylindrical geometry (d = 48 mm, h = 65 mm), while internally it is characterized by a truncated cone geometry upstream and downstream of the cylindrical central part (d = 24 mm, h = 15 mm), with a working volume of 2.5 mL. The inlet and outlet channels connect co-axially to the internal volume due to curved paths, and an O-ring is located on the top part of the chamber for radial sealing (Figure 1c). Based on CFD outcomes, CC2 was selected as the optimal layout that was then 3D-printed by stereolithography (SLA) using the biocompatible Dental SG Resin (Form 3, Formlabs, United States), setting a layer thickness of 50 μm (Figure 3.2a). Four cylindrical holders (internal d = 7, 8, 9, or 10 mm; external d = 24 mm; h = 15 mm) were manufactured by casting

biocompatible silicone (Sylgard 184, Dow Corning, United States) into modular acrylonitrile butadiene styrene (ABS) molds, 3D-printed by fused deposition modeling (uPrint SE Plus, Stratasys, United States), and curing them at 60°C for 5 h.

The culture chamber is connected to the perfusion unit (total culture medium volume = 50 mL), which is composed of: a culture medium reservoir with inlet and outlet ports, a medium sampling port, and air filters; oxygen permeable platinum-cured silicone tubing (Darwin Microfluidics, France); luer fittings (IDEX Health & Science, USA); and a peristaltic pump (G100-1J, Longer, China; for flow rate range see Supplementary Table 1) suitable to be incubated and to be connected to and controlled by the control unit (Figure 3.2b).

The control unit, connected to the pump via RS-485 serial communication, is enclosed in a compact box (135 x 130 x 60 mm3) and equipped with a microcontroller board (Arduino Micro, Arduino, Italy) that runs a purpose-built software. A user-friendly interface, based on four push buttons and one LCD display (Arduino, Italy), allows setting the perfusion parameters (Supplementary Table 3.S1, Figure 3.2b). In uni-directional mode, the flow direction can be set by selecting the direction of rotation of the pump head; however, in order to promote the outflow of possible air bubbles, a bottom-to-top flow is recommended. In bi-directional mode, the user can set the cycle duration, i.e., the time interval after which the flow direction is automatically inverted. Preliminary tests for assessing the bioreactor performance in terms of watertightness and reliability were performed (see Supplementary Material).

To deliver PEMF stimulation to the cultured constructs, a commercial PEMF stimulator composed of a generator and two solenoids was selected (magnetic field intensity = 1.5 mT, frequency = 75 Hz, IGEA Clinical Biophysics, Italy) and the bioreactor culture chamber was placed between the solenoids.
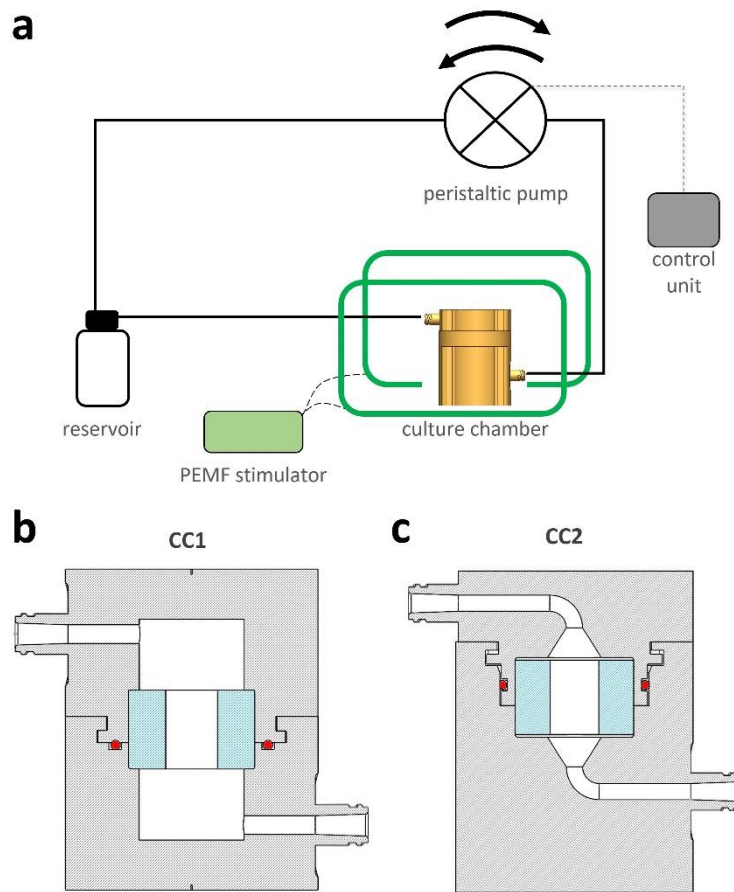
Figure 3.1. Bioreactor scheme and culture chamber design. (a) Schematic drawing of the bioreactor setup combined with the PEMF stimulator, with the connections among the culture chamber, the perfusion unit, and the control unit. Section views of the 3D models of CC1 (b) and CC2 (c), in grey the culture chamber, in blue the silicone holder, in red the o-ring.
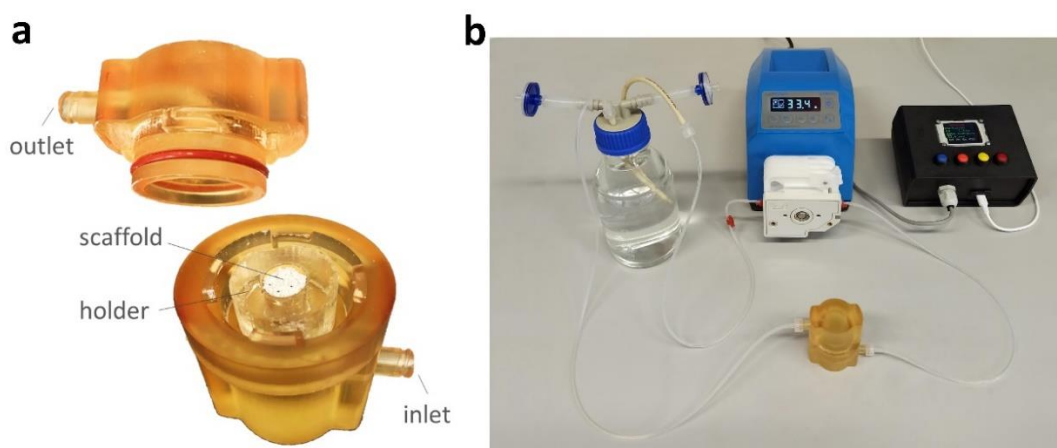
Figure 3.2. Bioreactor culture chamber. (a) The 3D printed CC2 is composed of a top part, equipped with the o-ring and the flow outlet, and a bottom part, housing the silicone holder and an exemplary scaffold. (b) Picture of the bioreactor components: culture chamber, perfusion unit, and control unit.

3.2.2 CFD simulations and wall shear stress estimation

For supporting the optimization of the culture chamber design, CFD simulations were performed. In detail, the 3D geometries of CC1 and CC2 were discretized with 3.41×10^6 and 4.99×10^5 elements, respectively, using tetrahedral elements for the bulk and hexahedral elements for the boundary layer (COMSOL Multiphysics 5.3, Comsol Inc., Sweden). The 3D construct, assumed as a reference cylinder (diameter = 10 mm, height = 15 mm), was modelled as a homogeneous and isotropic porous medium, imposing the properties (permeability $k = 3 \times 10^{-10}$ m^2, porosity $\varphi = 60\%$[196]) of the commercial Bio-Oss scaffold (Geistlich Pharma AG, Switzerland) adopted for the preliminary biological tests. The culture medium was modelled as an incompressible, Newtonian fluid (density $\rho = 9.94 \times 10^2$ kg/m^3, dynamic viscosity $\mu = 6.89 \times 10^{-4}$ Pa·s at 37 °C). Using a finite element-based commercial code (COMSOL), the governing equations of fluid motion were solved in their discretized form in the fluid domain, while the Brinkman equation[197] in its discretized form was adopted for describing perfusion in the porous domain. Four steady-state simulations were performed for each culture chamber layout, with and without the 3D construct and prescribing uni-directional perfusion with flow rate values of 0.3 and 1.0 mL/min (imposing a parabolic velocity profile) at the inlet of the culture chamber bottom. A reference pressure was imposed at the outlet, and the no-slip condition was applied at the internal walls of the culture chambers. Moreover, in order to investigate the development of the flow upstream of the construct within CC1 and CC2, the velocity field distributions were analyzed at 3 different horizontal sections of the culture chamber bottom (see Supplementary Figure 3.S1).

The simulated flow regimes within CC1 and CC2, expressed in terms of Reynolds number (Re) calculated considering the internal diameter of the inlet channel (3.7 mm) as the characteristic length, resulted to be laminar (Re = 2.48 for 0.3 mL/min; Re = 8.28 for 1.0 mL/min). Following the adoption of the Brinkman equation, the wall shear stress (τ_w) in the porous construct was evaluated using the expression obtained by Wang and Tarbell[198,199], which provides an accurate estimation for constructs with permeability higher than 10^{-10} m^2:

$$\tau_w = \frac{4}{\pi} \frac{\mu}{\sqrt{k}} v_{avg}$$

where μ is the dynamic viscosity of the culture medium, v_{avg} is the average velocity of the culture medium within the construct as obtained from CFD simulations, k is the construct permeability, and a null cell density was assumed.

3.2.3 Electromagnetic field simulations

Electromagnetic field simulations were performed to assess the suitability of the proposed bioreactor to be used in combination with a reference PEMF stimulator[96]. In detail, a 3D steady-state simulation was carried out adopting a finite element-based commercial code (COMSOL Multiphysics 5.3, Comsol Inc., Sweden) for investigating the distribution of the magnetic field within CC2 when placed between the two solenoids of the PEMF stimulator (see Supplementary Figure 3.S2). The CC2 internal geometry was discretized using 2.25×10^6 tetrahedral and 1.61×10^5 triangular elements. The Ampere's Law was solved in its discretized form imposing a current of 160 mA at each solenoid. A magnetic insulation condition (n × A = 0, where A is the magnetic potential) was prescribed at the domain boundaries. Each component was modelled according to its electromagnetic properties (Supplementary Table 3.S2).

3.2.4 3D bone tissue model preparation and culture

Commercially available bone marrow-derived human mesenchymal stem cells (hMSCs) were obtained from Merck (C-12974 PromoCell GmbH, Germany) and cultivated in low-glucose Dulbecco's modified Eagle Medium (DMEM, Sigma-Aldrich, United States) supplemented with 15% fetal bovine serum (FBS, Sigma-Aldrich, United States) and 1% penicillin/streptomycin into a standard incubator (37°C, 5% CO_2). Each 3D bone tissue model was obtained by seeding 4×10^6 cells into a pre-molded cylinder (diameter = 10 mm, height = 6 mm) of commercial bone substitute Bio-Oss (Geistlich Pharma AG, Switzerland), as previously described[200]. The 3D constructs were then statically pre-cultured in incubator for 48 h to allow full cell adhesion and spread.

For perfusion culture, the 3D bone tissue model was inserted in the flexible holder and housed in the bioreactor culture chamber, previously filled with 1 mL of fresh culture medium. The bioreactor was then located in incubator, the control unit was set (flow rate = 0.3 mL/min, uni- or bidirectional (cycle duration = 2 h) perfusion mode), and the pump was automatically put into operation (Supplementary Figure 3.S3a). The

construct was dynamically cultured for 3 or 6 days, under continuous perfusion, with a total culture medium volume of 50 mL. Analogous constructs were cultured in static conditions for the same time intervals as control tests (Supplementary Figure 3.S4), with a total culture medium volume of 3 mL that was changed every 3 days, following the physiological degradations of the culture medium key components, such as serum. Experiments were performed in triplicate.

3.2.5 Assessments of 3D bone tissue models culture under perfusion

At day 3 or day 6 time-points, the effect of the applied uni- or bi-directional perfusion was investigated in terms of cell viability and alkaline phosphatase (ALP) release. Cell viability was evaluated by assessing cell metabolic activity by the colorimetric Alamar blue assay (Life Technologies, Italy). At each time-point, constructs cultured under dynamic or static conditions were collected, then submerged by the Alamar blue solution and incubated for 4 h in the dark. Afterwards, 100 µL were moved into a black 96-well plate, and the fluorescence signals were evaluated with a spectrophotometer (Spark®, Tecan Trading AG, Switzerland) using a 590 nm wavelength for the reading. The early osteogenic marker ALP released by constructs cultured under dynamic or static conditions was measured in the supernatants using a colorimetric assay (ab83369 from AbCam, United Kingdom). Briefly, 80 µL of each supernatant was collected and mixed with 50 µL of the pNPP solution and 10 µL of the ALP enzyme. After 60 min, the optical density was evaluated by spectrophotometry (Spark®, Tecan Trading AG, Switzerland) using a 405 nm wavelength. Moreover, at day 6, the deposition of ECM was verified by histology. The 3D bone tissue models cultured under dynamic or static conditions were collected, fixed with 10% formalin, dehydrated by the alcohols' scale (70-90-100), and embedded in resin (Tecnovit 7200, Kulzer, Germany). Afterwards, the constructs were horizontally (top-down) sliced in parallel to the flow direction, along the mechanically polished diameter and surface, to a final thickness of 80 µm. Histological analysis was performed on the central slices representative of the core of the scaffolds by means of Toluidine blue. Images were acquired using an optical digital scanner (NanoZoomer S60, Hamamatsu Japan).

3.2.6 Combined bi-directional perfusion and PEMF stimulation culture and real-time PCR analysis

To verify the performances of the combined platform and to investigate the biological effect of combining bi-directional perfusion and PEMF stimulation, 3D bone tissue models, prepared as previously described, were cultured for 14 days under: i) static culture (control); ii) bi-directional perfusion (flow rate = 0.3 mL/min, cycle duration = 2 h); iii) bi-directional perfusion (flow rate = 0.3 mL/min, cycle duration = 2 h) combined with PEMF stimulation (magnetic field intensity = 1.5 mT, frequency = 75 Hz, exposure time = 24 h/day, see Supplementary Figure S3b). In order to avoid any interference due to biochemical stimulation, constructs were cultivated with maintenance medium (DMEM). At the end of the culture, real-time PCR was performed to evaluate the expression of the early osteogenic gene ALP and of the late osteogenic gene collagen type I (COL 1). Experiments were performed in triplicate. Total RNA extraction was performed using TRIzol (Invitrogen Life Technologies, Italy) according to the manufacturer's instructions. Briefly, samples were placed in multiwell cell culture plates and incubated with 500 µL of TRIzol solution at room temperature for 10 min. The resulting solutions were transferred to 1.5 ml microtubes, and 100 µL of chloroform was added on ice and mixed well. The samples were kept at room temperature for 2-3 min, and then centrifuged at 12000 g for 15 min at 4°C. The upper aqueous layers were transferred to new 1.5 ml microtubes, and the same corresponding volume of isopropanol was added and mixed well. The samples were kept on ice for 10 min, and then centrifuged at 12000 g for 10 min at 4°C. The resulting pellets were then washed twice with 75% ethanol, by adding 500 µL of 75% ethanol to the pellets, vortexing to detach the pellet, centrifuging at 7500 g for 5 min at 4°C, and then discarding the supernatant. The pellets were allowed to dry and then resuspended in 20 µL of diethylpyrocarbonate (DEPC)-treated water and stored at -80°C until use. The quantity and purity of the recovered RNA were determined via absorbance measurements at 230, 260, and 280 nm using the NanoPhotometer™ N60 Micro-Volume UV-VIS Spectrophotometer (Implen, CA, USA). Gene expression analysis was performed using the two-step RT-qPCR. First, retrotranscription was performed to the RNA templates (0.2 µg) using the iScript gDNA Clear cDNA Synthesis Kit (Bio-Rad Laboratories, CA, USA), according to the manufacturer's instructions, and a thermal cycler (Mastercycler X50s,

Eppendorf). The obtained cDNA templates were stored at -20°C until further use. Real-time qPCR was performed using the SsoAdvanced Universal SYBR® Green Supermix (Bio-Rad Laboratories, CA, USA) and a thermal cycler (C1000 Touch Thermal Cycler, CFX96 Real-Time System, Bio-Rad Laboratories, CA, USA). In brief, each reaction consisted of a total volume of 20 μL containing 1 μL of each primer, 2 μL of cDNA, 10 μL SYBR Green super mix and 6 μL of nuclease-free water. Each PCR reaction was run in technical triplicates. The thermal cycling conditions adopted were: 95°C for 30 s, followed by 40 cycles of amplification at 95°C for 5 s, and 60°C for 15 s, and eventually the melting curves were analyzed. The target genes used were ALP and collagen type I alpha 1 chain (COL1A1), whereas, the reference gene used was the ribosomal protein L34. For data analysis, the fold change (FC) of each gene expression was calculated using the $2^{-\Delta\Delta Ct}$ method, and the reference gene was used to normalize the results.

3.2.7 Statistical analysis

All biological experiments were performed in triplicate and results were statistically analyzed using the SPSS software (v.20.0, IBM, United States). Data normal distribution and homogeneity of variance were confirmed by the Shapiro-Wilk's and the Levene's test, respectively; then, groups were compared by the one-way ANOVA using the Tukey's test as post-hoc analysis. Significant differences were established at $p < 0.05$.

3.3 Results

3.3.1 CFD simulations and wall shear stress estimation

The CFD simulations allowed characterizing the hydrodynamics within CC1 and CC2 layouts at the imposed flow rates of 0.3 mL/min (Figure 3.3) and 1 mL/min (Supplementary Figure 3.S5) for finally defining the optimal layout. In detail, the flow streamlines developing within CC1 reveal recirculation regions in the bottom and top parts of culture chamber, both without (Figure 3.3a and Supplementary Figure 3.S5a) and with the construct inserted (Figure 3.3b and Supplementary Figure 3.S5b). Differently, within CC2 the flow streamlines follow the internal geometry of the culture chamber avoiding recirculation regions, both without (Figure 3.3c and Supplementary Figure 3.S5c) and with the construct inserted (Figure 3.3d and Supplementary Figure 3.S5d). As regards the velocity field upstream of the construct (Figure 3.4), the contour plots of the longitudinal velocity component show that the velocity field within CC1 is unevenly distributed (Figure 3.4a), with the maximum velocity value misaligned with respect to the longitudinal axis close to the inlet and a flattened flow profile at the entrance of the construct. As regards the in-plane velocity vectors, they present a diverging pattern close to the inlet while a converging pattern approaching the construct (Figure 3.4a). Differently, in CC2 the velocity profile is symmetric and parabolic everywhere upstream of the construct (Figure 3.4b). Moreover, within CC1 it is possible to observe the presence of wide regions characterized by very low or null velocity where flow stagnation can occur, particularly at the bottom of the culture chamber (Figure 3.4a), while in CC2 only the regions close to the walls are exposed to low or null velocities (Figure 3.4b). Therefore, CC2 was selected as the optimal layout to be manufactured. The wall shear stress values within the construct, calculated from the average velocity values obtained from the CFD analysis, turn out to be 3.23 or 10.75 mPa for both CC1 and CC2, depending on the imposed flow rates (0.3 and 1.0 mL/min, respectively, see Supplementary Table 3.S3).
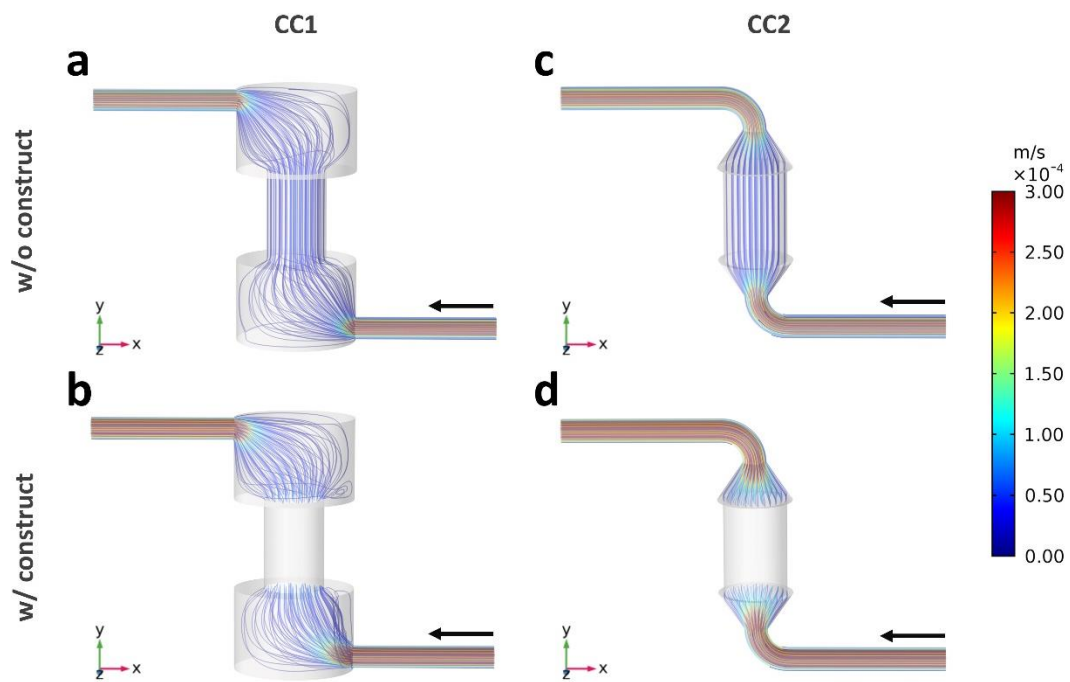
Figure 3.3. Flow streamlines developing within CC1 and CC2 imposing a modeled flow rate of 0.3 mL/min and color-coded with respect to velocity values. (a) CC1 without construct. (b) CC1 with an inserted construct modelled as porous medium. (c) CC2 without construct. (d) CC2 with an inserted construct modelled as porous medium.
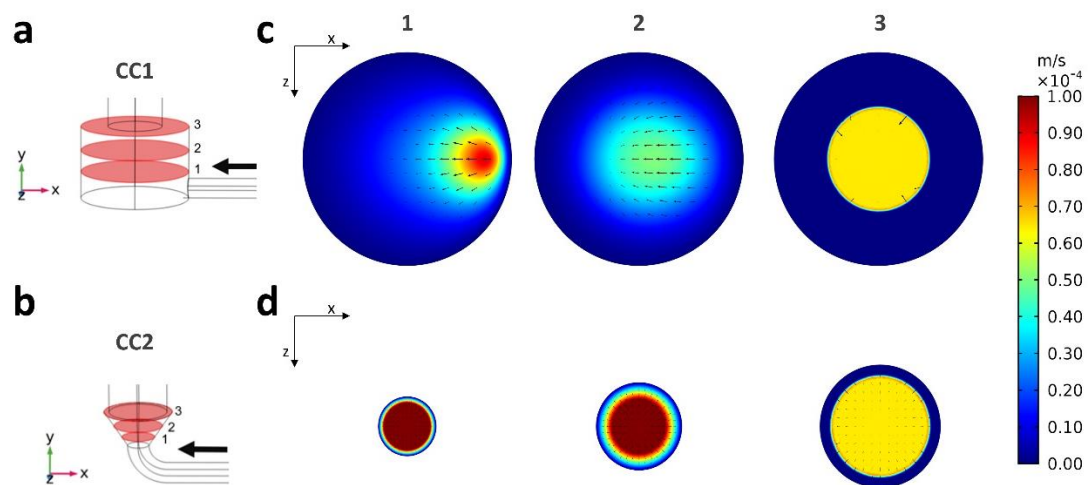
Figure 3.4. Development of the flow upstream of the construct within CC1 and CC2, analyzed at 3 different horizontal sections. (a) Bottom part of CC1 with horizontal sections. (b) Bottom part of CC2 with horizontal sections. Contour plots of the velocity component along the longitudinal axis of the culture chamber with vectors of in-plane velocity components for the three horizontal sections of CC1 (c) and of CC2 (d).

67

3.3.2 Electromagnetic field simulations

The electromagnetic field simulations confirmed that positioning the bioreactor culture chamber between the two solenoids of the PEMF stimulator does not affect the magnetic field distribution, neither on the xy (Figure 3.5a) or xz (Figure 3.5b) cross planes. Additionally, the simulations clearly showed that the construct housed in the bioreactor culture chamber is exposed to a uniform magnetic field, as testified by the magnetic field magnitude isolines and the contour plots on the longitudinal (Figure 3.5c) and transverse (Figure 3.5d) sections of the culture chamber. The magnetic field intensity resulting on the region occupied by the construct is 1.5 mT, in accordance with the nominal value specified by the stimulator manufacturer.
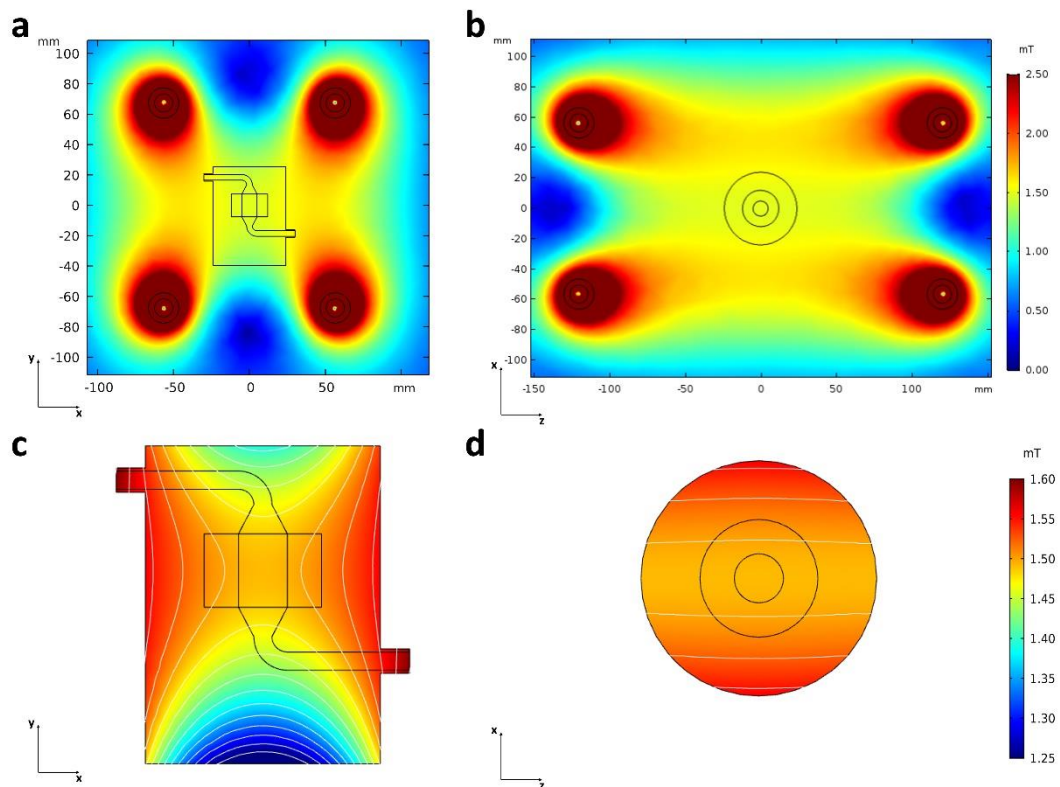
Figure 3.5. Contour plots with isolines of the magnetic field magnitude developing around and within the bioreactor culture chamber located between the PEMF stimulator solenoids. (a) Distribution of the magnetic field on the xy cross plane. (b) Distribution of the magnetic field on the xz cross plane. (c) Distribution of the magnetic field within the longitudinal section of the culture chamber. (d) Distribution of the magnetic field within the transverse section of the culture chamber.

3.3.3 Assessments of 3D bone tissue models culture under perfusion

To assess the suitability of the bioreactor culture, 3D bone tissue models were cultured under uni- or bi-directional perfusion and in static conditions. The metabolic activity of cells exposed to uni- or bi-directional perfusion was comparable (>90%, p>0.05) to that of constructs cultured under static conditions, at both day 3 and day 6 (Figure 3.6a). Interestingly and in accordance with literature, both uni- and bi-directional perfusion conditions determined an increase of the release of the early osteogenic marker ALP in the supernatant in comparison to static controls (p<0.05, indicated by §, Figure 3.6b). In particular, after 3 days of culture, an increase of almost 10-12% of ALP release was observed for the dynamic cultured constructs, and after 6 days of culture, the ALP release significantly increased up to 20-21%, as summarized in Table 3.1. No significant differences were observed by comparing the uni- and the bi-directional perfusion conditions (p>0.05). As regard ECM deposition and distribution, the histological analysis of the constructs harvested at day 6 showed that both uni- and bi-directional perfusion conditions were effective in stimulating adherent cells to produce ECM in comparison to the static control (Figure 3.7). In fact, the ECM deposits (stained in blue and indicated by arrows) were much more abundant in the perfused constructs (Figure 3.7b and 3.7c) than in the static cultured ones (Figure 3.7a), as it can be appreciated in both low and high magnification images. Moreover, comparing the uni- and the bi-directional perfusion conditions, a more homogeneous and consistent ECM deposition was observed for the bi-directional perfusion (Figure 3.7c), demonstrating that such condition is more efficient in stimulating adherent cells to secrete ECM.
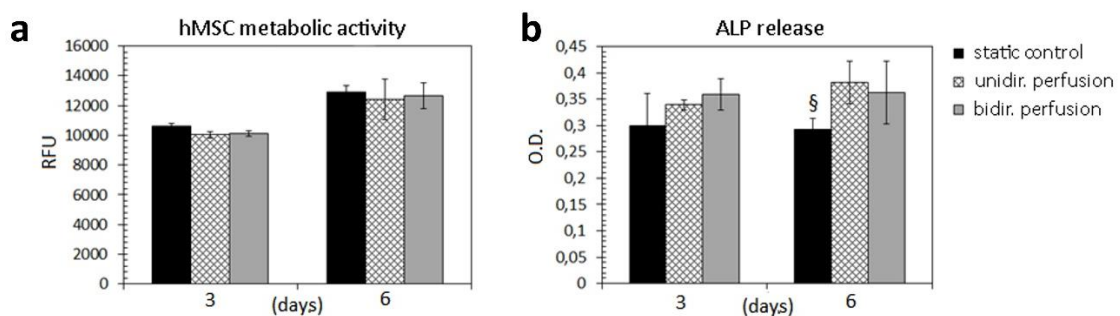
Figure 3.6. Biological assessments. (a) Metabolic activity of the 3D constructs cultured under static conditions (control), uni-directional

perfusion, and bi-directional perfusion assessed at day 3 and day 6. (b) ALP released by the 3D constructs cultured under static conditions (control), uni-directional perfusion, and bi-directional perfusion assessed at day 3 and day 6 (p<0.05 indicated by §). Bars represent means and standard deviations, replicates n = 3.

Table 3.1. Increase of ALP release under perfusion culture.

ALP release (% vs static control)		
Bioreactor setup	*Day 3*	*Day 6*
Uni-directional perfusion	+ 10.82%	+ 21.23%
Bi-directional perfusion	+ 12.23%	+ 20.72%
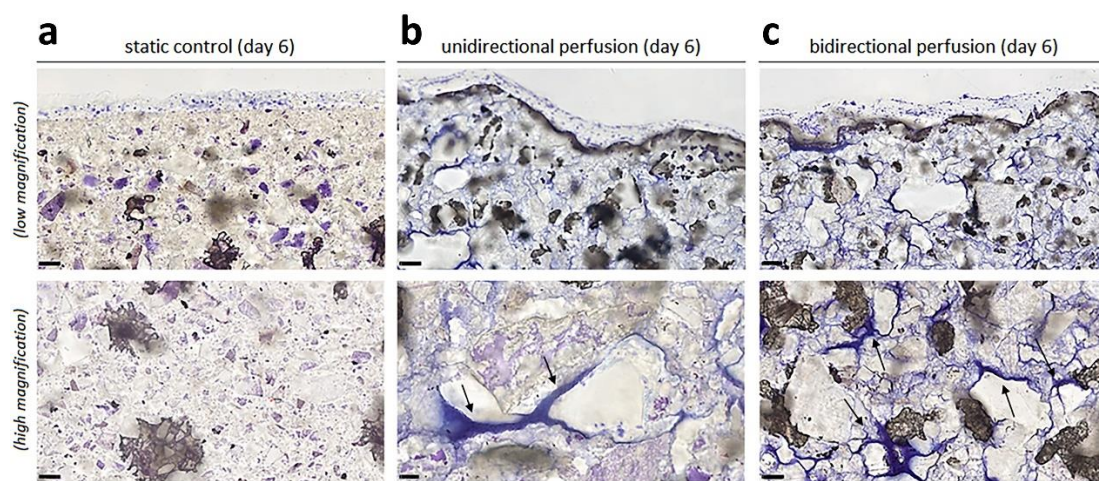
Figure 3.7. Histological images of the 3D constructs stained by Toluidine blue after 6 days of cultivation in (a) static conditions, (b) uni-directional perfusion, and (c) bi-directional perfusion. The black arrows indicate the ECM deposits throughout the constructs. Low magnification, bar scale = 100 μm; high magnification bar scale = 50 μm.

3.3.4 Combined bi-directional perfusion and PEMF stimulation culture and real-time PCR analysis

To verify the performances of the combined platform and to assess the biological effect induced by the combination of bi-directional perfusion and PEMF stimulation, 3D bone tissue models were cultured for 14 days under three defined conditions (static culture (control); bi-directional perfusion; bi-directional perfusion combined with PEMF stimulation) and using maintenance medium (DMEM) to avoid any biochemical osteogenic stimulus. At the end of the culture, the expression of the early ALP and late COL1 osteogenic genes was evaluated (Fig. 3.8). In particular, observing the

expression of COL1 gene normalized to static culture (Fig. 3.8a), the bi-directional perfusion condition caused a ~40-fold increase in comparison to the control, confirming that the fluid flow-induced shear stress plays a crucial role in fostering the expression of collagen type I, even without biochemical stimulation. More interestingly, the combination of bi-directional perfusion and PEMF stimulation induced an even stronger pro-osteogenic effect, with an almost 80-fold increase in comparison to the control. This suggests that the further ~40-fold higher expression with respect to the bi-directional perfusion condition could be due to the effect of the secondary electric field induced in the constructs by the PEMF stimulation.

Less evident differences were observed on the expression of the early osteogenic marker ALP among the three culture conditions (Fig. 3.8b). In fact, the bi-directional perfusion condition led to a ~1-fold increase, whereas the combination of bi-directional perfusion and PEMF stimulation induced a ~1.5-fold increase with respect to the control.
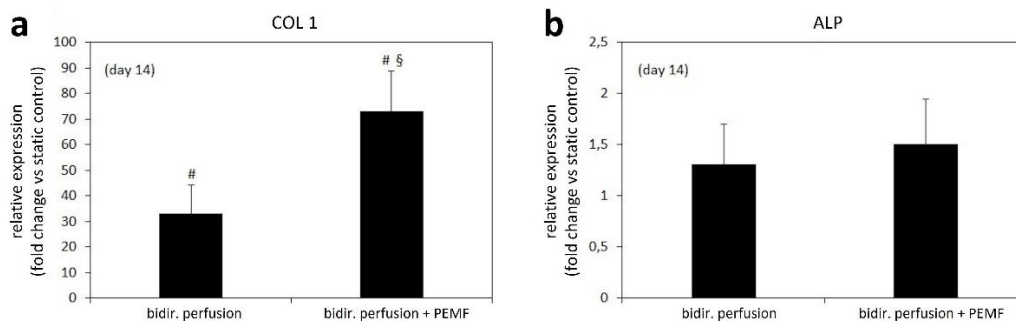
Figure 3.8. Real-time PCR results. (a) Collagen type I (COL 1) and (b) alkaline phosphatase (ALP) genes expression of 3D bone tissue models cultured for 14 days under static culture (control), bi-directional perfusion, or bi-directional perfusion combined with PEMF stimulation ($p < 0.05$ with respect to control indicated by #, $p < 0.05$ with respect to bi-directional perfusion indicated by §). Bars represent means and standard deviations, replicates n=3

3.4 Discussion

In the emerging and multidisciplinary research field of mechanobiology, it is clearly recognized that physical stimuli arising from the surrounding microenvironment or externally applied play a crucial role in influencing cell fate[5,201] and, at the tissue scale, tissue development, homeostasis, and even disease pathogenesis could be strictly dependent on physical forces[3]. In particular, bone and cartilage are among the tissues mostly influenced by mechanical stimuli *in vivo*: being deputed to the body support and mechanical stress dissipation, osteochondral tissues are highly exposed to compression and fluid flow-induced shear stress. In parallel, further physical stimuli, such as the non-invasive PEMF stimulation, are increasingly adopted in clinical practice for promoting endogenous bone healing[195]. However, a full understanding of the biological mechanisms induced in bone tissue by defined physical stimuli is still missing and the influence of different stimulation parameters and combinations is unknown[202], leading to empirical treatments.

Inspired by the need of unrevealing how physical stimuli regulate cell and tissue functions, we developed a versatile automated perfusion bioreactor combinable with PEMF stimulation devices. As regards the bioreactor culture chamber, two layouts were designed (Figures 3.1b and 3.1c) and compared in terms of hydrodynamic performances. The outcomes of the computational analysis confirmed that the internal geometry of the CC2 layout allows the development of a symmetric flow profile within the culture chamber and minimizes the regions with low or null longitudinal velocity (Figures 3.3 and 3.4), reducing the risk of recirculation and stagnation zones. For these reasons and due to the limited working volume (2.5 mL), CC2 design was selected as the optimal geometry and was then manufactured by the SLA 3D-printing technique, which allowed fabricating the bioreactor following a single-step procedure, reducing complexity, costs and lead time[69,72,185,203–205] (Figure 3.2a). To provide controlled uni- or bi-directional perfusion, the closed-loop perfusion unit was equipped with a peristaltic pump suitable to be incubated and to be externally controlled. For the control unit, the selection of a low-cost open-source microcontroller board allowed combining control accuracy and reliability with compactness, flexibility, and cost-efficiency (Figure 3.2b). Placed outside the incubator, the user-friendly control unit allows externally setting and

72

automatically controlling the perfusion unit, while keeping constant the incubator conditions and reducing the contamination risk.

The automated perfusion control, which enables selecting uni- or bi-directional perfusion mode within the same platform and without user intervention along the culture, is the first significant advantage and novelty of the proposed bioreactor. Indeed, conventional bioreactors providing uni-directional perfusion are either non-automated[178,182] or exploit automation strategies for regulating the flow rate, but do not allow reverting the flow direction[177]. On the other side, bioreactors delivering bi-directional perfusion are commonly based on syringe pumps[187,188,206], which are unsuitable for providing continuous uni-directional perfusion. The only study that compared uni- and bi-directional perfusion on 3D bone constructs adopted two non-automated perfusion systems characterized by different total culture medium volumes (250 mL vs 1.5 mL, respectively)[189]. Differently, our bioreactor allows comparing uni- and bi-directional perfusion modes using the same device and total culture medium volume (50 mL).

As concerns the shear stress values induced by direct perfusion, several studies investigated the optimal range for *in vitro* dynamic culture of 3D bone tissue modes[49,207]. In detail, shear stress values ranging from 0.55 mPa to 24 mPa were shown to stimulate osteogenic differentiation of hMSCs and to promote ECM mineralization in both β-tricalcium phosphate[208] and silk fibroin[209] scaffolds. Differently, values exceeding 60 mPa were shown to result in cell death/detachment[210], while values below 0.1 mPa did not stimulate any ECM mineralization[211]. In our study, the shear stress values developing within the construct under uni-directional perfusion were estimated to be 3.23 or 10.75 mPa, depending on the imposed flow rate (0.3 and 1.0 mL/min, respectively), thus confirming the suitability of the bioreactor for *in vitro* bone tissue culture and maturation.

As proof of concept, biological experiments imposing uni- or bi-directional perfusion mode on 3D bone tissue models, based on hMSCs seeded on Bio-Oss scaffolds, were performed. Being a pre-validated therapeutic product applied in clinic for small bone defects repair, Bio-Oss allowed specifically correlating the biological results with the applied perfusion conditions (uni- or bi-directional mode with respect to the static control). To our knowledge, this is the first time that, thanks to automation, uni- and bi-directional perfusion modes were compared using the same platform and total culture medium volume. Firstly, it was demonstrated

that the bioreactor perfusion culture does not introduce any disturbance for the cells in comparison to the static control in terms of metabolic activity (Figure 3.6a). Actually, the imposed flow rate (0.3 mL/min) was appositely selected to mimic the interstitial fluid features in the native tissue[212], providing native-like flow-induced shear stress to the cells. Moreover, no significant differences were observed between uni- and bi-directional perfusion conditions in terms of cell viability (Figure 3.6a). The biological effect of the perfusion culture emerged from the evaluation of the early osteogenic marker ALP (Figure 3.6b). In fact, just providing direct uni- or bi-directional perfusion for a short-term culture (6 days), without the use of osteogenic medium, a general increase of the ALP release was observed for the constructs cultured under perfusion with respect to the static controls (+10-12% at day 3 and +20-21% at day 6). This is in accordance with previous findings, showing that flow-induced shear stress alone is crucial for boosting osteogenic differentiation[189,213]. No significant differences were observed by comparing the uni- and the bi-directional perfusion modes in terms of ALP release; however, histological assessment enabled revealing the effect of the perfusion mode in terms of stimulation of cells in secreting and depositing ECM within the construct pores. Indeed, it is well known that flow-induced shear stress can influence ECM deposition[214,215]. In particular, in literature it was shown that uni-directional perfusion can induce an inhomogeneous ECM deposition within the construct, due to the different fluid transport and consequent shear stress values experienced by the cells located in the proximal and distal parts of the construct with respect to the main fluid direction[189]. Conversely, bi-directional perfusion has been reported as an effective strategy to provide uniform mechanical stimulation over time to the construct, promoting osteogenesis in a more effective manner and inducing homogeneous ECM deposition along the whole 3D bone tissue models[189]. In our study, the histological images of the 3D constructs harvested after 6 days of uni- or bi-directional perfusion and stained with Toluidine blue confirmed that perfusion favors cells to better penetrate the scaffold structure as well as to deposit more ECM with respect to static conditions. Notably, the ECM deposition was more marked for the constructs exposed to bi-directional perfusion, confirming the hypothesis that a bi-directional flow can represent a more efficient culture condition for 3D constructs mimicking physiological tissues. In particular, Toluidine blue was selected for the staining of the 3D bone tissue models as it specifically visualize the proteoglycan content in a tissue[216]. Proteoglycans and

glycoproteins represent the majority of the non-collagenous proteins of the bone matrix. During the bone healing process, proteoglycans such as decorin, biglycan, and osteoadherin play a pivotal role in promoting and supporting the early mineralization of the matrix in the first stages of osteogenesis. Therefore, it can be speculated that the regions positive to the Toluidine blue staining showing a dark-blue pigmentation are representative of early mineralization occurring in the pores of the constructs cultured under perfusion.

Lastly, as regards the PEMF stimulation, the results from the electromagnetic field modelling showed that the proposed bioreactor is in principle suitable to be combined with a commercial PEMF stimulator for exposing 3D bone tissue models to uni-/bi-directional flow-induced shear stress and uniform pulsed electromagnetic field (Figure 3.5). Dedicated biological tests were then performed for verifying the performances of the combined platform and for investigating the biological effect on 3D bone tissue models of combining bi-directional perfusion and PEMF stimulation. The constructs were cultured for 14 days under three different conditions (i.e., static culture (control), bi-directional perfusion, and bi-directional perfusion combined with PEMF stimulation) and, for all experiments, the maintenance medium (DMEM) was adopted for avoiding the interference of biochemical stimulation that could lead to misleading interpretation of the effects of the applied physical stimulations. At day 14, the expression of the early osteogenic gene ALP and the late osteogenic gene COL 1 were evaluated by real-time PCR (Figure 3.8). Results revealed that bi-directional perfusion *per se* induced a ~40-fold up-regulation of COL 1 in comparison to the control, and the further combination with PEMF stimulation boosted the up-regulation of COL1 up to ~80-fold (Figure 3.8a). This result represents a promising evidence that the combination of bi-directional perfusion and PEMF stimulation leads to a positive synergic contribution in promoting the expression of COL1, which is a fundamental component of the bone matrix. Indeed, collagen type I represents the 90-95% of the organic components of the bone tissue and is one of the key factors in determining the bone mechanical properties (particularly elasticity and flexibility)[217]. At the cellular and subcellular level, this synergic effect is due to the combination of the fluid flow-induced shear stress and the PEMF secondary electric field induced in the constructs. Fluid flow-induced shear stress acts on the cell membrane and can deform it, leading to alteration of membrane proteins and causing mechano-activated ion channels to open

and allow the influx of cations, such as Ca^{2+}, Na^+, and K^+, into the cell[180,218]. In parallel, PEMF stimulation can trigger the depolarization of the cell membrane and consequently stimulate ion currents, such as opening the Ca^{2+} channels and leading to an intracellular Ca^{2+} ion accumulation[219,220]. Such ions unbalance can activate specific cascades, such as the nuclear factors of activated cells (NFAT), enabling the transcription and the synthesis of osteogenic proteins[221]. Regarding the less evident effect of up-regulation observed for the ALP expression, although present (Figure 3.8b), it should be noted that several studies reported ALP to be upregulated within 2 days of osteogenic induction[222]; therefore, 14 days could represent a too long culture time for appreciating the effect of physical stimulation on ALP expression.

In literature, only the study of Wang and colleagues combined a perfusion bioreactor with a sinusoidal electromagnetic field (EMF) generator[192]. In detail, rabbit MSCs were seeded on hydroxyapatite/collagen scaffolds and the constructs were cultured for 14 days under uni-directional perfusion (10 mL/min) and EMF stimulation (magnetic field intensity = 1 mT, frequency = 15 Hz, exposure time = 4 h/day) with and without osteogenic culture medium, obtaining enhanced osteogenic differentiation at the end of the culture, similarly to our results. However, the system proposed by Wang et al. allowed delivering only uni-directional perfusion with no automated control of the pump[192]. Therefore, a further advantage and novelty of the here presented platform is related to its versatility to combine automated uni-/bi-directional perfusion and PEMF stimulation, which was demonstrated to be crucial for boosting pro-osteogenic differentiation in 3D bone tissue models.

Some limitations could affect this study. In the CFD modelling the construct was assumed as a homogeneous and isotropic porous medium, lacking the information about the real microarchitecture of the Bio-Oss scaffold and neglecting the presence of the cells. Moreover, the simulations did not take into account that along the culture the construct geometry is modified by cell proliferation and ECM deposition, which cause a decrease of the mean pore size and an increase of shear stress values over time. For these reasons, the computed shear stress values can be considered as a reasonable estimation for the early culture stage and in the future micro-computed tomography imaging of the constructs will be performed at day 0 and at different time points in order to precisely characterize the flow dynamics within the construct along its maturation[107,223,224]. As regards the

electromagnetic field modelling, it was performed in steady-state conditions. Although this approach neglects the temporal evolution of the magnetic field occurring during a PEMF pulse, the results were sufficiently accurate for describing the conditions occurring at the pulse peak while allowing a significant reduction of the computational costs. Concerning the biological tests, it should be noted that for the perfusion condition an higher culture medium volume was used with respect to the static condition (50 mL vs 3 mL changed every 3 days, respectively). A higher culture medium volume provides a higher amount of nutrients, and it could be speculated that this aspect, rather than fluid flow-induced shear stress, could favor the metabolic activity of the cells cultivated under perfusion with respect to the statically cultured ones. However, the fact that the ECM deposition was more marked for the constructs exposed to bi-directional perfusion with respect to the ones cultured under uni-directional perfusion (same culture medium volume) confirms that perfusion plays a beneficial role in ECM deposition. Lastly, the adopted Bio-Oss scaffold probably further contributed to stimulate osteogenesis due to its chemical composition. However, since all the constructs cultured under either static or dynamic conditions were based on Bio-Oss scaffolds and were cultured using the same basal medium (DMEM), the observed differences can be directly ascribed to the applied culture conditions.

3.5 Conclusion

In this study, we developed, characterized, and tested a tunable perfusion bioreactor based on automated control that can be combined with PEMF stimulation devices to be used as powerful tool for *in vitro* BTE production and investigations. The bioreactor is highly versatile as it allows housing constructs of different size and delivering individual or combined flow-induced shear stress and PEMF stimulations. Moreover, the adopted automation strategy enables providing uni- or bi-directional perfusion within the same platform and and using the same total culture medium volume, significantly reducing the user intervention and dependence along the culture, increasing robustness and reproducibility of the culture process. The preliminary biological tests demonstrated that the only application of perfusion was crucial for promoting osteogenic differentiation in the cultured constructs, even without the use of biochemical stimulation. In fact, uni- and bi-directional perfusion conditions were effective in stimulating the osteogenic differentiation of the cultured 3D bone tissue models, and highlighted that bi-directional perfusion better promoted the ECM deposition throughout the construct. Lastly, as regards PEMF stimulation, biological results demonstrated the synergic pro-osteogenic effect of combining bi-directional perfusion and PEMF stimulation and confirmed that the proposed platform could be used for both the production of BTE constructs and as powerful investigation tool. In the next future, an advanced investigation approach, based on the proposed bioreactor and high-throughput analyses, could lead to unravel molecular mechanisms activated by biophysical stimulation applied in clinic and to define the precise combinations of parameters inducing specific biological effects, paving the way for optimized orthopedic clinical protocols.

_____

Supplementary Material

Preliminary performance tests

The watertightness and reliability of the bioreactor were preliminarily tested in-house. Firstly, the CC2 underwent 5 autoclave cycles, to assess the maintenance of geometry and functionality. No deformations were observed in the CC2 components. Secondly, the CC2 was connected to the perfusion unit and tested in uni-directional perfusion mode with and without a reference scaffold (Bio-Oss, Geistlich Pharma AG, Switzerland), using distilled water at room temperature and imposing the highest flow rate provided by the pump (24 mL/min) for 58 h. No leakage was observed both with and without the reference scaffold inserted. Moreover, in the case of scaffold inserted, the applied bottom-to-top uni-directional perfusion efficiently promoted the outflow of air, preventing the residence of air bubbles that could impair the culture process. Lastly, the control unit was connected to the pump and the bi-directional perfusion mode was tested setting different cycle durations and checking the inversion timing using a stopwatch. The control unit timing respected the prescribed conditions.

Supplementary Table 3.S1. Perfusion parameters

Parameter	Range
Tubing size (internal diameter)	1.0 or 2.4 mm
Flow rate	0.006 - 6 mL/min (1.0 mm tubing)
	0.024 - 24 mL/min (2.4 mm tubing)
Perfusion mode	uni-directional/bi-directional
Direction of rotation	clockwise/counterclockwise
Cycle duration	1 s - 24 hours

Supplementary Table 3.S2. Electromagnetic properties of the modelled domains (when the properties were unknown, an analogous material was considered).

Domain	Electric conductivity (S/m)	Relative permittivity	Relative permeability
Culture chamber (photopolymer)	$1*10^{-14}$	3.1	1
Holder (PDMS)	$2.5*10^{-14}$	2.4	1

Construct (glass ceramic) [225]	1*10⁻⁷	24.5	1
Culture medium [83,150]	1.45	80	1
Coils (copper)	5.998*10⁷	1	1
Coils' cover (PVC) [226]	1.33*10⁻¹³	4.46	1
Air	0	1	1

Supplementary Table 3.S3. Mean velocity and wall shear stress values within the construct calculated for the different modelled conditions.

Chamber layout	Flow rate (mL/min)	Mean velocity within the construct (m/s)	Wall shear stress (mPa)
CC1 and CC2	0.3	$6.37×10^{-5}$	3.23
	1	$2.12×10^{-4}$	10.75
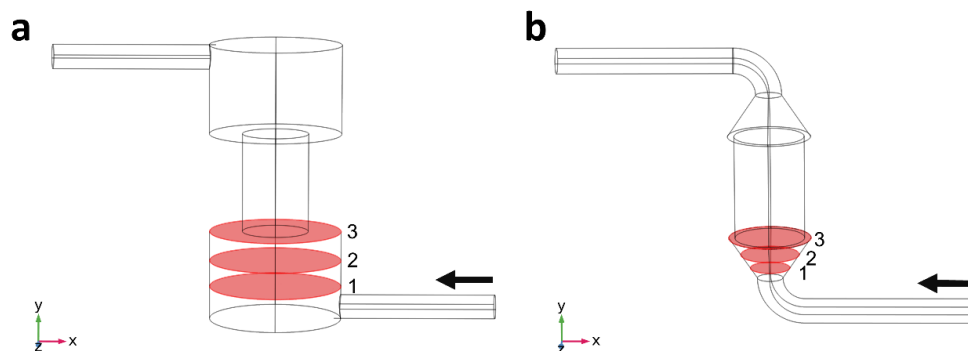
Supplementary Figure 3.S1. 3D view of the internal geometry of CC1 (a) and CC2 (b), highlighting the direction of flow perfusion and the 3 horizontal sections where the fluid velocity field distributions were analyzed: 1) at 0.5 mm above the end of the inlet channel; 2) at midway between the construct and the end of the inlet channel (i.e., 4.5 mm below the construct for CC1 and 2.5 mm below the construct for CC2); 3) tangent to the construct.
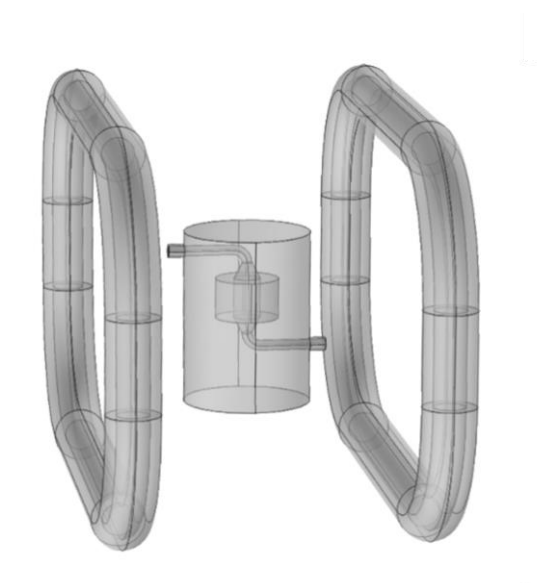
Supplementary Figure 3.S2. 3D geometry considered for the stationary electromagnetic field modelling.
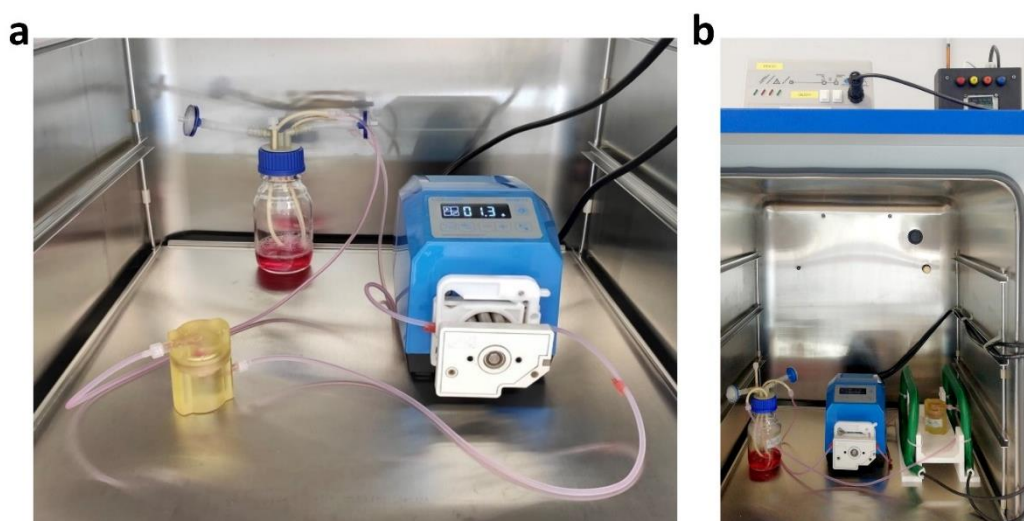
Supplementary Figure 3.S3. (a) Picture of the bioreactor setup within the incubator, with CC2 connected by silicone tubing to the reservoir and the peristaltic pump. This latter is connected by electric wires to the control unit located outside the incubator. (b) Picture of the bioreactor setup combined with the PEMF stimulator. Within the incubator, CC2 is placed between the PEMF stimulator coils and connected by silicone tubing to the reservoir and the peristaltic pump. The coils are connected by electric wires to the PEMF stimulator located outside the incubator. Similarly, the pump is connected to the control unit located outside the incubator.
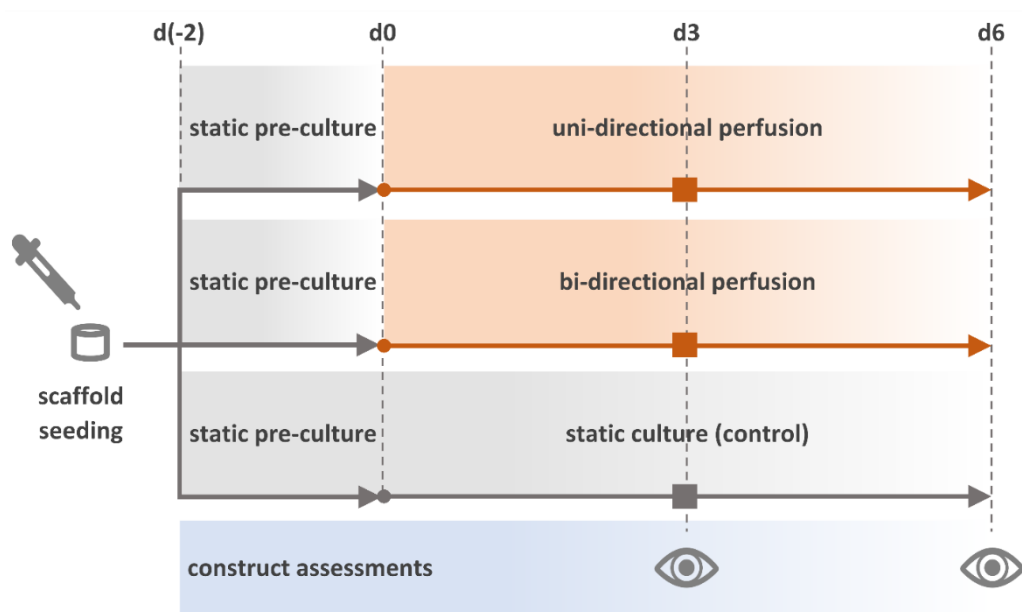
Supplementary Figure 3.S4. Timeline of the performed culture protocols.

Supplementary Figure 3.S5. Flow streamlines developing within CC1 and CC2 imposing a modeled flow rate of 1 mL/min and color-coded with respect to velocity values. (a) CC1 without construct. (b) CC1 with an inserted construct modelled as porous medium. (c) CC2 without construct. (d) CC2 with an inserted construct modelled as porous medium.

Chapter 4

Permeability Test Bench for Characterizing Hard and Soft Samples for Tissue Engineering Applications

Abstract

Tissue engineering (TE) strategies are based on the active interplay among cells, three-dimensional (3D) scaffolds, and physiological signals in view of developing in vitro functional tissue substitutes. Scaffold effectiveness is strongly influenced by its microstructure and ability to be permeated by fluids (i.e., scaffold permeability) and consequently to be colonized by cells. Permeability depends on the combination of porosity, pore size, tortuosity, and interconnectivity and its characterization is crucial for an effective evaluation of the overall scaffold performance.

Several methods and set-ups have been proposed to characterize the permeability of hard or soft materials, but no systems able to characterize both types of materials have yet been developed. Inspired by this context, we developed a versatile permeability test bench (PTB), based on the pump method, for characterizing hard and soft scaffolds. The permeability chamber (PC), designed using the Solidworks software and manufactured by stereolithography, consists of two parts coupled by screws, with an internal cylindrical geometry. Interchangeable silicone holders and a grid allow housing hard or soft cylindrical samples (height = 1-14 mm, diameter = 8-27 mm). The PC is part of a closed loop hydraulic circuit based on a peristaltic pump, a reservoir for demineralized water, silicone tubing, 3-way stopcocks, and two in-line relative pressure sensors located upstream and downstream the PC, respectively, to measure the pressure drop across it. The sensor signals are acquired by a DAQ, controlled by a computer running a purpose-built LabView interface. Upon imposing a defined flow rate (selected for guaranteeing laminar flow), scaffold permeability (k) was calculated by using the Darcy flow transport model and considering the pressure drop across the sample (subtracting the mean pressure drop due to the empty chamber).

For validating the PTB, commercial biomimetic scaffolds for bone TE (SmartBone) were tested. For each sample, 6 tests were carried out (flow rate = 5 ml/min), and for each test 5 pressure recordings were performed. As reference test bench (RTB), a previously validated device based on the acoustic method and developed by the National Institute of Metrological Research (INRiM) was used.

The mean permeability values of the SmartBone scaffolds were $2.3 \cdot 10^{-10} \pm 3.4 \cdot 10^{-10}$ m2 (PTB) and $1.8 \cdot 10^{-10} \pm 4.2 \cdot 10^{-11}$ m2 (RTB). Although the PTB measurements were affected by a higher dispersion, the normalized

errors between the results obtained with the PTB and RTB resulted to be less than 1, confirming the suitability of the PTB as permeability test bench for hard scaffolds. For reducing measurement uncertainty, the optimization of the PTB data acquisition system is in process. In parallel, measurements with a USB digital differential pressure transducer, selected for reducing the transient phenomena, are ongoing together with further tests varying the flow rates. Finally, tests are currently underway for assessing the suitability of the PTB to be used for soft scaffolds characterization.

4.1 Introduction

The development of *in vitro* biomimetic and functional substitutes of native human tissues requires the substantial understanding of how cells respond to signals, interact with their 3D environment, and organize themselves in response to the surrounding physical stimuli[157].

In native tissues there are two main regions: the vascular space, consisting of blood and lymph vessels, and the extravascular area. This region is a porous medium, composed by cells, ECM and interstitial fluid which saturates the pores that exist between cells as a part of a granular structure or between the ECM fibrous molecules[227,228]. The interstitial pores can be isolated or interlinked to form channel for the transport of nutrients, metabolites, inhibitors and other signaling molecules. The proper mimicking of the native ECM is particularly important for generating models of tissue which are not vascularized (e.g., cartilage).

In vitro the porous substrate that mimics the ECM, called scaffold, is responsible for supporting the entire cell architecture and promoting cell adhesion, differentiation, proliferation, and migration. With a view to obtaining a porous 3D support capable of providing a native-like environment, it is necessary to control some of its characteristics including porosity, pore size, distribution and interconnectivity, surface area and pore tortuosity. However, these microscopic quantities are not sufficient for scaffold's characterization because they can lead to unclear correlation to transport phenomena, some are hard to measure and for their evaluation inertial forces at solid-fluid interface must be considered[106,229].

The macroscopic variable encompassing the effects of the parameters mentioned above is the intrinsic permeability (k), which embodies the porous medium ability to be penetrated by a fluid and reflects the role of contributing indicators in the structures such as porosity and pore dimension and orientation to flow direction[199]. Several systems for evaluating scaffolds permeability, either based on direct or indirect methods, have been developed during the past decades and their performances are described in literature. However, the lack of standards in measurement and testing procedures for evaluating TE scaffold permeability makes the comparison of results achieved in different laboratories unworkable[106]. Moreover, soft scaffolds pose challenging tasks due to their deformability and the need to be tested in hydrated conditions to preserve their mechanical properties[230–232].

As indirect methods are affected by shortcomings related to the measurement techniques applied for measuring pore size and porosity of the scaffold, direct methods based on measurements of pressure drop and volumetric flow rate of a test fluid across the sample have been preferred[233].

Among direct methods, different test benches for characterizing hard and soft samples permeability have been developed exploiting the gravity-based method, consisting in the use of 2 reservoirs: the first is filled with water and placed at a fixed height to supply a constant or falling pressure head on the chamber holding the sample and the second placed downstream of the chamber to collect the water[229,234,235]. Interestingly, Nasrollahzadeh and Pioletti[236] designed a chamber to subject viscoelastic scaffolds to increasing compression values (ε=10%- 20%) and exploited the constant head method to estimate the strain dependent permeability, according to Darcy law. Although similar setups proved suitable for samples with high permeability (k $\approx 10^{-12}$-10^{-8} m^2), they induce a very low flow rate through the sample, making the reading unreliable for lower permeability values due to water evaporating from the container. Increasing the pressure head results often impractical and unsuitable for testing inside a laboratory, as considerable heights would be needed.

To overcome this issue, test benches have been developed exploiting the use of a pump to impose a known flow rate through the sample. The pump-based method offer the possibility to cover a wide range of permeability values by appropriately tuning the imposed flow rate and several test benches have been developed for investigating scaffolds and tissue samples permeability over a wide range (10^{-18}–10^{-9} m^2), which is limited only by the accuracy and range of the pressure transducers[231,237–240]. Moreover, by applying different flow rates on the same sample the permeability can be characterized under different flow regimes. In a comprehensive study, Santos et al.[241] developed a test bench for housing rigid samples based on a syringe pump and tested 3D-printed scaffolds by applying increasing flow rates (Q=1-100 mL/min). They observed a gradual transition from Darcy flow regime to Forchheimer flow regime and calculated scaffold permeability accordingly to the occurring flow regime in the range 10^{-10}-10^{-9} m^2.

Finally, besides the two direct methods described, which constitute most of the literature covering the subject, test benches exploiting the flow of air through the sample have also been developed[242]. Notably, Schiavi et al.[108] proposed a rapid permeability evaluation technique based on acoustic

pressure measurements, which allows measuring permeability of rigid scaffolds over several orders of magnitude (k~10^{-14}-10^{-8} m^2) with a confidence level of 95%.

Based on the reported considerations, a new test bench for the characterization of the permeability of rigid and soft materials is proposed here. In particular, the test bench was designed to be suitable for measuring a wide range of permeability values and give the possibility to host different rigid and soft samples. Following the development of the test bench, a protocol for carrying out the measurements and calculating the permeability considering its extended uncertainty was devised. To validate the test bench, permeability measurements on rigid scaffolds were compared with those obtained from a reference test bench based validated for rigid materials and located at the National Institute of Metrological Research (INRiM).

4.2 Materials and Methods

4.2.1 Permeability test bench

The design and development of the test bench were guided by specific requirements. Firstly, the test bench must enable to test rigid and soft samples having different dimensions. Moreover, the test bench must allow the measurement of permeability in the widest possible range, which for biological scaffolds and materials covers 10 orders of magnitudes (k~10^{-9}-10^{-19} m^2). The fluid flow parameters have to be tunable, in order to run the tests under defined conditions, therefore knowing the occurring flow regime. Finally, the test bench must allow to run long-lasting tests to guarantee the extinguishment of transient phenomena and record measurements under stationary conditions.

To thoroughly fulfil this set of requirements, a test bench exploiting the pump-based method was developed.

The main component of the test bench is the permeability chamber (PC), consisting of two parts coupled by screws. The chamber has a parallelepiped shape with limited footprint (length = 70 mm, width = 50 mm, height = 62.56 mm) and an internal cylindrical geometry. Watertightness is guaranteed by a o ring placed circumferentially in the upper part. The lower part of the PC allows the housing of cylindrical samples (height = 1-14 mm, diameter = 8-27 mm), which are positioned and held by using a set of interchangeable customized silicone gaskets and a grid. Both parts of the permeability chamber have a central channel with diameter = 8 mm which allows the fluid to uniformly flow through the sample. Female luer lock connections are directly implemented in both the parts of the chamber to ensure a watertight connection to the rest of the circuit. When the sample to be tested is rigid, a single gasket with an internal diameter matching that of the sample is used (Figure 4.1). In case there are spaces between the sample and the gasket, a white Teflon tape is used to wrap around the sample to prevent the flow from passing sideways instead of flowing through the central part of porous surface.
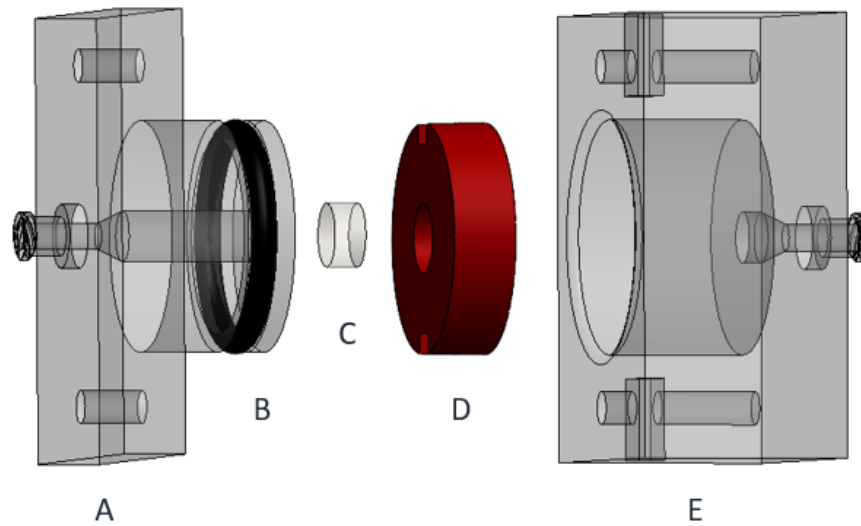
Figure 4.1. Exploded view of the permeability chamber assembly for tests on rigid samples: A) upper part, B) o ring, C) rigid sample, D) gasket, E) bottom part

If the sample is soft, two silicon gaskets are necessary to avoid water leakage on the sides of the structure and to clamp the sample and a grid with four squared holes (side=2.4 mm) serves to support the sample avoiding longitudinal movements due to the flow (Figure 4.2).
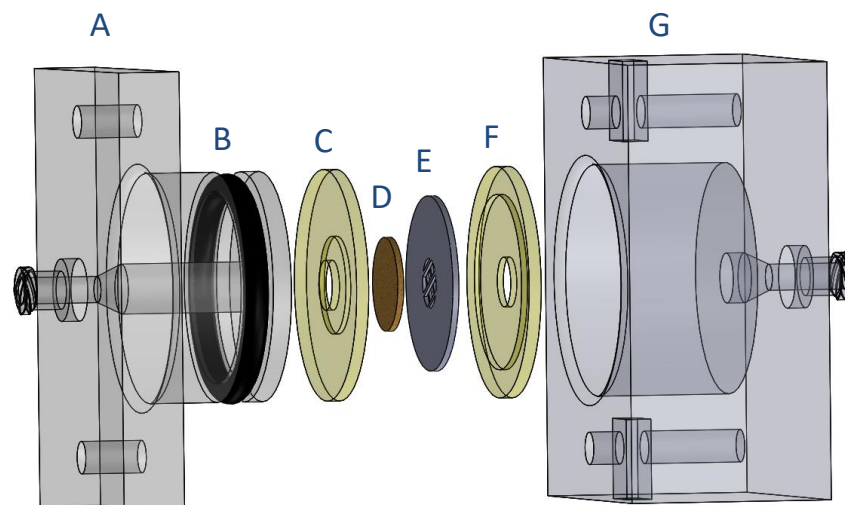
Figure 4.2. Exploded view of the permeability chamber assembly for tests on soft samples: A) upper part, B) o ring, C) sample gasket, D) soft sample, E) grid, F) grid gasket, G) bottom part.

The chamber parts were drawn using the CAD software Solidworks (Dassault Systemes, France) and realized by stereolithography in the Clear Resin using the Form 3 3D printer (FormLabs, United States), selecting a resolution of 25 μm (Figure 4.3a). The flexible gaskets were manufactured by pouring PDMS (Sylgard 184, Dow Corning, USA) or liquid silicone

_____

rubber (R Pro Tech 33, Reschimica, Italy) in modular molds and allowing it to solidify at room temperature for three days (Figure 4.3b and c). Mold components were manufactured in acrylonitrile-butadiene-styrene (ABS) by fused deposition modelling (FDM). The grid for supporting the soft sample was also manufactured in ABS by fused deposition modelling (Figure 4.3d).
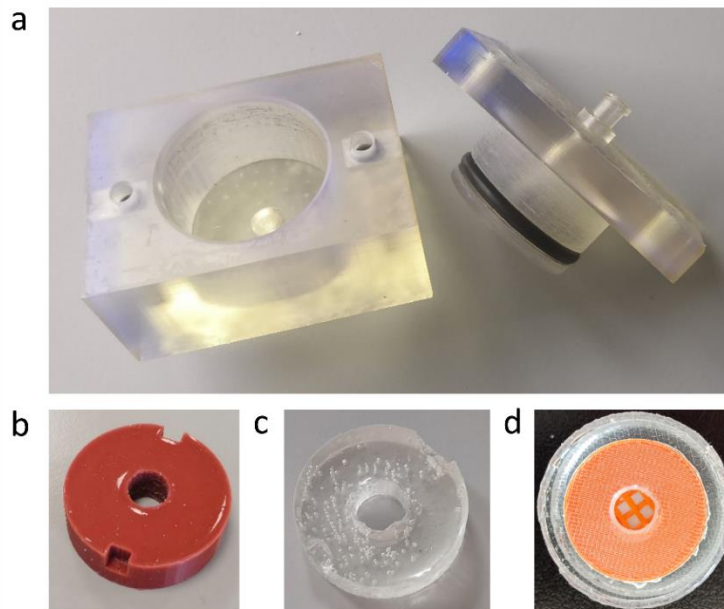
Figure 4.3. Permeability chamber components after manufacturing: a) top and bottom part with o ring inserted; b) silicone rubber holder for hard samples; c) PDMS holder for hard samples; d) gaskets and grid assembly for soft samples.

The permeability chamber is part of a closed-loop hydraulic circuit, composed of a reservoir, a peristaltic pump (Masterflex, Cole-Parmer, USA), oxygen impermeable Tygon S3 tubing (internal diameter=3.2 mm), and 3-way stopcocks. The selected pump and tubing guarantee flow rates in the range of 0.8 - 480 mL/min. Two in-line physiological relative pressure sensors (SP844, HJK Sensoren, Germany) are placed upstream and downstream the permeability chamber to measure the pressure drop across the chamber. Additional tubing is used to allow complete removal of bubbles trapped inside the sensor membrane. The sensors have a measurement range between -30 mmHg and 300 mmHg and sensitivity $S =$ 5 µV/V/mmHg. Their signals are acquired by a data acquisition (DAQ) system composed of a NI9237 module connected to the cDAQ9191 (National Instruments, USA). The DAQ is controlled a computer running a purpose-built LabView interface (Figure 4.4). Demineralized water (dynamic viscosity µ = 1 mPa·s) is used as test fluid.
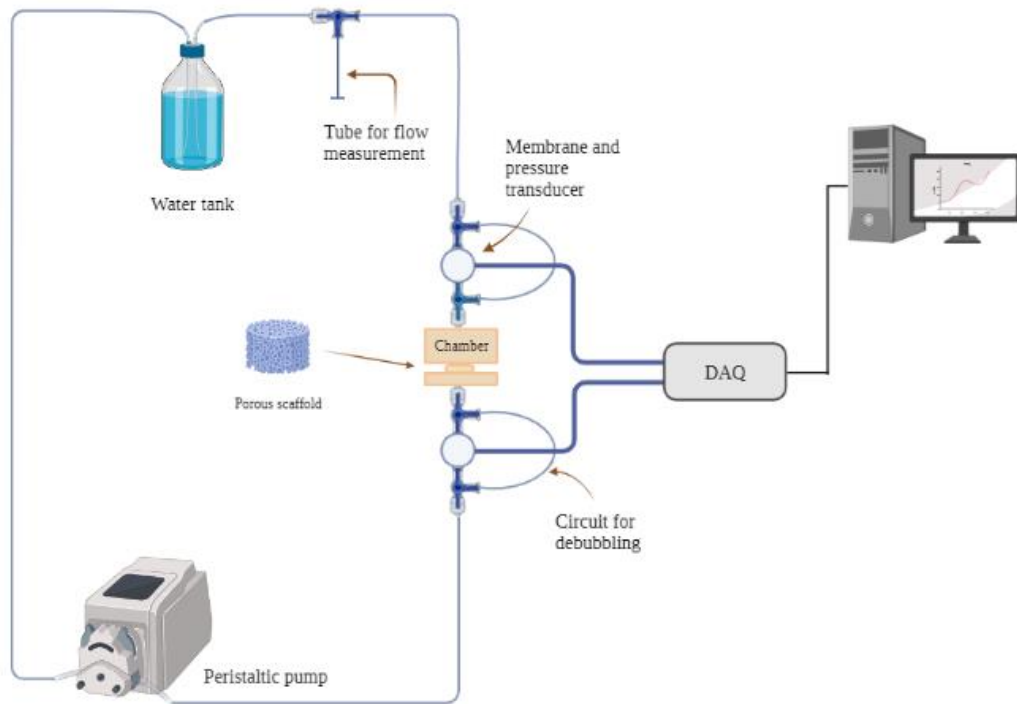
Figure 4.4. Schematic drawing of the permeability test bench

Recorded signals are post-processed using Matlab (Mathworks, USA) and Excel (Microsoft, USA).

4.2.2 Test protocol

A defined test protocol was developed in order to obtain reliability and repeatability of permeability measurements.

Firstly, the sample dimensions are measured with a caliper (10 measurements are taken for each dimension of interest). The sample is then inserted inside the appropriate gaskets. In case of soft samples, attention is paid to ensuring contact between the gasket and the sample in the lateral portion, to avoid water leaking from the sides. In case of a rigid scaffold, Teflon tape is wrapped on the lateral surface to ensure watertightness between sample and gasket. Once the sample is inserted into the gasket, the assembly is inserted into the bottom part of the chamber, the top part is coupled, and the permeability chamber is closed by tightening the screws. The permeability chamber is then connected to the hydraulic circuit. 500 mL of demineralized water are boiled to achieve microbiological purity, left to cool, and poured into the reservoir. The pump is then activated to completely fill the circuit. Additional tubing is used for ensuring complete air bubble removal from the chamber and from the sensor membranes. To ease air bubble removal, the chamber and the reservoir are positioned on a wooden support structure purposely developed (Figure 4.5).
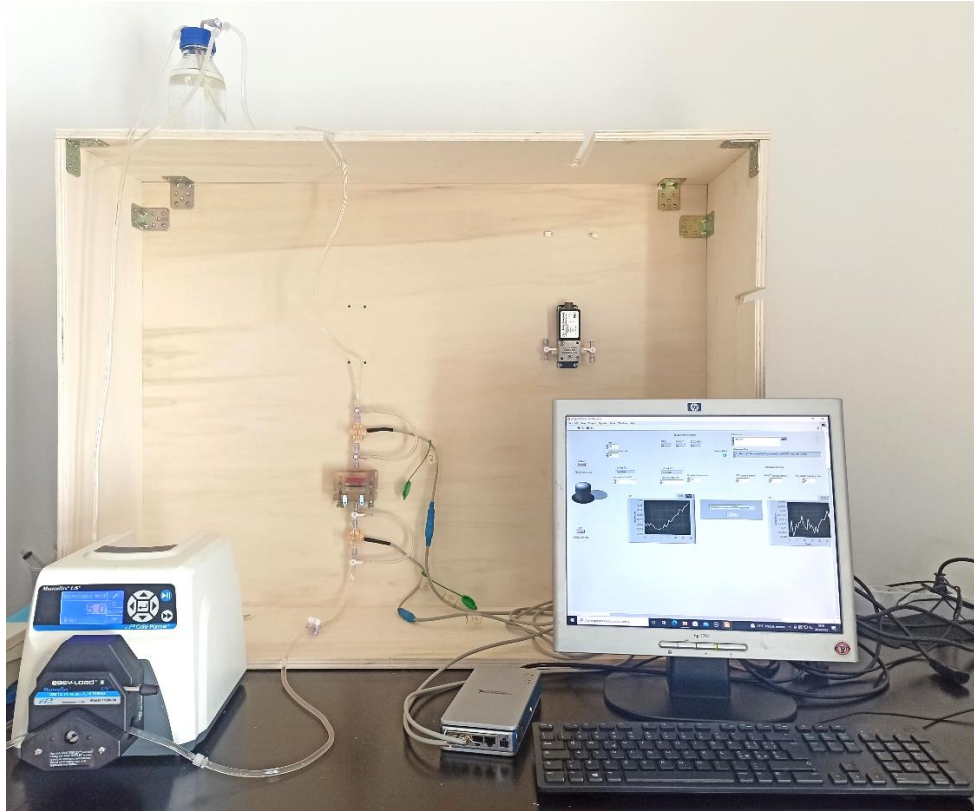
Figure 4.5. Assembled permeability test bench. The chamber and the reservoir are positioned on the wooden support structure

To ensure that the sample is completely wet before the test and that all residual air is removed, the pump is set at a flow rate Q=10 mL/min and run overnight. The day after, the flow rate is set to a value compatible with Darcy flow regime. To do so, the interstitial Reynolds number (Re_D) is calculated as:

$$Re_D = \frac{\rho \ v \ D}{\mu}$$

where v is the linear fluid velocity, and D is the mean pore diameter. The flow rate is then selected to guarantee the condition $Re_D < 1$, which identifies Darcy flow regime[243–245].

After turning on the pump, the flow rate is measured by opening the circuit after the chamber and using a balance scale to quantify the volume that flows in 2 minutes. After that, the circuit is closed again. At this moment the pressure sensors are zeroed to avoid the presence of any offset. Subsequently, the pump is restarted, and 5 recordings of pressure readings are conducted at a sample frequency f = 750 Hz. The first recording lasts one hour, the subsequent 4 have a duration of 15 minutes. Between each recording, 30 minutes pass. In this way, time series of pressure values allow to assess that all transient phenomena have ended. If the end of the transient

is detected, pressure data after that moment are averaged to obtain the average pressure. Pressure drop across the chamber is obtained as the difference between the average pressure recorded by each sensor. For each sample, 4 to 6 tests are conducted by repeating the whole procedure detailed above.

Prior to testing the sample, tests are run imposing the same flow rate on the chamber without the sample inserted. Pressure drop due to the presence of the sample is then obtained as:

$$\Delta p_{sample} = \Delta p_{full} - \Delta p_{empty}$$

Using the mean Δp_{sample}, the permeability k of the sample is obtained from Darcy law[246]:

$$k = \mu \frac{Q}{\Delta p} \frac{L}{A}$$

where Δp is the pressure drop across the sample, L is the thickness of the sample, Q is the flow rate, and A is the area of the sample cross-section.

To obtain a range of permeability with 95% confidence, the extended uncertainty is calculated in accordance with the guidelines developed by the International Bureau of Weights and Measures (BIPM)[247]. At first, measurement uncertainty is calculated from the definition as

$$s_k = \sqrt{\left(\frac{\partial k}{\partial \mu}\right)^2 \cdot s_\mu^2 + \left(\frac{\partial k}{\partial Q}\right)^2 \cdot s_Q^2 + \left(\frac{\partial k}{\partial \Delta p}\right)^2 \cdot s_{\Delta p}^2 + \left(\frac{\partial k}{\partial L}\right)^2 \cdot s_L^2 + \left(\frac{\partial k}{\partial A}\right)^2 \cdot s_A^2}$$

where $\partial k / \partial x$ is the partial derivative of k with respect to the parameter x and s_x is the uncertainty on the value of the parameter, which for measured parameters is their standard deviation.

Extended uncertainty is then obtained as:

$$U_k = c \cdot s_k$$

where c is the Student-t coverage factor, which for a confidence value of 95% is equal to 2.

In case a soft sample (i.e. a sample characterized by a low elastic modulus: 10^{-1} MPa $< E < 10^2$ MPa), the compressive strain is calculated as the ratio between the thickness of the sample before the test and the height of the socket where it is positioned. Permeability of the uncompressed sample using the formula[230]:

$$k_1 = k_0 \, e^{M\varepsilon}$$

where k_1 is the permeability of the compressed sample, k_0 is the permeability of the uncompressed sample, M is a material constant, ε is the strain applied.

4.2.3 Validation tests

For a preliminary validation of the permeability test bench (PTB), 3 commercial cylindrical hard scaffolds (SmartBone IBI S.A, Switzerland) were tested for 4 independent repetitions at 5 mL/min (Figure 4.6). Based on the mean pore size of Smartbone scaffold ($D = 378 \pm 145$ μm[248]) and on the measured geometrical features of the scaffolds (reported in Section 4.3), the flow rate was selected to ensure Darcy flow regime ($Re_D = 0.379 \pm 0.146$). Mean permeability value and extended uncertainty were calculated for each scaffold (respectively named SmartBone 1, SmartBone 2 and SmartBone 3).
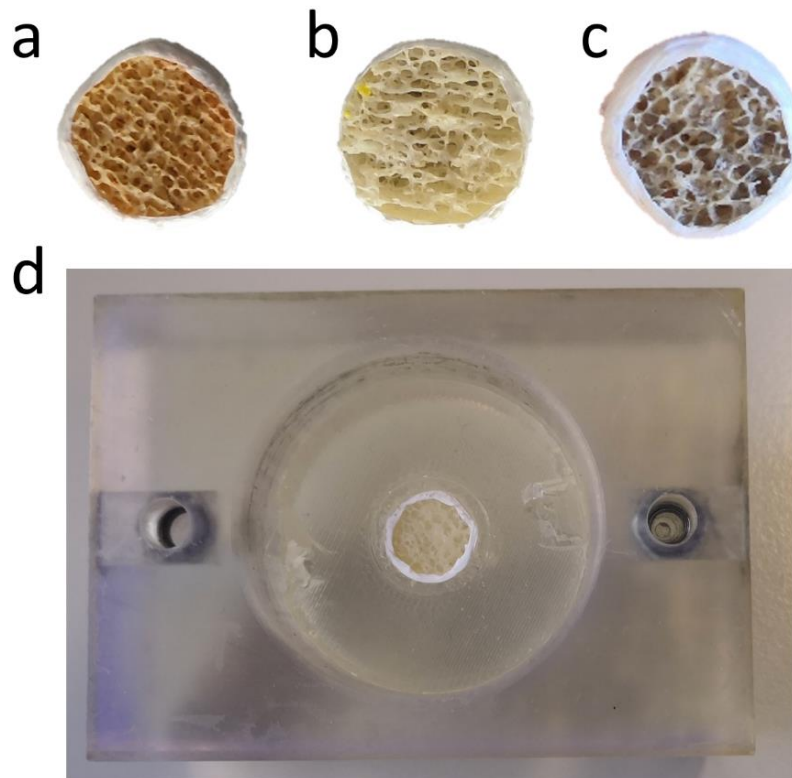
Figure 4.6. a) SmartBone 1, b) SmartBone 2 and c) SmartBone 3 hard scaffolds used in the validation tests wrapped in Teflon tape; d) SmartBone 3 scaffold positioned in the permeability chamber

Results were compared with a reference test bench (RTB), consisting in the test bench based on the acoustic method, validated for rigid materials, and located at the National Institute of Metrological Research (INRiM).

For each sample, the normalized error was calculated as:

$$E_n = \frac{|k_1 - k_2|}{\sqrt{U_{k_1}^2 + U_{k_2}^2}}$$

where k_1 and k_2 are the mean permeability values obtained with the two different test benches and U_{k1} and U_{k2} are the respective extended uncertainties. Measurements from the two test benches were considered compatible for $E_n < 1$.

4.3 Results

4.3.1 Permeability test bench

The test bench was assembled, and preliminary test were run to assess its suitability for the intended purpose. Using test specimens, it was demonstrated that the permeability chamber design allows effectively holding the sample, preventing deformations, and ensuring watertightness. Moreover, tests conducted with these sacrificial specimens allowed to refine the test protocol in order to guarantee complete air bubble removal.

Pressure sensors cables were assembled with RJ50 connectors for allowing easy interface with the DAQ. The calibration data of the sensors were loaded to the DAQ, in order to convert the measured analog voltage to the corresponding pressure value. The DAQ software, developed in the LabView environment, allows the user to remove the offset from the pressure sensors reading and then set the parameters for data recording (sample frequency, recording duration, duration of interval between recordings).

4.3.2 Validation tests

To validate the test bench, the permeability of 3 commercial cylindrical hard scaffolds was evaluated. Table 4.1 reports the measured values of the variables that appear in Darcy equation and the resulting permeability values for the scaffolds. Data are presented as mean ± SD. For the geometric quantities, n = 10 (measurements with the caliper), for Q and Δp n = number of tests = 4. From the measured quantities, the uncertainty was calculated using the equation detailed in Section 4.2. The permeability of the 3 samples resulted in the order of 10^{-10} m^2.

Table 4.1. Measured and calculated data for the SmartBone samples tested with the proposed test bench

	SmartBone 1	SmartBone 2	SmartBone 3
L (m)	$3.32 \pm 0.05 \cdot 10^{-3}$	$3.20 \pm 0.01 \cdot 10^{-3}$	$3.29 \pm 0.07 \cdot 10^{-3}$
A (m^2)	$8.32 \pm 0.55 \cdot 10^{-5}$	$9.27 \pm 0.15 \cdot 10^{-5}$	$8.31 \pm 0.30 \cdot 10^{-5}$
μ (Pa·s)	$1.00 \pm 0.01 \cdot 10^{-3}$	$1.00 \pm 0.01 \cdot 10^{-3}$	$1.00 \pm 0.01 \cdot 10^{-3}$
Q (m^3/s)	$7.99 \pm 0.04 \cdot 10^{-8}$	$8.19 \pm 0.13 \cdot 10^{-8}$	$7.96 \pm 0.03 \cdot 10^{-8}$
Δp_{sample} (Pa)	11.4 ± 8.6	9.7 ± 8.6	28.3 ± 13.6
k (m^2)	$2.804 \cdot 10^{-10}$	$2.926 \cdot 10^{-10}$	$1.117 \cdot 10^{-10}$
U_k (m^2)	$2.112 \cdot 10^{-10}$	$2.586 \cdot 10^{-10}$	$6.243 \cdot 10^{-11}$

Measurements obtained with the PTB show an extended uncertainty of the same order of magnitude of the measured k. The most significant relative contribution to the uncertainty is due to the pressure measurements.

The comparison between the permeability measured with the PTB and the RTB on the same rigid scaffolds is reported in Table 4.2. The measurements are compatible, as for each sample $E_n < 1$. The 95% confidence interval for measurements obtained with the RTB is from 4 to 13 times smaller than the interval for measurements with the PTB.

Table 4.2. Comparison between the measurements obtained with the proposed test bench and the reference test bench

		SmartBone 1	SmartBone 2	SmartBone 3
$k \pm U_k$ (10^{-10} m²)	RTB	1.097 ± 0.158	2.733 ± 0.363	1.67 ± 0.13
	PTB	2.804 ± 2.112	2.926 ± 2.586	1.117 ± 0.624
E_n		0.81	0.07	0.87

For the samples named SmartBone 1 and Smartbone 2 the confidence intervals obtained with the two test benches show a complete overlap, while for measurements on sample Smartbone 3 the confidence intervals partially overlap (Figure 4.7).
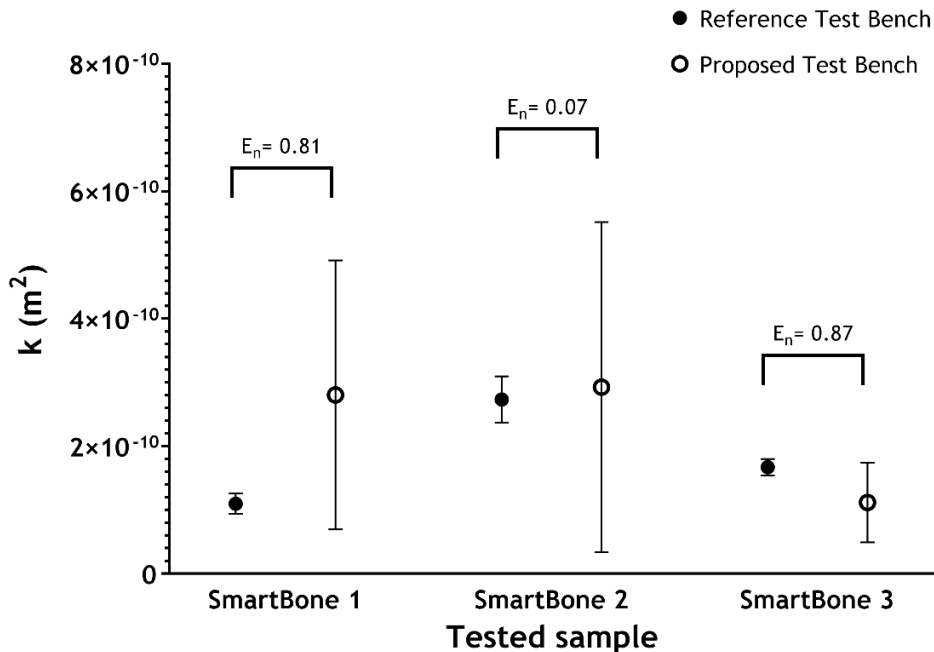
Figure 4.7. Comparison between the measurements obtained with the proposed test bench and the reference test bench

4.4 Discussion

Intrinsic permeability is a fundamental parameter that embodies the ability of a porous medium to be penetrated by a fluid and is a key determinant for the success of a scaffold in *in vitro* 3D cell cultures. In fact, intrinsic permeability affects oxygen and nutrient transport, cell seeding efficiency, and the transmission of appropriate physical stimuli (in particular shear stresses) to the cultured cells[238]. Consequently, the accurate measurement of scaffold permeability is highly useful as part of a scaffold design process.

Several methods have been proposed to characterize the permeability of hard and soft scaffolds, however defined protocols are still missing, due to the differences between them that make the comparisons of results often inconsistent[106]. Firstly, soft scaffolds are difficult to characterize due to their deformability, as their permeability exhibits a strain-dependent behavior. In addition, the different developed architectures are affected by significant shortcomings. The gravity-based method is impractical for samples with low permeability, as high pressures must be generated to force the fluid through the scaffold, or large time intervals are needed to allow the fluid to flow through the scaffold[236]. Moreover, since the flow rate is not set, different flow regimes might develop inside the samples. For the pump-based method, since the evaluation is based on simultaneous measurement of multiple quantities (i.e., upstream and downstream pressure, and flow rate), accuracy and sensitivity of transducers are fundamental and prescribe the limits on the measurable permeability range.

Inspired by this scenario, we developed a test bench for measuring the permeability of hard and soft scaffolds for tissue engineering under Darcy flow regime. The selected architecture, based on a closed-loop hydraulic circuit drove by a peristaltic pump, allows to run long-term tests, ensuring that all transient phenomena are extinguished. Moreover, the pump allows fine-tuning the flow rate, in order to guarantee the development of Darcy flow regime inside the samples.

The design of the permeability chamber guaranteed to fulfil all the envisioned requirements: ease of use, versatility, modularity, and watertightness. In detail, thanks to the manufactured customized flexible gaskets, the chamber can effectively house hard and soft scaffolds, avoiding excessive deformations and ensuring watertightness.

The developed test protocol ensures that no air is present in the circuit during the recording. Running tests without a sample inserted in the permeability chamber allowed to evaluate the pressure drop due to the chamber alone and consequently avoid considering it when evaluating the permeability of the tested scaffold. Moreover, the timed recordings guarantee to observe the presence of any residual transient behavior and consequently analyze only the values corresponding to a stationary condition.

Preliminary validation tests, performed on 3 commercially available hard scaffolds, showed repeatable results, with the permeability of the 3 scaffolds being in the 10^{-10} m^2 range. With respect to the average permeability value, the 95% confidence interval has the same order of magnitude. Analyzing the contribution to the measurement extended uncertainty, it emerges that the uncertainty on the measured pressure values provides the most significant contribution to the extended uncertainty (Table 4.1).

When compared to the measurements obtained with the validated RTB, permeability values obtained using the PTB were compatible with RTB values ($E_n < 1$), although the PTB measurements were affected by a higher dispersion (Figure 4.8). In detail, the 95% confidence interval of PTB permeability measurements is one order of magnitude bigger than that of the RTB.

The considerable uncertainty of pressure readings constitutes the main limitation of the PTB and could affect the performed study. This uncertainty is due to the choice of the sensors. The PTB is equipped with membrane pressure sensors for measurements on liquids, with a wide range for covering several orders of magnitude of k. As the tested SmartBone samples are characterized by a high permeability, this determines low pressure drop across the sample, which are close to the resolution of the DAQ system. The RTB instead uses a microphone calibrated for samples with a permeability between 10^{-8} and 10^{-14} m^2 [108].

For reducing measurement uncertainty, the optimization of the PTB data acquisition system is in process. Firstly, the hydraulic circuit is being reviewed, considering the possibility to add a pulse damper in series to the pump, to obtain a continuous flow instead of a pulsating one. Despite the use of a syringe pump would guarantee a continuous flow by design, the use of such a pump is impractical when long-term tests need to be performed. Moreover, the tests could be repeated increasing the flow rate,

provided that Darcy flow regime is still guaranteed to occur inside the samples. Finally, the chamber could be equipped with different pressure sensors, with measurement range and accuracy selected for specific pressure ranges. In detail, different interchangeable sensors could be provided and then used based on the expected permeability range of the scaffold to test.

Finally, despite the higher precision of the RTB, it has to be considered that the PTB was conceived as suitable for measurements on soft scaffolds, as they are kept in wet conditions throughout the test. This constitutes a significant improvement with respect to the RTB, which is limited to work with dry samples. Based on the testing protocol described in section 4.2, the deformation of the samples can be measured and therefore the permeability values for undeformed scaffolds can be retrieved. Following the validation of the PTB described in this chapter, tests on soft scaffolds are ongoing to refine the measurement protocol and determine the permeability of such scaffolds.

Chapter 5

Conclusions and Future Works

5.1 Summary and main contributions

The objectives of this PhD thesis concerned the design, development, and validation of advanced technological platforms for automated dynamic culture and electro-mechanical characterization of biological tissues and scaffolds.

The core reason for developing these technologies was to provide powerful tools for supporting the tissue engineering research field, in view of fully elucidating mechanotransduction pathways in living cells and tissues. A full understanding of the cascade of the biological responses triggered at the cell and tissue level by physical stimulation would be fundamental for elucidating both the development of tissues and the pathogenesis of many diseases and for developing new medical therapies[4,5]. To understand the interplay of phenomena implied in tissue regeneration and homeostasis, reliable and robust *in vitro* models need to be developed[60]. In addition, the physical properties of the developed constructs and adopted substrates need to be accurately characterized. Up to now, the generalizability of the published research in mechanobiology has been problematic due to the incomplete achievement of these two goals: *in vitro* models recapitulate a small subset of physical cues with limited accuracy, and testing tools and machinery were developed for materials and substrates used in the industrial sector and are not easily adaptable.

In this view, the technologies presented in this thesis aim to overcome some of the limitations affecting state-of-the-art technologies. The faithful mimicking of *in vivo* conditions, the tunability of the delivered stimuli, and the possibility to obtain repeatable quantitative information were the main points addressed in this work.

This thesis introduced three different technologies:

1. a compact, easy to use, versatile electrical stimulator for cardiac tissue engineering investigations, designed to provide tunable stimuli to the cultured cells/constructs in view of studying the effect of different protocols of electrical stimulation *in vitro*;
2. an automated bioreactor for bone tissue engineering that allows combining flow induced shear stress and PEMF stimulation;
3. a novel test bench for the characterization of the permeability of hard and soft biological samples.

Besides the systems having notably different intended uses, the engineering processes leading to their finalization share many aspects. In each case, a design process based on the concurrent engineering concept was adopted[249]: the different phases of system and subsystem development were identified and performed in parallel. Each of the technologies proposed in this thesis is the result of an iterative engineering approach, conducted following the general guidelines and engineering standards elaborated for the development of medical devices, laboratory equipment, measurement systems and space payloads[247,250–254].

Technically, computer-aided design (CAD) and electronics design assembly (EDA) software were used to support the design of functional components. Multiphysics computational simulations enabled precise characterization of the physical stimuli and consequent refinement of the components in view of their intended use. Additive manufacturing technologies (FDM and SLA) allowed fast prototyping of the systems. Different software suites were used for developing the firmware controlling the various systems. Acceptance and validation tests were conducted on each system and the resulting data were statistically analyzed using numeric computing software.

The main contributions from each chapter of this thesis are reported below.

Chapter 1 - Introduction

The first chapter introduces the biological and technological background necessary to understand the work of this thesis and provides the motivations for the conducted research. The main objectives that were pursued are also reported.

Chapter 2 – Versatile Electrical Stimulator for Cardiac Tissue Engineering Investigations

A novel compact, easy-to-use, tunable electrical stimulator for cardiac tissue engineering, named ELETTRA, is proposed in this chapter. Upon construction, the stimulator was coupled to customized culture chambers, designed for delivering uniform electrical stimulation to the samples, and was adopted in biological experiments aimed at investigating the effects of 3 different electrical stimulation patterns on neonatal rat cardiomyocytes functionality. Results demonstrated the reliability and versatility of ELETTRA and confirmed the crucial role of electrical stimulation in

_____

promoting cardiac cell functionality and maturation. In particular, biological experiments demonstrated that 5V/cm monophasic and ±5V/cm symmetric biphasic electrical stimulations were effective in enhancing cardiac functionality by reducing the excitation threshold and highlighted that the ±5V/cm symmetric biphasic waveform also induced a higher maximum capture rate.

Chapter 3 – An Automated 3D-Printed Perfusion Bioreactor Combinable with Pulsed Electromagnetic Field Stimulators for Bone Tissue Investigations

This chapter details the design, development, manufacturing, and testing of an automated bioreactor for bone tissue engineering. The bioreactor introduced the possibility of combining two different physical stimulation: flow-induced shear stress and PEMF stimulation. The adopted automation strategy enables providing uni- or bi-directional perfusion within the same platform and without user intervention along the culture, a feature that is not implemented in currently available perfusion bioreactors. Moreover, automation significantly reduces user intervention and dependence along the culture, increasing robustness and reproducibility of the culture process. The preliminary biological tests demonstrated that uni- and bi-directional perfusion conditions effectively stimulated osteogenic differentiation of the cultured 3D bone tissue models, based on a commercial scaffold seeded with human bone marrow stem cells. Readouts of the experiments indicated that perfusion culture promoted osteogenic differentiation and favored cells to deposit more ECM with respect to the static culture, and notably bi-directional perfusion better promoted ECM deposition across the constructs with respect to uni-directional perfusion, indicating that the proposed bioreactor represents a powerful tool for in depth bone mechanobiology investigations.

Chapter 4 – Permeability Test Bench for Characterizing Hard and Soft Samples for Tissue Engineering Applications

Here a versatile test bench for characterizing the permeability of hard and soft scaffolds under Darcy flow regime is presented. For a clearer comprehension, the chapter provides details about flow regimes occurring in porous media. Noteworthy examples of systems for measuring hard and soft scaffolds permeability are described and their main limitations are analyzed. The proposed test bench, developed on a pump-based hydraulic

circuit, can house hard or soft samples within a customized permeability chamber and, upon imposing a defined flow rate (guaranteeing laminar flow), permeability is measured by using the Darcy flow transport model.- Preliminary validation tests, performed on a commercially available bone scaffold, showed that the permeability values obtained using the proposed test bench are compatible with those obtained with a reference system, confirming the suitability of the proposed approach.

All the proposed technologies were developed for overcoming current limitations affecting the tissue engineering and mechanobiology research fields (i.e., incomplete recapitulation of the physical cues, limited tunability and versatility of the equipment, uncertainty in characterizing material properties and stimuli). The application of engineering design methods and processes ensured the development of reliable automated platform which increase reproducibility of experiments and in turn enhance the robustness of the obtained results. Overall, the results of the present PhD thesis demonstrated the potential of the proposed technological platforms and provided evidence that they can strongly support the advancement of tissue engineering and mechanobiology research, fulfilling the main purpose of this PhD thesis.

5.2 Limitations

Notwithstanding their consistency, the described studies could be affected by some potentially significant limitations. Due to the variety of technologies described, the restraints are not easily generalizable and will be addressed peculiarly for each of the presented study.

Chapter 2 – Versatile Electrical Stimulator for Cardiac Tissue Engineering Investigations

The stimulator at the moment offers the possibility of tuning the parameters, which remain constant over the stimulation period. In reality, electrical stimulation *in vivo* presents an intrinsic variability both in physiological and in pathological conditions.

The biological tests were conducted using NRCMs and concentrated on assessing the effects of electrical stimulation of these cells. In view of developing a reliable *in vitro* model for future investigation, the validation

of the beneficial effects of biphasic stimulation with human origin CMs would increase the clinical relevance of the presented findings.

Chapter 3 – An Automated 3D-Printed Perfusion Bioreactor Combinable with Pulsed Electromagnetic Field Stimulators for Bone Tissue Investigations

The CFD model considered the construct as a homogeneous and isotropic porous medium and neglected the presence of the cells. Moreover, the simulations did not consider that along the culture the construct geometry is modified by cell proliferation and ECM deposition. For these reasons, the computed shear stress values are a reasonable estimation for the early culture stage. The electromagnetic field modelling was performed in steady-state conditions, neglecting the temporal evolution of the magnetic field occurring during a PEMF pulse, therefore describing the conditions occurring at the pulse peak. Lastly, biological tests combining perfusion and PEMF have not been conducted yet, therefore the effects of the combined physical stimuli are yet to be investigated.

Chapter 4 – Permeability Test Bench for Characterizing Hard and Soft Samples for Tissue Engineering Applications

A clear limitation of the test bench is the long time needed for priming the system. Up to now, for ensuring that the entirety of the sample is wet, and all air is removed in the circuit, the protocol involves running the system for several hour before starting the test. This procedure is automatically carried on overnight, but in turns, also due to the time to extinguish the transient, limits the number of tests to one per day.

Moreover, measurements performed with the proposed test bench, although compatible with those of a reference a system, are affected by a high extended uncertainty. Finally, the flow regime occurring inside the sample is determined *a priori* by calculating the flow rate that guarantees $Re_D\sim1$. If the internal geometry of the sample is not known, this condition can only be verified afterwards by measuring the pressure drop at different flow rates, therefore needing additional time for these tests.

5.3 Future works

In the multidisciplinary research field of mechanobiology, it is clearly acknowledged that physical stimuli arising from the surrounding

microenvironment or externally applied play a crucial role in influencing cell fate[5,201]. This in turn determines tissue development, homeostasis, and disease pathogenesis[3]. However, a complete understanding of the biological mechanisms induced in different biological tissues by peculiar physical stimuli is still missing and the influence of different stimulation parameters and combinations is unknown[202].

All the contributions reported in this thesis constitute the result of an attempt to introduce novel technological platforms which could overcome some of the limitations in mechanobiology research.

In detail, ELETTRA (introduced in Chapter 2) can be used as powerful tool for cardiac tissue engineering investigations, as it is combinable with different cell culture set-ups, and allows testing different stimulation patterns at the same time stimulating multiple constructs in parallel. The reported findings constitute the basis for the future use of ELETTRA in advanced investigations aimed to identify the precise combinations of stimulation parameters inducing specific biological effects. Moreover, coupled with existing bioreactors, ELETTRA can be used to provide combined physical stimuli in a physiologically relevant way, for future production of functional CTE constructs in vitro. In this view, human CMs derived by iPSCs (induced Pluripotent Stem Cells) represent one of the best cell candidates for repeating the results obtained so far in 2D and 3D cardiac *in vitro* models.

The automated bioreactor for bone tissue engineering (Chapter 3), allows providing uni/bi-directional perfusion without user intervention, and combining perfusion and PEMF stimulation. Due to its simple architecture, it can be easily parallelized, representing a powerful tool for investigating *in vitro* the biological response of 3D bone tissue models to defined physical stimuli. Biological tests adopting 3D-printed biomimetic scaffolds resembling the microarchitecture of trabecular bone and imposing perfusion and PEMF stimulation are ongoing. In the next future, an advanced investigation approach, based on the proposed bioreactor and high-throughput analyses, could lead to unravel molecular mechanisms activated by biophysical stimulation applied in clinic and to define the precise combinations of parameters inducing specific biological effects, paving the way for optimized orthopedic clinical protocols.

Concerning the permeability test bench (Chapter 4), the obtained results demonstrate the suitability of the test bench for measuring the permeability of hard samples. Preliminary results on commercially available rigid

scaffolds show that the developed approach guarantees repeatable and robust results, although the confidence interval remains large. For reducing measurement uncertainty, the optimization of the test bench data acquisition system is in process, and in parallel tests varying the imposed flow rates and using different hard and soft samples are ongoing. Once completed, the test bench and protocol will constitute a robust framework for measuring the permeability of soft deformable scaffolds for TE, a challenge that is yet unsolved in soft tissue biomechanics. Such framework could be used in combination with bioreactors, such as the system described in Chapter 3, in view of a complete and quantitative characterization of scaffold performances.

The advanced technologies presented in this dissertation will allow overcoming some of the current limitations of the tissue engineering research field. In the near future, the proposed technologies will be used as powerful investigation tools for unravelling cell-scale mechanotransduction signaling pathways, providing meaningful insights to increase the tissue regeneration knowledge base, finally contributing to boost the translation of promising tissue engineering strategies to clinical use.

List of Publications

Journal Articles

Putame, G., <u>Gabetti, S.</u>, Carbonaro, D., Di Meglio, F., Romano, V., Sacco, A. M., Belviso, I., Serino, G., Bignardi, C., Morbiducci, U., Castaldo, C., Massai, D., Compact and tunable stretch bioreactor advancing tissue engineering implementation. Application to engineered cardiac constructs, *Medical Engineering & Physics*, Elsevier, pp. 9, 2020, Vol. 84, ISSN: 1873-4030, DOI: 10.1016/j.medengphy.2020.07.018

Maffiodo, D., Sesana, R., <u>Gabetti, S.</u>, Colombo, A., Innovative force sensor for indoor climbing holds – real-time measurements and data processing, design and validation, *Proceedings of The Institution of Mechanical Engineers. Part P, Journal of Sports Engineering and Technology*, SAGE, pp. 14, 2020, ISSN: 1754-3371, DOI: 10.1177/1754337120927122

Articles under revision

<u>Gabetti, S.</u>, Masante, B., Cochis, A., Putame, G., Sanginario, A., Armando, I., Fiume, E., Scalia, A. C., Baino, F., Morbiducci, U., Rimondini, L., Bignardi, C., Massai, D., An Automated 3D-Printed Perfusion Bioreactor Combinable with Pulsed Electromagnetic Field Stimulators for Bone Tissue Investigations, *Scientific Reports*

Articles under submission

<u>Gabetti, S.</u>, Sileo, A., Montrone, F., Putame, G., Audenino, A., Marsano, A., Massai, D., Versatile and tunable Monophasic/Biphasic Electrical Stimulator for Cardiac Tissue Engineering Investigations, *Biotechnology & Bioengineering*

Masante, B., <u>Gabetti, S.</u>, Putame, G., Massai, D., Biological Mechanisms Induced by Non-Invasive Pulsed Electromagnetic Field Stimulation in vivo and in vitro, *Bioengineering*

_____

Gabetti, S., Masante, B., Massini, C., Tassi, R., Mochi, F., Del Gaudio, C., Morbiducci, U., Audenino, A., Schiavi, A., Massai, D., Permeability Test Bench for Characterizing Hard and Soft Scaffolds for Tissue Engineering Applications

Conference Proceedings

Masante, B., Gabetti, S., Cochis, A., Putame, G., Sanginario, A., Fiume, E., Baino, F., Verné, E., Rimondini, L., Bignardi, C., Massai, D., 3D-Printed Bioreactor Combining Direct Perfusion and PEMF Stimulation for Investigating the Biological Responses of Bone Tissue Models to Controlled Physical Stimuli, presented at ICFD 2021, 18th International Conference on Fluid Dynamics, Online, October 27-29 2021

Serino, G., Lugas, A. T., Bernava, G., Ragazzini, S., Gabetti, S., Terzini, M., Morbiducci, U., Audenino, A., Pesce, M., Massai, D., PDMS Substrates with tunable stiffness for cardiac mechanobiology investigation: A nanoindentation study, *Biomedical Science and Engineering*, In: Proceedings of the third Centro 3R Annual Meeting, PAGEPress, III Convegno Annuale "L'era delle 3R: modelli in silico, in vitro e in vivo per promuovere la ricerca traslazionale", Online September 30th - October 1st 2021, pp. 2, 2021, Vol. 4, ISSN: 2531-9892, DOI: 10.4081/bse.2021.192

Gabetti, S., Masante, B., Cochis, A., Putame, G., Sanginario, A., Fiume, E., Baino, F., Verne', E., Rimondini, L., Bignardi, C., Massai, D., Bioreactor platform combining perfusion and PEMF stimulation for in vitro bone research, In: Book of abstracts of ESB-ITA 2021, ESB-ITA, Italian Chapter of the European Society of Biomechanics, 2021 Annual Meeting of the ESB ITA, Online 23 September – 24 September 2021, pp. 1, 2021

Gabetti, S., Sileo, A., Montrone, F., Putame, G., Audenino, A., Marsano, A., Massai, D., Tunable Monophasic/Biphasic Electrical Stimulator for Cardiac Tissue Engineering Investigations, In: Book of abstracts of ESB2021, European Society of Biomechanics, 26th Congress of the European Society of Biomechanics, Milan (IT) July 11-14, 2021, pp. 1, 2021

Masante, B., Gabetti, S., Cochis, A., Putame, G., Fiume, E., Armando, I., Sanginario, A., Baino, F., Rimondini, L., Verne', E., Bignardi, C., Massai, D.,

Versatile Bioreactor Combining Perfusion and PEMF Stimulation for Bone Mechanobiology Research, In: Book of abstracts of ESB2021, European Society of Biomechanics, 26th Congress of the European Society of Biomechanics, Milan (IT) July 11-14, 2021, pp. 1, 2021

Serino, G., Bernava, G., Lugas, A. T., Gabetti, S., Midei, F., Terzini, M., Morbiducci, U., Audenino, A., Pesce, M., Massai, D., Nanoindentation of PDMS Substrates with Tunable Stiffness for Cardiac Mechanobiology Investigations, In: Book of abstracts of ESB2021, European Society of Biomechanics, 26th Congress of the European Society of Biomechanics, Milan (IT) July 11-14, 2021, pp. 1, 2021

Torta, E., Caridi, G. C. A., Gabetti, S., Chiastra, C., Gallo, D., Compin, M., Morbiducci, U., A Compact In Vitro Test Bench for Cardiovascular Flow Analysis for Space Application: Feasibility Study, In: Book of abstracts of ESB2021, European Society of Biomechanics, 26th Congress of the European Society of Biomechanics, Milan (IT) July 11-14, 2021, pp. 1, 2021

Canova, A., Quercio, M., Gabetti, S., Massai, D., A tunable magnetic stimulation system for elucidating the role of PEMF stimulation in bone tissue maturation in vitro in view of precision orthopedic medicine, In: Book of abstracts of EMF 2021, The 12th International Symposium on Electric and Magnetic Fields, Online Conference, July 6-8 2021

Massai D., Gabetti S., Putame G., Armando I., Fiume E., Sanginario A., Carbonaro D., Baino F., Audenino A. L., Verné E., Bignardi C., "Versatile perfusion and electrical stimulation bioreactor for bone tissue engineering", GNB2020, June 10th-12th 2020, Trieste, Italy

Gabetti, S., Putame, G., Montrone, F., Isu, G., Marsano, A., Audenino, A., Massai, D., Versatile electrical stimulator for providing cardiac-like electrical impulses in vitro, *Biomedical Science and Engineering*, PAGEPress, pp. 2, 2020, Vol. 3, ISSN: 2531-9892, DOI: 10.4081/bse.2019.111

Gabetti S., Putame G., Montrone F., Isu G., Marsano A., Audenino A., Massai D., "ELETTRA: a versatile electrical stimulator for cardiac tissue engineering", ESB-ITA Meeting 2019, 30th September – 1st October 2019, Bologna, Italy

Torta E., Drayson O., Bernardini N., Bakkali Abderrahaman A., Dalfó Ferrer B., Gabetti S., Compin M., Morbiducci U., "Artery in Microgravity: a compact in vitro testbench for cardiovascular flow analysis in space", SimBio-M 2020, 18th - 19th June 2020, Virtual Conference

Drayson O., Bernardini N., Bakkali Abderrahaman A., Cerquetani L., Cipolletta A., Dalfó Ferrer B., Falcone F., Gabetti S., Genoni M., Torta E., Vagnone F., Aguzzi M., Audas C., Compin M., Favier J. J., Lizy-Destrez S. and Morbiducci U., "AIM (Artery In Microgravity): Design And Development Of An Ice Cubes Experiment" 70th International Astronautical Congress, 21 - 25 October 2019, Washington D.C., United States

Drayson O., Bernardini N., Bakkali Abderrahaman A., Cerquetani L., Cipolletta A., Dalfó Ferrer B., Falcone F., Gabetti S., Genoni M., Torta E., Vagnone F., Aguzzi M., Audas C., Compin M., Favier J. J., Lizy-Destrez S. and Morbiducci U, "AIM (Artery In Microgravity): An ICE Cubes Mission by University Students", SSEA19: 3rd ESA Symposium on Space Educational Activities, , September 16-18 2019, Leicester, UK

Patents

WO application 2020250121A1, Gallo D., Massai D., Bignardi C., Gabetti S., Serino G., Putame G., Carbonaro D., Castaldo C., Di Meglio F., Romano V., Belviso I., Sacco A., Montagnani S., "Rotation Supporting Unit for Biological Samples / Scaffold and Mass Transfer Method Using the Same", published 2020-12-17, assigned to: Politecnico di Torino, Università degli Studi di Napoli Federico II

References

1. Alberts, B. *et al. Molecular biology of the cell*. (Garland Science, 2008).

2. Suresh, S. Biomechanics and biophysics of cancer cells. *Acta Biomaterialia* **3**, 413–438 (2007).

3. Ethier, C. R. & Simmons, C. A. *Introductory biomechanics from cells to organisms*. (Cambridge University Press, 2007).

4. Wang, J. H.-C. & Thampatty, B. P. An Introductory Review of Cell Mechanobiology. *Biomech Model Mechanobiol* **5**, 1–16 (2006).

5. Martino, F., Perestrelo, A. R., Vinarský, V., Pagliari, S. & Forte, G. Cellular Mechanotransduction: From Tension to Function. *Frontiers in Physiology* **9**, 824 (2018).

6. Thompson, D. W. *On Growth and Form*. (Cambridge University Press, 1942).

7. Kim, T.-J. Mechanobiology: A New Frontier in Biology. *Biology* **10**, 570 (2021).

8. Bao, G. & Suresh, S. Cell and molecular mechanics of biological materials. *Nature Mater* **2**, 715–725 (2003).

9. Chicurel, M. E., Chen, C. S. & Ingber, D. E. Cellular control lies in the balance of forces. *Current Opinion in Cell Biology* **10**, 232–239 (1998).

10. Bronzino, J. D. & Peterson, D. R. *Tissue Engineering and Artificial Organs*. (CRC Press, 2006).

11. Chen, C. S., Tan, J. & Tien, J. Mechanotransduction at Cell-Matrix and Cell-Cell Contacts. *Annu. Rev. Biomed. Eng.* **6**, 275–302 (2004).

12. Stewart, S., Darwood, A., Masouros, S., Higgins, C. & Ramasamy, A. Mechanotransduction in osteogenesis. *Bone & Joint Research* **9**, 1–14 (2020).

13. Wang, N., Butler, J. P. & Ingber, D. E. Mechanotransduction Across the Cell Surface and Through the Cytoskeleton. **260**, 5 (1993).

14. Chowdhury, F., Huang, B. & Wang, N. Cytoskeletal prestress: The cellular hallmark in mechanobiology and mechanomedicine. *Cytoskeleton* **78**, 249–276 (2021).

15. Davies, P. F. & Tripathi, S. C. Mechanical stress mechanisms and the cell. An endothelial paradigm. *Circ Res* **72**, 239–245 (1993).

16. Sims, J. R., Karp, S. & Ingber, D. E. Altering the cellular mechanical force balance results in integrated changes in cell, cytoskeletal and nuclear shape. *Journal of Cell Science* **103**, 1215–1222 (1992).

17. Ingber, D. E. Cellular tensegrity: defining new rules of biological design that govern the cytoskeleton. *Journal of Cell Science* **104**, 613–627 (1993).

18. Duncan, R. L. & Turner, C. H. Mechanotransduction and the functional response of bone to mechanical strain. *Calcif Tissue Int* **57**, 344–358 (1995).

19. Orr, A. W., Helmke, B. P., Blackman, B. R. & Schwartz, M. A. Mechanisms of mechanotransduction. *Dev Cell* **10**, 11–20 (2006).

20. Giancotti, F. G. & Ruoslahti, E. Integrin Signaling. *Science* **285**, 1028–1033 (1999).

21. Davies, P. F. Flow-mediated endothelial mechanotransduction. *Physiol Rev* **75**, 519–560 (1995).

22. Torrent-Guasp, F. *et al.* The Structure and Function of the Helical Heart and Its Buttress Wrapping. I. The Normal Macroscopic Structure of the Heart. *Seminars in Thoracic and Cardiovascular Surgery* **13**, 301–319 (2001).

23. Bouten, C. V. C. *et al.* Substrates for cardiovascular tissue engineering. *Adv Drug Deliv Rev* **63**, 221–241 (2011).

24. Kuznetsova, T. *et al.* Left ventricular strain and strain rate in a general population. *Eur Heart J* **29**, 2014–2023 (2008).

25. Holubarsch, C. *et al.* Shortening versus isometric contractions in isolated human failing and non-failing left ventricular myocardium: dependency of external work and force on muscle length, heart rate and inotropic stimulation. *Cardiovasc Res* **37**, 46–57 (1998).

26. Massai, D. *et al.* Bioreactors as Engineering Support to Treat Cardiac Muscle and Vascular Disease. *Journal of Healthcare Engineering* **4**, 329–370 (2013).

27. Jacot, J. G., Martin, J. C. & Hunt, D. L. Mechanobiology of cardiomyocyte development. *Journal of Biomechanics* **43**, 93–98 (2010).

28. van Putten, S., Shafieyan, Y. & Hinz, B. Mechanical control of cardiac myofibroblasts. *Journal of Molecular and Cellular Cardiology* **93**, 133–142 (2016).

29. Voorhees, A. P. & Han, H.-C. Biomechanics of Cardiac Function. 48 (2016).

30. Fahrenbach, J. P., Mejia-Alvarez, R. & Banach, K. The relevance of non-excitable cells for cardiac pacemaker function. *The Journal of Physiology* **585**, 565–578 (2007).

31. *Cardiovascular Biomechanics*. (Springer International Publishing, 2017). doi:10.1007/978-3-319-46407-7.

32. Tandon, N. *et al.* Electrical stimulation systems for cardiac tissue engineering. *Nat Protoc* **4**, 155–173 (2009).

33. Bronzino, J. D. *Biomedical Engineering Handbook*. (CRC Press, 1999).

34. Stoppel, W. L., Kaplan, D. L. & Black, L. D. Electrical and mechanical stimulation of cardiac cells and tissue constructs. *Advanced Drug Delivery Reviews* **96**, 135–155 (2016).

35. Mesirca, P., Torrente, A. G. & Mangoni, M. E. Functional role of voltage gated Ca2+ channels in heart automaticity. *Front. Physiol.* **6**, (2015).

36. Zhu, R. *et al.* Physical developmental cues for the maturation of human pluripotent stem cell-derived cardiomyocytes. *Stem Cell Res Ther* **5**, 117 (2014).

37. Bers, D. M. Calcium Cycling and Signaling in Cardiac Myocytes. *Annu. Rev. Physiol.* **70**, 23–49 (2008).

38. Jorba, I. *et al.* In Vitro Methods to Model Cardiac Mechanobiology in Health and Disease. *Tissue Engineering Part C: Methods* **27**, 139–151 (2021).

39. Gaetani, R. *et al.* When Stiffness Matters: Mechanosensing in Heart Development and Disease. *Frontiers in Cell and Developmental Biology* **8**, (2020).

40. Lyon, R. C., Zanella, F., Omens, J. H. & Sheikh, F. Mechanotransduction in Cardiac Hypertrophy and Failure. *Circulation Research* **116**, 1462–1476 (2015).

41. Wolff, J. *The Law of Bone Remodelling*. (Springer Berlin Heidelberg, 1986). doi:10.1007/978-3-642-71031-5.

42. Assanah, F. & Khan, Y. Cell responses to physical forces, and how they inform the design of tissue-engineered constructs for bone repair: a review. *J Mater Sci* **53**, 5618–5640 (2018).

43. Klein-Nulend, J., Bacabac, R. G. & Bakker, A. D. Mechanical loading and how it affects bone cells: the role of the osteocyte cytoskeleton in maintaining our skeleton. *Eur Cell Mater* **24**, 278–291 (2012).

44. Pedrero, S. G., Llamas-Sillero, P. & Serrano-López, J. A Multidisciplinary Journey towards Bone Tissue Engineering. *Materials (Basel)* **14**, 4896 (2021).

45. Lakes, R. S., Katz, J. L. & Sternstein, S. S. Viscoelastic properties of wet cortical bone—I. Torsional and biaxial studies. *Journal of Biomechanics* **12**, 657–678 (1979).

46. Fritton, S. P. & Weinbaum, S. Fluid and Solute Transport in Bone: Flow-Induced Mechanotransduction. *Annu Rev Fluid Mech* **41**, 347–374 (2009).

47. Sladkova, M. & de Peppo, G. Bioreactor Systems for Human Bone Tissue Engineering. *Processes* **2**, 494–525 (2014).

48. Knothe Tate, M. L. "Whither flows the fluid in bone?" An osteocyte's perspective. *Journal of Biomechanics* **36**, 1409–1424 (2003).

49. Yeatts, A. B. & Fisher, J. P. Bone tissue engineering bioreactors: Dynamic culture and the influence of shear stress. *Bone* **48**, 171–181 (2011).

50. Fukada, E. & Yasuda, I. On the Piezoelectric Effect of Bone. *J. Phys. Soc. Jpn.* **12**, 1158–1162 (1957).

51. Bassett, C. A. L. & Becker, R. O. Generation of Electric Potentials by Bone in Response to Mechanical Stress. *Science* **137**, 1063–1064 (1962).

52. Friedenberg, Z. B., Harlow, M. C., Heppenstall, R. B. & Brighton, C. T. The cellular origin of bioelectric potentials in bone. *Calc. Tis Res.* **13**, 53–62 (1973).

53. Kuzyk, P. R. & Schemitsch, E. H. The science of electrical stimulation therapy for fracture healing. *Indian J Orthop* **43**, 127–131 (2009).

54. Leppik, L. *et al.* Construction and Use of an Electrical Stimulation Chamber for Enhancing Osteogenic Differentiation in Mesenchymal Stem/Stromal Cells In Vitro. *JoVE (Journal of Visualized Experiments)* e59127 (2019) doi:10.3791/59127.

55. Cadossi, R., Massari, L., Racine-Avila, J. & Aaron, R. K. Pulsed Electromagnetic Field Stimulation of Bone Healing and Joint Preservation: Cellular Mechanisms of Skeletal Response. *J Am Acad Orthop Surg Glob Res Rev* **4**, e19.00155 (2020).

56. Thompson, M. S., Epari, D. R., Bieler, F. & Duda, G. N. In vitro models for bone mechanobiology: Applications in bone regeneration and tissue engineering. *Proc Inst Mech Eng H* **224**, 1533–1541 (2010).

57. Martin, I., Wendt, D. & Heberer, M. The role of bioreactors in tissue engineering. *Trends in Biotechnology* **22**, 80–86 (2004).

58. Asnaghi, M. A. *et al.* Trends in biomedical engineering: Focus on regenerative medicine. *Journal of Applied Biomaterials and Biomechanics* **9**, 73–86 (2011).

59. Mattei, G. Design Criteria for Generating Physiologically Relevant In Vitro Models in Bioreactors. 22 (2014).

60. Vunjak Novakovic, G., Eschenhagen, T. & Mummery, C. Myocardial Tissue Engineering: In Vitro Models. *Cold Spring Harbor Perspectives in Medicine* **4**, a014076–a014076 (2014).

61. Rouwkema, J. *et al.* In vitro platforms for tissue engineering: implications to basic research and clinical translation. *J Tissue Eng Regen Med* **5**, e164–e167 (2011).

62. Wendt, D., Riboldi, S. A., Cioffi, M. & Martin, I. Bioreactors in Tissue Engineering: Scientific Challenges and Clinical Perspectives. in *Bioreactor Systems for Tissue Engineering* (eds. Kasper, C., van Griensven, M. & Pörtner, R.) 1–27 (Springer, 2009). doi:10.1007/10_2008_1.

63. Chen, H.-C. & Hu, Y.-C. Bioreactors for tissue engineering. *Biotechnol Lett* **28**, 1415–1423 (2006).

64. Riboldi, S. A., Bertoldi, S. & Mantero, S. In vitro dynamic culture of cell-biomaterial constructs. in *Characterization of Polymeric Biomaterials* 339–363 (2017). doi:10.1016/B978-0-08-100737-2.00014-5.

65. Lim, D. *et al.* Bioreactor design and validation for manufacturing strategies in tissue engineering. *Bio-des. Manuf.* (2021) doi:10.1007/s42242-021-00154-3.

66. Ratcliffe, A. & Niklason, L. E. Bioreactors and bioprocessing for tissue engineering. *Ann N Y Acad Sci* **961**, 210–215 (2002).

67. Brown, M. A., Iyer, R. K. & Radisic, M. Pulsatile perfusion bioreactor for cardiac tissue engineering. *Biotechnology Progress* **24**, 907–920 (2008).

68. Martin, Y. & Vermette, P. Bioreactors for tissue mass culture: Design, characterization, and recent advances. *Biomaterials* **26**, 7481–7503 (2005).

69. Putame, G. *et al.* Compact and tunable stretch bioreactor advancing tissue engineering implementation. Application to engineered cardiac constructs. *Medical Engineering & Physics* **84**, 1–9 (2020).

70. Vunjak-Novakovic, G. *et al.* Challenges in Cardiac Tissue Engineering. *Tissue Eng Part B Rev* **16**, 169–187 (2010).

71. Massai, D. *et al.* Bioreactor Platform for Biomimetic Culture and in situ Monitoring of the Mechanical Response of in vitro Engineered Models of Cardiac Tissue. *Frontiers in Bioengineering and Biotechnology* **8**, 733 (2020).

72. Putame, G. *et al.* Application of 3D Printing Technology for Design and Manufacturing of Customized Components for a Mechanical Stretching Bioreactor. *Journal of Healthcare Engineering* **2019**, e3957931 (2019).

73. Béland, J. *et al.* Development of an open hardware bioreactor for optimized cardiac cell culture integrating programmable mechanical and electrical stimulations. *AIP Advances* **10**, 035133 (2020).

74. Cortes, D. *et al.* BEaTS-α an open access 3D printed device for in vitro electromechanical stimulation of human induced pluripotent stem cells. *Scientific Reports* **10**, 11274 (2020).

75. Kluge, J. A. *et al.* Bioreactor System Using Noninvasive Imaging and Mechanical Stretch for Biomaterial Screening. *Ann Biomed Eng* **39**, 1390–1402 (2011).

76. Mantero, S., Sadr, N., Riboldi, S. A., Lorenzoni, S. & Montevecchi, F. M. A new electro-mechanical bioreactor for soft tissue engineering. *Journal of Applied Biomaterials and Biomechanics* **5**, 107–116 (2007).

77. Eschenhagen, T. *et al.* 3D engineered heart tissue for replacement therapy. *Basic Res Cardiol* **97 Suppl 1**, I146-152 (2002).

78. Zimmermann, W.-H. *et al.* Tissue Engineering of a Differentiated Cardiac Muscle Construct. *Circulation Research* **90**, 223–230 (2002).

79. Zimmermann, W.-H. *et al.* Engineered heart tissue grafts improve systolic and diastolic function in infarcted rat hearts. *Nat Med* **12**, 452–458 (2006).

80. Pavesi, A. *et al.* Electrical conditioning of adipose-derived stem cells in a multi-chamber culture platform: Electrical Conditioning of Adipose-Derived Stem Cells. *Biotechnol. Bioeng.* **111**, 1452–1463 (2014).

81. Ronaldson-Bouchard, K. *et al.* Engineering of human cardiac muscle electromechanically matured to an adult-like phenotype. *Nat Protoc* **14**, 2781–2817 (2019).

82. Radisic, M. *et al.* Functional assembly of engineered myocardium by electrical stimulation of cardiac myocytes cultured on scaffolds. *Proceedings of the National Academy of Sciences* **101**, 18129–18134 (2004).

83. Tandon, N. *et al.* Optimization of electrical stimulation parameters for cardiac tissue engineering. *J Tissue Eng Regen Med* **5**, e115–e125 (2011).

84. Ronaldson-Bouchard, K. *et al.* Advanced maturation of human cardiac tissue grown from pluripotent stem cells. *Nature* **556**, 239–243 (2018).

85. Xiao, Y. *et al.* Microfabricated perfusable cardiac biowire: a platform that mimics native cardiac bundle. *Lab Chip* **14**, 869–882 (2014).

86. Barash, Y. *et al.* Electric field stimulation integrated into perfusion bioreactor for cardiac tissue engineering. *Tissue Eng Part C Methods* **16**, 1417–1426 (2010).

87. Maidhof, R. *et al.* Biomimetic perfusion and electrical stimulation applied in concert improved the assembly of engineered cardiac tissue: Cardiac tissue

engineering with perfusion and electrical stimulation. *J Tissue Eng Regen Med* **6**, e12–e23 (2012).

88. Morgan, K. Y. & Black, L. D. Mimicking Isovolumic Contraction with Combined Electromechanical Stimulation Improves the Development of Engineered Cardiac Constructs. *Tissue Engineering Part A* **20**, 1654–1667 (2014).

89. Marijanovic, I., Antunovic, M., Matic, I., Panek, M. & Ivkovic, A. Bioreactor-Based Bone Tissue Engineering. in *Advanced Techniques in Bone Regeneration* (eds. Zorzi, A. R. & de Miranda, J. B.) (InTech, 2016). doi:10.5772/62546.

90. Schwarz, R. P., Goodwin, T. J. & Wolf, D. A. Cell culture for three-dimensional modeling in rotating-wall vessels: an application of simulated microgravity. *J Tissue Cult Methods* **14**, 51–57 (1992).

91. Rauh, J., Milan, F., Günther, K.-P. & Stiehler, M. Bioreactor systems for bone tissue engineering. *Tissue Eng Part B Rev* **17**, 263–280 (2011).

92. Wendt, D., Marsano, A., Jakob, M., Heberer, M. & Martin, I. Oscillating perfusion of cell suspensions through three-dimensional scaffolds enhances cell seeding efficiency and uniformity. *Biotechnol Bioeng* **84**, 205–214 (2003).

93. Kavlock, K. D. & Goldstein, A. S. Effect of Pulse Frequency on the Osteogenic Differentiation of Mesenchymal Stem Cells in a Pulsatile Perfusion Bioreactor. *Journal of Biomechanical Engineering* **133**, 091005 (2011).

94. Jagodzinski, M. *et al.* Influence of perfusion and cyclic compression on proliferation and differentiation of bone marrow stromal cells in 3-dimensional culture. *Journal of Biomechanics* **41**, 1885–1891 (2008).

95. Leppik, L., Oliveira, K. M. C., Bhavsar, M. B. & Barker, J. H. Electrical stimulation in bone tissue engineering treatments. *Eur J Trauma Emerg Surg* **46**, 231–244 (2020).

96. Fassina, L. *et al.* Effects of Electromagnetic Stimulation on Calcified Matrix Production by SAOS-2 Cells over a Polyurethane Porous Scaffold. *Tissue Engineering* **12**, 1985–1999 (2006).

97. Fassina, L. *et al.* In vitro electromagnetically stimulated SAOS-2 osteoblasts inside porous hydroxyapatite. *Journal of Biomedical Materials Research Part A* **93A**, 1272–1279 (2010).

98. Zhang, B., Xie, Y., Ni, Z. & Chen, L. Effects and Mechanisms of Exogenous Electromagnetic Field on Bone Cells: A Review. *Bioelectromagnetics* **41**, 263–278 (2020).

99. Trichet, L. *et al.* Evidence of a large-scale mechanosensing mechanism for cellular adaptation to substrate stiffness. *Proceedings of the National Academy of Sciences* **109**, 6933–6938 (2012).

100. Marsano, A. *et al.* Scaffold stiffness affects the contractile function of three-dimensional engineered cardiac constructs. *Biotechnol Progress* **26**, 1382–1390 (2010).

101. Griffin, M., Premakumar, Y., Seifalian, A., Butler, P. E. & Szarko, M. Biomechanical Characterization of Human Soft Tissues Using Indentation and Tensile Testing. *J Vis Exp* 54872 (2016) doi:10.3791/54872.

102. Maeda, E., Sugimoto, M. & Ohashi, T. Cytoskeletal tension modulates MMP-1 gene expression from tenocytes on micropillar substrates. *J Biomech* **46**, 991–997 (2013).

103. Matsui, T. S., Deguchi, S., Sakamoto, N., Ohashi, T. & Sato, M. A versatile micro-mechanical tester for actin stress fibers isolated from cells. *Biorheology* **46**, 401–415 (2009).

104. Do, T.-D., Katsuyoshi, J., Cai, H. & Ohashi, T. Mechanical Properties of Isolated Primary Cilia Measured by Micro-tensile Test and Atomic Force Microscopy. *Frontiers in bioengineering and biotechnology* **9**, (2021).

105. Zhao, F., Lacroix, D., Ito, K., van Rietbergen, B. & Hofmann, S. Changes in scaffold porosity during bone tissue engineering in perfusion bioreactors considerably affect cellular mechanical stimulation for mineralization. *Bone Reports* **12**, 100265 (2020).

106. Pennella, F. *et al.* A Survey of Methods for the Evaluation of Tissue Engineering Scaffold Permeability. *Ann Biomed Eng* **41**, 2027–2041 (2013).

107. Pecci, R., Baiguera, S., Ioppolo, P., Bedini, R. & Del Gaudio, C. 3D printed scaffolds with random microarchitecture for bone tissue engineering applications: Manufacturing and characterization. *Journal of the Mechanical Behavior of Biomedical Materials* **103**, 103583 (2020).

108. Schiavi, A., Guglielmone, C., Pennella, F. & Morbiducci, U. Acoustic method for permeability measurement of tissue-engineering scaffold. *Meas. Sci. Technol.* **23**, 105702 (2012).

109. Hirt, M. N., Hansen, A. & Eschenhagen, T. Cardiac tissue engineering: state of the art. *Circ Res* **114**, 354–367 (2014).

110. Pitoulis, F. G., Watson, S. A., Perbellini, F. & Terracciano, C. M. Myocardial slices come to age: an intermediate complexity in vitro cardiac model for translational research. *Cardiovasc Res* **116**, 1275–1287 (2020).

111. Weinberger, F., Mannhardt, I. & Eschenhagen, T. Engineering Cardiac Muscle Tissue: A Maturating Field of Research. *Circ Res* **120**, 1487–1500 (2017).

112. Zhao, Y., Feric, N. T., Thavandiran, N., Nunes, S. S. & Radisic, M. The Role of Tissue Engineering and Biomaterials in Cardiac Regenerative Medicine. *Canadian Journal of Cardiology* **30**, 1307–1322 (2014).

113. Stein, J. M., Mummery, C. L. & Bellin, M. Engineered models of the human heart: directions and challenges. *Stem Cell Reports* S2213671120304616 (2020) doi:10.1016/j.stemcr.2020.11.013.

114. Zhuang, R. Z., Lock, R., Liu, B. & Vunjak-Novakovic, G. Opportunities and challenges in cardiac tissue engineering from an analysis of two decades of advances. *Nat. Biomed. Eng* **6**, 327–338 (2022).

115. Monteiro, L. M., Vasques-Nóvoa, F., Ferreira, L., Pinto-do-Ó, P. & Nascimento, D. S. Restoring heart function and electrical integrity: closing the circuit. *npj Regen Med* **2**, 9 (2017).

116. Montero, P. *et al.* Cells, Materials, and Fabrication Processes for Cardiac Tissue Engineering. *Front. Bioeng. Biotechnol.* **8**, 955 (2020).

117. Bhana, B. *et al.* Influence of substrate stiffness on the phenotype of heart cells. *Biotechnol. Bioeng.* **105**, 1148–1160 (2010).

118. Guilak, F., Butler, D. L., Goldstein, S. A. & Baaijens, F. P. T. Biomechanics and mechanobiology in functional tissue engineering. *Journal of Biomechanics* **47**, 1933–1940 (2014).

119. Birla, R. k., Huang, Y. c. & Dennis, R. g. Development of a Novel Bioreactor for the Mechanical Loading of Tissue-Engineered Heart Muscle. *Tissue Engineering* **13**, 2239–2248 (2007).

120. Mihic, A. *et al.* The effect of cyclic stretch on maturation and 3D tissue formation of human embryonic stem cell-derived cardiomyocytes. *Biomaterials* **35**, 2798–2808 (2014).

121. Pang, Q., Zu, J. W., Siu, G. M. & Li, R.-K. Design and Development of a Novel Biostretch Apparatus for Tissue Engineering. *Journal of Biomechanical Engineering* **132**, (2009).

122. Hernández, D. *et al.* Electrical Stimulation Promotes Cardiac Differentiation of Human Induced Pluripotent Stem Cells. *Stem Cells International* **2016**, 1–12 (2016).

123. Nunes, S. S. *et al.* Biowire: a platform for maturation of human pluripotent stem cell–derived cardiomyocytes. *Nature Methods* **10**, 781–787 (2013).

124. Sathaye, A., Bursac, N., Sheehy, S. & Tung, L. Electrical pacing counteracts intrinsic shortening of action potential duration of neonatal rat ventricular cells in culture. *Journal of Molecular and Cellular Cardiology* **41**, 633–641 (2006).

125. Zhang, F. *et al.* Gelatin-based hydrogels combined with electrical stimulation to modulate neonatal rat cardiomyocyte beating and promote maturation. *Bio-des. Manuf.* **4**, 100–110 (2021).

126. Chiu, L. L. Y., Iyer, R. K., King, J.-P. & Radisic, M. Biphasic Electrical Field Stimulation Aids in Tissue Engineering of Multicell-Type Cardiac Organoids. *Tissue Engineering Part A* **17**, 1465–1477 (2011).

127. Pietronave, S. *et al.* Monophasic and Biphasic Electrical Stimulation Induces a Precardiac Differentiation in Progenitor Cells Isolated from Human Heart. *Stem Cells and Development* **23**, 888–898 (2014).

128. Hirt, M. N. *et al.* Functional improvement and maturation of rat and human engineered heart tissue by chronic electrical stimulation. *J Mol Cell Cardiol* **74**, 151–161 (2014).

129. Lasher, R. A., Pahnke, A. Q., Johnson, J. M., Sachse, F. B. & Hitchcock, R. W. Electrical stimulation directs engineered cardiac tissue to an age-matched native phenotype. *J Tissue Eng* **3**, 2041731412455354 (2012).

130. Pretorius, D., Kahn-Krell, A. M., LaBarge, W. C., Lou, X. & Zhang, J. Engineering of thick human functional myocardium via static stretching and electrical stimulation. *iScience* **25**, (2022).

131. Visone, R., Talò, G., Lopa, S., Rasponi, M. & Moretti, M. Enhancing all-in-one bioreactors by combining interstitial perfusion, electrical stimulation, on-line monitoring and testing within a single chamber for cardiac constructs. *Sci Rep* **8**, 16944 (2018).

132. Visone, R. *et al.* A microscale biomimetic platform for generation and electro-mechanical stimulation of 3D cardiac microtissues. *APL Bioengineering* **2**, 046102 (2018).

133. Zhao, Y. *et al.* A Platform for Generation of Chamber-Specific Cardiac Tissues and Disease Modeling. *Cell* **176**, 913-927.e18 (2019).

134. Baumgartner, S. *et al.* Electrophysiological and Morphological Maturation of Murine Fetal Cardiomyocytes During Electrical Stimulation In Vitro. *J Cardiovasc Pharmacol Ther* **20**, 104–112 (2015).

135. Chan, Y.-C. *et al.* Electrical stimulation promotes maturation of cardiomyocytes derived from human embryonic stem cells. *J Cardiovasc Transl Res* **6**, 989–999 (2013).

136. Kroll, K. *et al.* Electro-mechanical conditioning of human iPSC-derived cardiomyocytes for translational research. *Progress in Biophysics and Molecular Biology* **130**, 212–222 (2017).

137. LaBarge, W. *et al.* Maturation of three-dimensional, hiPSC-derived cardiomyocyte spheroids utilizing cyclic, uniaxial stretch and electrical stimulation. *PLoS One* **14**, e0219442 (2019).

138. Ruan Jia-Ling *et al.* Mechanical Stress Conditioning and Electrical Stimulation Promote Contractility and Force Maturation of Induced Pluripotent Stem Cell-Derived Human Cardiac Tissue. *Circulation* **134**, 1557–1567 (2016).

139. Martherus, R. S. R. M., Zeijlemaker, V. A. & Ayoubi, T. A. Y. Electrical stimulation of primary neonatal rat ventricular cardiomyocytes using pacemakers. *Biotechniques* **48**, 65–67 (2010).

140. Klingensmith, M. E., Washington University (Saint Louis, Mo.), & Department of surgery. *The Washington manual of surgery.* (2020).

141. Schneck, D. An outline of cardiovascular structure and function. in *Tissue Engineering* I-1-I–12 (CRC Press, 2003).

142. Tandon, N., Cannizzaro, C., Figallo, E., Voldman, J. & Vunjak-Novakovic, G. Characterization of Electrical Stimulation Electrodes for Cardiac Tissue Engineering. in *2006 International Conference of the IEEE Engineering in Medicine and Biology Society* 845–848 (IEEE, 2006). doi:10.1109/IEMBS.2006.259747.

143. Randles, J. E. B. Kinetics of rapid electrode reactions. *Discuss. Faraday Soc.* **1**, 11–19 (1947).

144. Radisic, M., Marsano, A., Maidhof, R., Wang, Y. & Vunjak-Novakovic, G. Cardiac tissue engineering using perfusion bioreactor systems. *Nat Protoc* **3**, 719–738 (2008).

145. Tandon, N., Marsano, A., Cannizzaro, C., Voldman, J. & Vunjak-Novakovic, G. Design of electrical stimulation bioreactors for cardiac tissue engineering. in *2008 30th Annual International Conference of the IEEE Engineering in Medicine and Biology Society* 3594–3597 (IEEE, 2008). doi:10.1109/IEMBS.2008.4649983.

146. Marsano, A. *et al.* Beating heart on a chip: a novel microfluidic platform to generate functional 3D cardiac microtissues. *Lab Chip* **16**, 599–610 (2016).

147. Scuderi, G. J. & Butcher, J. Naturally Engineered Maturation of Cardiomyocytes. *Frontiers in Cell and Developmental Biology* **5**, (2017).

148. Voldman, J. Electrical Forces for Microscale Cell Manipulation. *Annual Review of Biomedical Engineering* **8**, 425–454 (2006).

149. Tsai, P. J., Nayak, S., Ghosh, S. & Puri, I. K. Influence of particle arrangement on the permittivity of an elastomeric composite. *AIP Advances* **7**, 015003 (2017).

150. Chen, M.-T., Jiang, C., Vernier, P. T., Wu, Y.-H. & Gundersen, M. A. Two-dimensional nanosecond electric field mapping based on cell electropermeabilization. *PMC Biophys* **2**, 9 (2009).

151. El-Rashidy, A. A., Roether, J. A., Harhaus, L., Kneser, U. & Boccaccini, A. R. Regenerating bone with bioactive glass scaffolds: A review of in vivo studies in bone defect models. *Acta Biomater* **62**, 1–28 (2017).

152. Suryani, L. *et al.* Effects of Electromagnetic Field on Proliferation, Differentiation, and Mineralization of MC3T3 Cells. *Tissue Engineering Part C: Methods* **25**, 114–125 (2019).

153. Borgström, F. *et al.* Fragility fractures in Europe: burden, management and opportunities. *Arch Osteoporos* **15**, 59 (2020).

154. Kanis, J. A. *et al.* SCOPE 2021: a new scorecard for osteoporosis in Europe. *Arch Osteoporos* **16**, 82 (2021).

155. Nauth, A., Schemitsch, E., Norris, B., Nollin, Z. & Watson, J. T. Critical-Size Bone Defects: Is There a Consensus for Diagnosis and Treatment? *J Orthop Trauma* **32 Suppl 1**, S7–S11 (2018).

156. Migliorini, F. *et al.* Strategies for large bone defect reconstruction after trauma, infections or tumour excision: a comprehensive review of the literature. *Eur J Med Res* **26**, 118 (2021).

157. Amini, A. R., Laurencin, C. T. & Nukavarapu, S. P. Bone Tissue Engineering: Recent Advances and Challenges. *Crit Rev Biomed Eng* **40**, 363–408 (2012).

158. Kargozar, S. *et al.* Bone Tissue Engineering Using Human Cells: A Comprehensive Review on Recent Trends, Current Prospects, and Recommendations. *Applied Sciences* **9**, 174 (2019).

159. Evans, C. H. Barriers to the Clinical Translation of Orthopedic Tissue Engineering. *Tissue Eng Part B Rev* **17**, 437–441 (2011).

160. Campana, V. *et al.* Bone substitutes in orthopaedic surgery: from basic science to clinical practice. *J Mater Sci Mater Med* **25**, 2445–2461 (2014).

161. Mittwede, P. N., Gottardi, R., Alexander, P. G., Tarkin, I. S. & Tuan, R. S. Clinical Applications of Bone Tissue Engineering in Orthopedic Trauma. *Curr Pathobiol Rep* **6**, 99–108 (2018).

162. Quarto, R. & Giannoni, P. Bone Tissue Engineering: Past-Present-Future. *Methods Mol Biol* **1416**, 21–33 (2016).

163. Frost, H. M. A 2003 update of bone physiology and Wolff's Law for clinicians. *Angle Orthod* **74**, 3–15 (2004).

164. Manokawinchoke, J. *et al.* Mechanical loading and the control of stem cell behavior. *Archives of Oral Biology* **125**, 105092 (2021).

165. Wan, X., Liu, Z. & Li, L. Manipulation of Stem Cells Fates: The Master and Multifaceted Roles of Biophysical Cues of Biomaterials. *Advanced Functional Materials* **31**, 2010626 (2021).

166. Duval, K. *et al.* Modeling Physiological Events in 2D vs. 3D Cell Culture. *Physiology (Bethesda)* **32**, 266–277 (2017).

167. Wendt, D., Riboldi, S. A., Cioffi, M. & Martin, I. Bioreactors in tissue engineering: scientific challenges and clinical perspectives. *Adv Biochem Eng Biotechnol* **112**, 1–27 (2009).

168. Salter, E. *et al.* Bone Tissue Engineering Bioreactors: A Role in the Clinic? *Tissue Engineering Part B: Reviews* **18**, 62–75 (2012).

169. Martin, I., Smith, T. & Wendt, D. Bioreactor-based roadmap for the translation of tissue engineering strategies into clinical products. *Trends Biotechnol* **27**, 495–502 (2009).

170. Hambor, J. E. Bioreactor design and bioprocess controls for industrialized cell processing: Bioengineering strategies and platform technologies. *BioProcess International* **10**, 22–33 (2012).

171. Massai, D. *et al.* A Versatile Bioreactor for Dynamic Suspension Cell Culture. Application to the Culture of Cancer Cell Spheroids. *PLoS ONE* **11**, e0154610 (2016).

172. Thorpe, S. D. *et al.* The Response of Bone Marrow-Derived Mesenchymal Stem Cells to Dynamic Compression Following TGF-β3 Induced Chondrogenic Differentiation. *Ann Biomed Eng* **38**, 2896–2909 (2010).

173. Steward, A. J., Wagner, D. R. & Kelly, D. J. Exploring the roles of integrin binding and cytoskeletal reorganization during mesenchymal stem cell mechanotransduction in soft and stiff hydrogels subjected to dynamic compression. *Journal of the Mechanical Behavior of Biomedical Materials* **38**, 174–182 (2014).

174. Zhao, Y.-H. *et al.* Hydrostatic pressure promotes the proliferation and osteogenic/chondrogenic differentiation of mesenchymal stem cells: The roles of RhoA and Rac1. *Stem Cell Research* **14**, 283–296 (2015).

175. Sart, S., Agathos, S. N., Li, Y. & Ma, T. Regulation of mesenchymal stem cell 3D microenvironment: From macro to microfluidic bioreactors. *Biotechnol J* **11**, 43–57 (2016).

176. Alvarez-Barreto, J. F., Linehan, S. M., Shambaugh, R. L. & Sikavitsas, V. I. Flow Perfusion Improves Seeding of Tissue Engineering Scaffolds with Different Architectures. *Ann Biomed Eng* **35**, 429–442 (2007).

177. Schmid, J. *et al.* A Perfusion Bioreactor System for Cell Seeding and Oxygen-Controlled Cultivation of Three-Dimensional Cell Cultures. *Tissue Engineering Part C: Methods* **24**, 585–595 (2018).

178. Bancroft, G. N. *et al.* Fluid flow increases mineralized matrix deposition in 3D perfusion culture of marrow stromal osteoblasts in a dose-dependent manner. *Proc Natl Acad Sci U S A* **99**, 12600–12605 (2002).

179. Carpentier, B., Layrolle, P. & Legallais, C. Bioreactors for Bone Tissue Engineering. *Int J Artif Organs* **34**, 259–270 (2011).

180. Wittkowske, C., Reilly, G. C., Lacroix, D. & Perrault, C. M. In Vitro Bone Cell Models: Impact of Fluid Shear Stress on Bone Formation. *Front. Bioeng. Biotechnol.* **4**, (2016).

181. Bancroft, G. N., Sikavitsas, V. I. & Mikos, A. G. Technical Note: Design of a Flow Perfusion Bioreactor System for Bone Tissue-Engineering Applications. *Tissue Engineering* **9**, 549–554 (2003).

182. Datta, N. *et al.* In vitro generated extracellular matrix and fluid shear stress synergistically enhance 3D osteoblastic differentiation. *Proc Natl Acad Sci U S A* **103**, 2488–2493 (2006).

183. Du, D., Furukawa, K. & Ushida, T. Oscillatory perfusion seeding and culturing of osteoblast-like cells on porous beta-tricalcium phosphate scaffolds. *J. Biomed. Mater. Res.* **86A**, 796–803 (2008).

184. Koch, M. A., Vrij, E. J., Engel, E., Planell, J. A. & Lacroix, D. Perfusion cell seeding on large porous PLA/calcium phosphate composite scaffolds in a perfusion bioreactor system under varying perfusion parameters. *J. Biomed. Mater. Res.* **95A**, 1011–1018 (2010).

185. Engel, N. *et al.* An optimized 3D-printed perfusion bioreactor for homogeneous cell seeding in bone substitute scaffolds for future chairside applications. *Sci Rep* **11**, 22228 (2021).

186. Tseng, C.-L., Chang, K.-M., Wu, C.-C., Wang, Y.-K. & Wang, I.-K. Rabbit Mesenchymal Stem Cells Cultured in a Dynamic Culture System Displayed Superior Cell Proliferation and Osteogenetic Induction. *Journal of Experimental & Clinical Medicine* **6**, 10–15 (2014).

187. Chen, G., Xu, R., Zhang, C. & Lv, Y. Responses of MSCs to 3D Scaffold Matrix Mechanical Properties under Oscillatory Perfusion Culture. *ACS Appl. Mater. Interfaces* **9**, 1207–1218 (2017).

188. Beşkardeş, I. G., Aydın, G., Bektaş, Ş., Cengiz, A. & Gümüşderelioğlu, M. A systematic study for optimal cell seeding and culture conditions in a perfusion mode bone-tissue bioreactor. *Biochemical Engineering Journal* **132**, 100–111 (2018).

189. Du, D., Furukawa, K. S. & Ushida, T. 3D culture of osteoblast-like cells by unidirectional or oscillatory flow for bone tissue engineering. *Biotechnology and Bioengineering* **102**, 1670–1678 (2009).

190. Ceccarelli, G. *et al.* A Comparative Analysis of the In Vitro Effects of Pulsed Electromagnetic Field Treatment on Osteogenic Differentiation of Two Different Mesenchymal Cell Lineages. *BioResearch Open Access* **2**, 283–294 (2013).

191. Daish, C., Blanchard, R., Fox, K., Pivonka, P. & Pirogova, E. The Application of Pulsed Electromagnetic Fields (PEMFs) for Bone Fracture Repair: Past and Perspective Findings. *Ann Biomed Eng* **46**, 525–542 (2018).

192. Wang, H. *et al.* Enhanced osteogenesis of bone marrow stem cells cultured on hydroxyapatite/collagen I scaffold in the presence of low-frequency magnetic field. *J Mater Sci: Mater Med* **30**, 89 (2019).

193. Varani, K. *et al.* Pulsed Electromagnetic Field Stimulation in Osteogenesis and Chondrogenesis: Signaling Pathways and Therapeutic Implications. *IJMS* **22**, 809 (2021).

194. Markov, M. S. Pulsed electromagnetic field therapy history, state of the art and future. *Environmentalist* **27**, 465–475 (2007).

195. Hu, H. *et al.* Promising application of Pulsed Electromagnetic Fields (PEMFs) in musculoskeletal disorders. *Biomedicine & Pharmacotherapy* **131**, 110767 (2020).

196. Zhang, X., Tiainen, H. & Haugen, H. J. Comparison of titanium dioxide scaffold with commercial bone graft materials through micro-finite element modelling in flow perfusion. *Med Biol Eng Comput* **57**, 311–324 (2019).

197. Brinkman, H. C. A calculation of the viscous force exerted by a flowing fluid on a dense swarm of particles. *Appl. Sci. Res.* **1**, 27 (1949).

198. Wang, D. M. & Tarbell, J. M. Modeling Interstitial Flow in an Artery Wall Allows Estimation of Wall Shear Stress on Smooth Muscle Cells. *Journal of Biomechanical Engineering* **117**, 358–363 (1995).

199. Vossenberg, P., Higuera, G. A., van Straten, G., van Blitterswijk, C. A. & van Boxtel, A. J. B. Darcian permeability constant as indicator for shear stresses in regular scaffold systems for tissue engineering. *Biomech Model Mechanobiol* **8**, 499–507 (2009).

200. Sohrabi, M. *et al.* Enhancing Mechanical Properties and Biological Performances of Injectable Bioactive Glass by Gelatin and Chitosan for Bone Small Defect Repair. *Biomedicines* **8**, 616 (2020).

201. Kim, M.-H. & Kino-oka, M. Mechanobiological conceptual framework for assessing stem cell bioprocess effectiveness. *Biotechnology and Bioengineering* **118**, 4537–4549 (2021).

202. Zhou, J. *et al.* Different electromagnetic field waveforms have different effects on proliferation, differentiation and mineralization of osteoblasts in vitro: Effects of Electromagnetic Fields on Osteoblasts. *Bioelectromagnetics* **35**, 30–38 (2014).

203. Smith, L. J., Li, P., Holland, M. R. & Ekser, B. FABRICA: A Bioreactor Platform for Printing, Perfusing, Observing, & Stimulating 3D Tissues. *Sci Rep* **8**, 7561 (2018).

204. Wendt, D., Riboldi, S. A., Cioffi, M. & Martin, I. Potential and Bottlenecks of Bioreactors in 3D Cell Culture and Tissue Manufacturing. *Advanced Materials* **21**, 3352–3367 (2009).

205. Hansmann, J., Groeber, F., Kahlig, A., Kleinhans, C. & Walles, H. Bioreactors in tissue engineering-principles, applications and commercial constraints. *Biotechnology Journal* **8**, 298–307 (2013).

206. Stavenschi, E., Labour, M.-N. & Hoey, D. A. Oscillatory fluid flow induces the osteogenic lineage commitment of mesenchymal stem cells: The effect of shear stress magnitude, frequency, and duration. *Journal of Biomechanics* **55**, 99–106 (2017).

207. Zhao, F., van Rietbergen, B., Ito, K. & Hofmann, S. Flow rates in perfusion bioreactors to maximise mineralisation in bone tissue engineering in vitro. *Journal of Biomechanics* **79**, 232–237 (2018).

208. Li, D., Tang, T., Lu, J. & Dai, K. Effects of Flow Shear Stress and Mass Transport on the Construction of a Large-Scale Tissue-Engineered Bone in a Perfusion Bioreactor. *Tissue Engineering Part A* **15**, 2773–2783 (2009).

209. Vetsch, J. R., Betts, D. C., Müller, R. & Hofmann, S. Flow velocity-driven differentiation of human mesenchymal stromal cells in silk fibroin scaffolds: A combined experimental and computational approach. *PLOS ONE* **12**, e0180781 (2017).

210. McCoy, R. j., Jungreuthmayer, C. & O'Brien, F. j. Influence of flow rate and scaffold pore size on cell behavior during mechanical stimulation in a flow perfusion bioreactor. *Biotechnology and Bioengineering* **109**, 1583–1594 (2012).

211. Olivares, A. L., Marsal, È., Planell, J. A. & Lacroix, D. Finite element study of scaffold architecture design and culture conditions for tissue engineering. *Biomaterials* **30**, 6142–6149 (2009).

212. Najmi, Z. *et al.* Evaluation of Nisin and LL-37 Antimicrobial Peptides as Tool to Preserve Articular Cartilage Healing in a Septic Environment. *Frontiers in Bioengineering and Biotechnology* **8**, 561 (2020).

213. Holtorf, H. L., Jansen, J. A. & Mikos, A. G. Flow perfusion culture induces the osteoblastic differentiation of marrow stromal cell-scaffold constructs in the absence of dexamethasone. *Journal of Biomedical Materials Research Part A* **72A**, 326–334 (2005).

214. Ding, C.-M., Zhou, Y., He, Y.-N. & Tan, W.-S. Perfusion seeding of collagen–chitosan sponges for dermal tissue engineering. *Process Biochemistry* **43**, 287–296 (2008).

215. Seddiqi, H. *et al.* Inlet flow rate of perfusion bioreactors affects fluid flow dynamics, but not oxygen concentration in 3D-printed scaffolds for bone tissue engineering: Computational analysis and experimental validation. *Computers in Biology and Medicine* **124**, 103826 (2020).

216. Bergholt, N. L., Lysdahl, H., Lind, M. & Foldager, C. B. A Standardized Method of Applying Toluidine Blue Metachromatic Staining for Assessment of Chondrogenesis. *Cartilage* **10**, 370–374 (2019).

217. Lehmann, T. P. *et al.* The Regulation of Collagen Processing by miRNAs in Disease and Possible Implications for Bone Turnover. *Int J Mol Sci* **23**, 91 (2021).

218. McMahon, L. A., Campbell, V. A. & Prendergast, P. J. Involvement of stretch-activated ion channels in strain-regulated glycosaminoglycan synthesis in mesenchymal stem cell-seeded 3D scaffolds. *Journal of Biomechanics* **41**, 2055–2059 (2008).

219. Murillo, G. *et al.* Electromechanical Nanogenerator–Cell Interaction Modulates Cell Activity. *Advanced Materials* **29**, 1605048 (2017).

220. More, N. & Kapusetti, G. Piezoelectric material - A promising approach for bone and cartilage regeneration. *Med Hypotheses* **108**, 10–16 (2017).

221. Jacob, J., More, N., Kalia, K. & Kapusetti, G. Piezoelectric smart biomaterials for bone and cartilage tissue engineering. *Inflamm Regener* **38**, 2 (2018).

222. Golub, E. E. & Boesze-Battaglia, K. The role of alkaline phosphatase in mineralization. *Current Opinion in Orthopaedics* **18**, 444–448 (2007).

223. Massai, D. *et al.* Image-Based Three-Dimensional Analysis to Characterize the Texture of Porous Scaffolds. *BioMed Research International* **2014**, e161437 (2014).

224. Zermatten, E. *et al.* Micro-Computed Tomography Based Computational Fluid Dynamics for the Determination of Shear Stresses in Scaffolds Within a Perfusion Bioreactor. *Ann Biomed Eng* **42**, 1085–1094 (2014).

225. Pisitpipathsin, N. *et al.* Effect of BCZT on Electrical Properties and Bioactivity of 45S5 Bioglass. *Integrated Ferroelectrics* **142**, 144–153 (2013).

226. Mukherjee, A. K. & Patri, M. Electrical properties of chlorinated atactic polypropylene (CAPP) and PVC–DOP–CAPP system. *Journal of Applied Polymer Science* **39**, 1485–1493 (1990).

227. Nield, D. A. & Bejan, A. *Convection in porous media.* (Springer, 2006).

228. Truskey, G. A., Yuan, F. & Katz, D. F. *Transport phenomena in biological systems.* (Pearson/Prentice Hall, 2004).

229. Dias, M. R., Fernandes, P. R., Guedes, J. M. & Hollister, S. J. Permeability analysis of scaffolds for bone tissue engineering. *Journal of Biomechanics* **45**, 938–944 (2012).

230. Lai, W. M. & Mow, V. C. Drag-induced compression of articular cartilage during a permeation experiment. *Biorheology* **17**, 111–123 (1980).

231. Mohee, L., Offeddu, G. S., Husmann, A., Oyen, M. L. & Cameron, R. E. Investigation of the intrinsic permeability of ice-templated collagen scaffolds as a function of their structural and mechanical properties. *Acta Biomaterialia* **83**, 189–198 (2019).

232. Podichetty, J. T. & Madihally, S. V. Modeling of porous scaffold deformation induced by medium perfusion: Deformation of Porous Scaffolds. *J. Biomed. Mater. Res.* **102**, 737–748 (2014).

233. Pennella, F. *et al.* A Virtual Test Bench to Study Transport Phenomena in 3D Porous Scaffolds Using Lattice Boltzmann Simulations. in *Volume 1A: Abdominal Aortic Aneurysms; Active and Reactive Soft Matter; Atherosclerosis; BioFluid Mechanics; Education; Biotransport Phenomena; Bone, Joint and Spine Mechanics; Brain Injury; Cardiac Mechanics; Cardiovascular Devices, Fluids and Imaging; Cartilage and Disc Mechanics; Cell and Tissue Engineering; Cerebral Aneurysms; Computational Biofluid Dynamics; Device Design, Human Dynamics, and Rehabilitation; Drug Delivery and Disease Treatment; Engineered Cellular Environments* V01AT07A020 (American Society of Mechanical Engineers, 2013). doi:10.1115/SBC2013-14489.

234. Fernandez, M., Vink, J., Yoshida, K., Wapner, R. & Myers, K. M. Direct Measurement of the Permeability of Human Cervical Tissue. *Journal of Biomechanical Engineering* **135**, 021024 (2013).

235. Lipowiecki, M. *et al.* Permeability of rapid prototyped artificial bone scaffold structures. *Journal of Biomedical Materials Research Part A* **102**, 4127–4135 (2014).

236. Nasrollahzadeh, N. & Pioletti, D. P. Experimental method to characterize the strain dependent permeability of tissue engineering scaffolds. *Journal of Biomechanics* **49**, 3749–3752 (2016).

237. Ochoa, I. *et al.* Permeability evaluation of 45S5 Bioglass®-based scaffolds for bone tissue engineering. *Journal of Biomechanics* **42**, 257–260 (2009).

238. Truscello, S. *et al.* Prediction of permeability of regular scaffolds for skeletal tissue engineering: A combined computational and experimental study. *Acta Biomaterialia* **8**, 1648–1658 (2012).

239. Kleinhans, K. L. & Jackson, A. R. Hydraulic permeability of meniscus fibrocartilage measured via direct permeation: Effects of tissue anisotropy, water volume content, and compressive strain. *Journal of Biomechanics* **72**, 215–221 (2018).

240. Giuliani, N. *et al.* Use of an optimized automatic procedure for measuring the hydraulic permeability of articular cartilage. in 4 (2020).

241. Santos, J., Pires, T., Gouveia, B. P., Castro, A. P. G. & Fernandes, P. R. On the permeability of TPMS scaffolds. *Journal of the Mechanical Behavior of Biomedical Materials* **110**, 103932 (2020).

242. Chor, M. V. & Li, W. A permeability measurement system for tissue engineering scaffolds. *Meas. Sci. Technol.* **18**, 208–216 (2007).

243. Bear, J. *Dynamics of fluids in porous media*. (Dover, 1988).

244. Fand, R. M., Kim, B. Y. K., Lam, A. C. C. & Phan, R. T. Resistance to the Flow of Fluids Through Simple and Complex Porous Media Whose Matrices Are Composed of Randomly Packed Spheres. *Journal of Fluids Engineering* **109**, 268–273 (1987).

245. Dybbs, A. & Edwards, R. V. A New Look at Porous Media Fluid Mechanics — Darcy to Turbulent. in *Fundamentals of Transport Phenomena in Porous Media* (eds. Bear, J. & Corapcioglu, M. Y.) 199–256 (Springer Netherlands, 1984). doi:10.1007/978-94-009-6175-3_4.

246. Darcy, H. *Les fontaines publiques de la ville de Dijon : Exposition et application des principes à suivre et des formules à employer dans les questions de distribution d'eau : Ouvrage terminé par un appendice relatif aux fournitures d'eau de plusieurs villes, au filtrage des eaux et à la fabrication des tuyaux de fonte, de plomb, de tôle et de bitume*. (Paris : V. Dalmont, 1856).

247. JCGM 100:2008 (GUM 1995 with minor corrections): Evaluation of measurement data - Guide to the expression of uncertainty in measurement. (2008).

248. Perale, G. *et al.* Biomimetic Biomolecules in Next Generation Xeno-Hybrid Bone Graft Material Show Enhanced In Vitro Bone Cells Response. *JCM* **8**, 2159 (2019).

249. Ma, Y.-S., Chen, G. & Thimm, G. Paradigm shift: unified and associative feature-based concurrent and collaborative engineering. *J Intell Manuf* **19**, 625–641 (2008).

250. Active Engineering standards | European Cooperation for Space Standardization. https://ecss.nl/standards/active-standards/engineering/.

251. Design Control Guidance For Medical Device Manufacturers. (1997).

252. Ogrodnik, P. J. *Medical device design: innovation from concept to market*. (Elsevier/Academic Press, 2013).

253. JCGM_200_2012: International vocabulary of metrology - Basic and general concepts and associated terms (VIM). (2012).

254. OECD. *OECD Principles on Good Laboratory Practice*. (Organisation for Economic Co-operation and Development, 1998).